ABSTRACT

The Effects of Freezing on the Material Properties
and Structure of Bovine Medial Meniscus

D. Scott Morgan, M.S.

Mentor: Carolyn T. Skurla, Ph.D.

Menisci serve as shock absorbers and stabilizers in the knee. Bovine meniscus is often used as a model for human meniscus because it is inexpensive and readily available. During experiments, the bovine menisci are usually frozen and thawed repeatedly to maintain freshness through specimen transport and during the study. Previous studies did not take into account the effects of multiple freezing and thawing cycles (FTCs) on the mechanical properties [32, 33, 35, 47]. The current study will observe the effects, if any, of repeated FTC's on the viscoelastic properties and structure of bovine meniscus. Five test groups were created consisting of five menisci each. After treatment, a plug was taken from each meniscus and compressed in a confined compression chamber for 20,000 seconds. Displacement and specimen dimensions were measured, and aggregate Modulus (H_A) and tissue permeability (λ) were calculated. A scanning electron microscope (SEM) was used to view the structure.

The Effects of Freezing on the Material Properties
and Structure of Bovine Medial Meniscus

by

D. Scott Morgan, B.S.

A Thesis

Approved by the Department of Mechanical Engineering

_____
William M. Jordan, Ph.D., Chairperson

Submitted to the Graduate Faculty of
Baylor University in Partial Fulfillment of the
Requirements for the Degree
of
Master of Science in Biomedical Engineering

Approved by the Thesis Committee

_____
Carolyn T. Skurla, Ph.D., Chairperson

_____
William M. Jordan, Ph.D.

_____
Ann E. Rushing, Ph.D.

Accepted by the Graduate School
August 2009

_____
J. Larry Lyon, Ph.D., Dean

Page bearing signatures is kept on file in the Graduate School.

TABLE OF CONTENTS

LIST OF FIGURES

LIST OF TABLES

ACKNOWLEDGMENTS

The author would like to acknowledge Dr. Carolyn Skurla for her years of direction and assistance on two theses as well as her overall mentorship for the past four years. Also, the author would like to thank Dr. Anne Rushing for the use of her laboratory and for training on using a scanning electron microscope as well as Dr. Bill Jordan for his support during the thesis project. The time, effort, and assistance of the thesis committee is greatly appreciated. The author would also like to acknowledge the efforts of Dr. Ian Gravagne, Dr. Stephen McClain, Dr. Brian Garner, and Mr. Ashley Orr of Baylor University, as well as Dr. Harry Hogan of Texas A&M. Finally, the author would like to thank John Miller, Jason Head, Heather Benoit, Jace Kelley, and Gilbert Narvaez for their assistance both inside and outside of the laboratory and especially thank Jonathan Golightly of Texas A&M for his assistance with the data analysis.

CHAPTER ONE

Introduction

General Knee Anatomy

The human knee joint contains a pair of fibro-cartilaginous, semi-lunar menisci, located medially and laterally (Figure 1), which serve a variety of functions necessary for normal and pain-free knee movement. The human knee is also formed by four major ligaments, a tendon, and three major bones along with numerous smaller structures (Figure 1). Situated between the femur and the tibia, attached to the top of the tibial plateau and conforming around the femoral condyles, the meniscus is ideally placed to serve as a shock absorber and stabilizer in the legs. The knee joints must support as much as 10 to 20 times the body weight of the person during athletic activities such as running, which alone causes high joint reaction forces, as well as support some of the largest muscles in the human body [2]. The menisci cover most of the tibial plateau, with the medial meniscus occupying 51-75 percent of the medial pleateau and the lateral meniscus occupying 75-93 percent of the lateral plateau [3].

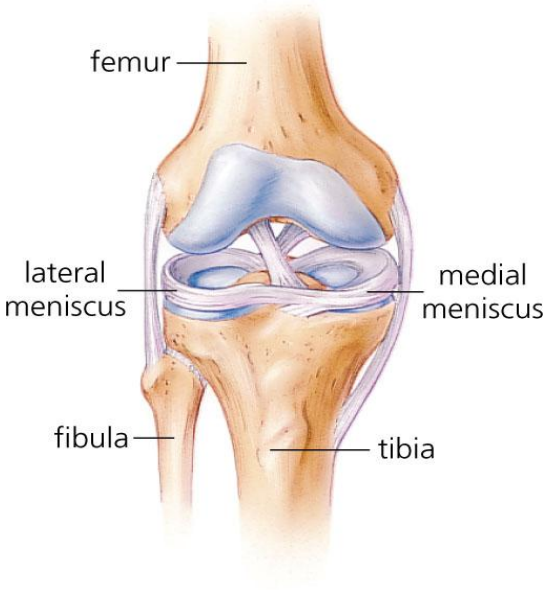

Figure 1: The knee joint from American Heritage Dictionary [1]

Fibro-cartilage serves two important mechanical functions. First it limits the stresses transferred to the bone surfaces because it has the ability to deform and thereby to evenly distribute the applied load across the joint. Second, together with synovial fluid, the menisci provide an extremely efficient bearing surface which is typical of normal, healthy, joints.

The unique shape of the meniscus allows for increased joint stability and the more enhanced load bearing capabilities of the knee. The femoral condyles are two, semi-circular, smooth extensions of the femur, which form the proximal articulating surface of the knee joint and allow for easy articulation. The distal articulating surface is a mostly flat region, known as the tibial plateau. The menisci act as a bearing surface that provides for greater congruence between the round femoral condyles and the flat tibial plateau by utilizing a concave surface that fits with the femoral condyles on the proximal side. The distal side of the meniscus is flat to conform to the tibial plateau and allow for an increased surface area across which forces are transmitted, thereby reducing the stress. Also, the concave shape of the proximal meniscal surface allows for them to wrap around the outside of the femoral condyles providing greater stability for the entire joint [2]. Finally, cartilage is a visco-elastic material, which will appear stiffer when loaded at high strain rates than when loaded at low strain rates [4]. This allows the meniscus to serve as a natural shock absorber which can handle greater impacts while preventing damage to the body.

Importance of the Meniscus

Before Fairbank's paper in 1948, menisci were originally considered vestigial structures within the knee that served no important function; however, menisci are now

recognized as integral components in the complex biomechanics of load transmission, shock absorption, and joint stability [3, 5-11]. Research has shown that the removal of all or part of the meniscus results in increased stress on the fibro- and articular cartilage which triggers progressive degeneration of the load bearing surfaces of the joint [11]. Knee injuries accounted for 19.4 million visits to the doctor in 2003 and are the most common reason for individuals to visit an orthopedic surgeon [12]. While ligament injuries tend to be more common, meniscal injuries still account for a very large portion of doctor visits. Meniscal injuries, such as tears, are caused by a number of factors including age-related cartilage degradation, which causes the meniscus to wear thin, and injuries caused by knee movement in an unnatural direction [12]. Sports related meniscal injuries usually result from a compressive force being placed on the joint coupled with rotational movement which usually happens during cutting, pivoting, decelerating, or tackling [12].

Treatment Options

Under normal, healthy conditions, diarthrodial joints function in a nearly frictionless and wear resistant manner. Failure of the menisci, as with engineering bearings, means an increase in wear, friction, and ultimately pain. In biomedical terms, injury to diarthrodial joints leads to degenerative changes which in turn cause the development of osteoarthritis (OA). The synovial fluid, cartilage, and supporting bones are the essential materials forming the bearing system for the body [2]. The performance of these bearings depends on the mechanical behaviors of the materials comprising the joint [13, 14].

Initial treatment of a meniscal injury usually follows the R.I.C.E. formula: rest, ice, compression, and elevation, coupled with anti-inflammatory medication [12]. This can be effective for shallow injuries that occur in the red, outer third of the meniscus which is vascularized and thus has a good chance of healing, especially with surgery, due to the abundant blood supply. However, since many injuries occur within the white, inner two-thirds of the meniscus, which is avascular and receives nutrients via diffusion through the synovial fluid, a need for better treatment options is clear. For these injuries deeper within the joint, such as bucket handle tears (Figure 2), there are very few treatment options. The choice of treatment depends on numerous factors, such as the patient's age, health, life style, willingness to undergo invasive surgery and lengthy rehabilitation, and the type of injury in the meniscus. Partial meniscectomy, attempted surgical repair, and meniscal allograft are currently the three primary choices [11, 16, 17]. There is also experimental work focusing on meniscal prosthetics made from various artificial materials and biomaterials which could be a viable fourth option within the foreseeable future [8, 18, 19]. For instance, work done by J.H. de Groot et. al. and T.G. Tienen et. al. has shown that a porous polyurethane has potential as an artificial meniscal prosthetic [20, 21].

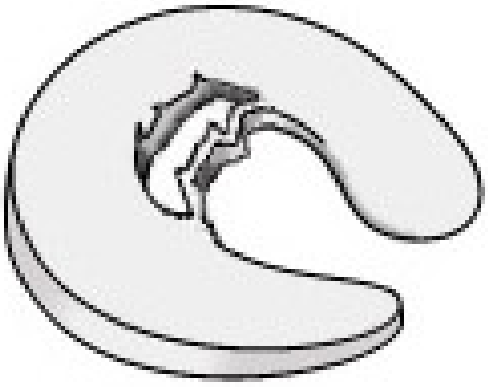

Figure 2: Bucket handle tear of the meniscus from AAOS[15]

A first step in understanding OA in order to treat the disease is to characterize the structure-material property-function relationships existing for fibro-cartilage [14]. No procedure currently exists for replacement of a removed or severely injured meniscus even though eventual use of meniscal allografts may represent a potential method of replacing damaged tissue or at least minimizing the degenerative changes attendant to meniscectomy. However, consistently obtaining fresh graft material is complicated due to finding viable human donors who have undamaged tissue, and while the use of human tissue is an admirable goal, finding appropriately sized graft tissue can be extremely difficult . These issues necessitate the development of suitable preservation and storage methods for the meniscus [11]. Allograft options include fresh, deep-frozen, cryopreserved, and freeze dried (lyophilized) grafts [19]. However, the clinical success of meniscal allografts will be partially dependent on the effects of the preservation and storage methods on the biological and biomechanical integrity of the tissue [11]. Also, to create potential meniscal prosthetics, a full understanding of the material properties is necessary to make the prosthetics effective.

Meniscus Structure & Function

The material properties of the meniscus are specifically dependent on the composition and organization of the tissue [11]. The structure of meniscus is incredibly complex in order to offer the necessary set of properties to allow for smooth and easy function of the knee joint. Fibro-cartilage is a visco-elastic, multiphasic, anisotropic and non-homogenous material [2, 4, 22]. The matrix is formed primarily of fibrous elements embedded in a gel-like ground substance which causes the menisci to act as a fiber-reinforced, porous, permeable, composite solid filled with water [23, 24]. Three primary

elements compose the meniscus: 1) the solid matrix of Type I collagen and proteoglycan macromolecules (~16-27 percent of the total wet weight), 2) a large amount of fluid, primarily water (~60-70 percent of the total wet weight), and 3) various electrolytes with positive and negative charges (Na+, Ca++, Cl-, etc.; ~1 percent of the total wet weight) [2, 25, 26].

Collagen is the basic structural fiber in mammals with Type I being the most abundant in the human body [2, 16, 27]. The collagen fibers' primary purpose is to resist tensile forces while the hydrophilic proteoglycan molecules assist in resisting compressive loading [2, 16]. Acting together, the three primary components of the composite allow for the meniscus to be extremely versatile in resisting the forces and stresses placed on the knees during normal activity [28].

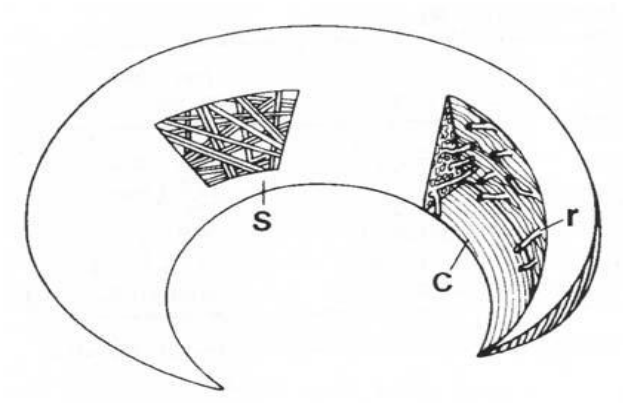

Figure 3: Circumferential (c), Radial (r), and Surface (s) Collagen Fiber Orientation from Mow [2]

The overall structural shape is semi-lunar and the outer, femoral surface of the meniscus is composed of collagen fibrils in a random, mesh-like, woven matrix (Figure 3) [2]. Approximately 100 μm below the surface, the peripheral two-thirds of the structure are composed of collagen fiber bundles that are arranged circumferentially around the outside of the semi-lunar shape with smaller radial

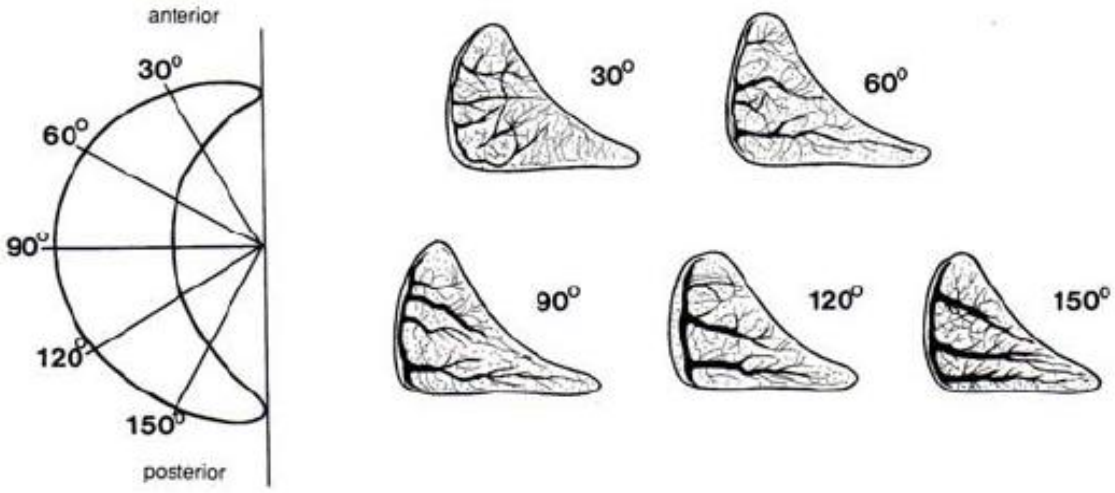

Figure 4: Architecture of radial tie fibers in the meniscus vary by region [2]

fibers tying the large circumferential fiber bundles together and providing reinforcement to the overall structure of the meniscus (Figure 4). The circumferential fibers are long and continuous around the outside of the structure and connect to the attachment points on the tibial plateau. This arrangement allows for the compressive forces that are placed on the meniscus to be transferred not just vertically down the leg, but radially around the half-moon so that the meniscus holds the forces in tension where the collagen fibers are strongest. Since the major joint reaction force is broken up into a radial (angular) component and a tibial (vertical) component (Figure 5), large hoop stresses result from the radial force caused by the concave shape of the structure.

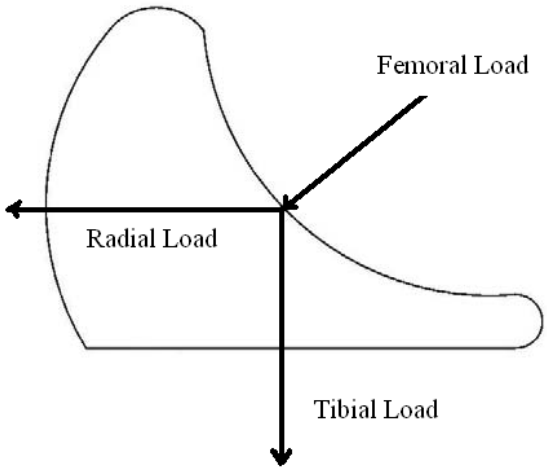

Figure 5: Forces on the Meniscus [46]

The overall function and failure of the meniscus is dominated by the large, radial hoop stresses, but the collagen fibers are strongest in this direction and able to resist the stresses that are placed upon it [16]. The inner third of the meniscus experiences far less hoop stress than the outer regions; therefore, the collagen fibers are arranged in random order and hold less of a load than the circumferentially-arranged collagen fibers. However, the randomly arranged fibers in the inner third of the meniscus provide a clean contact point for the vertical, tibial force to travel along the leg and be supported by the bone and foot structures.

The stiffness of fibro-cartilage is a major factor in determining how much stress the meniscus can hold and is likely to affect the efficiency of the bearing surface [29]. Mechanical testing to determine the strength and stiffness has been at the focus of meniscal studies [11, 16, 27, 30-36]. Previously, the circumferential tensile properties of meniscus were studied by the author; so the current study will focus primarily on the viscoelastic properties.

The mechanical properties of collagen fibers in tension are mostly known through the study of tendon and ligament [2]. The fibers are arranged in a parallel structure that has a high modulus of elasticity and a high tensile strength. The results of tensile testing on tendon to failure indicated that failure occurred due to random flaws in the material [37].

Collagen is the name given to a class of proteins which, through similarities in amino acid sequence, have similar structure and physical properties [37]. The amino acids glycine, proline, and hydroxyproline play a major role in determining the three-dimensional conformation of collagen with approximately one-third of the total amino acids being glycine and another 20% being proline and hydroxyproline[37]. The overall structure of collagen is a triple helical arrangement of three polypeptide α chains composed of glycine, proline, and either hydroxyproline or another amino acid. Each chain has a left-handed helical shape around its own central axis. Together, the three chains form a right-handed helix structure around a central axis where every third amino-acid in the polypeptide chains is glycine. The glycine side chains are only single hydrogen atoms that face towards the center of the triple helix, which allows the three helical chains to be packed closely together into the triple helix conformation of collagen (Figure 6) [37]. This tight, highly organized, rope-like structure offers a high modulus and ultimate tensile strength. Collagen is then arranged hierarchically into four levels of structure for the meniscus: tropocollagen, which is formed by a triple helix of three collagen molecules, fibrils, fascicles, and fibrocartilage.

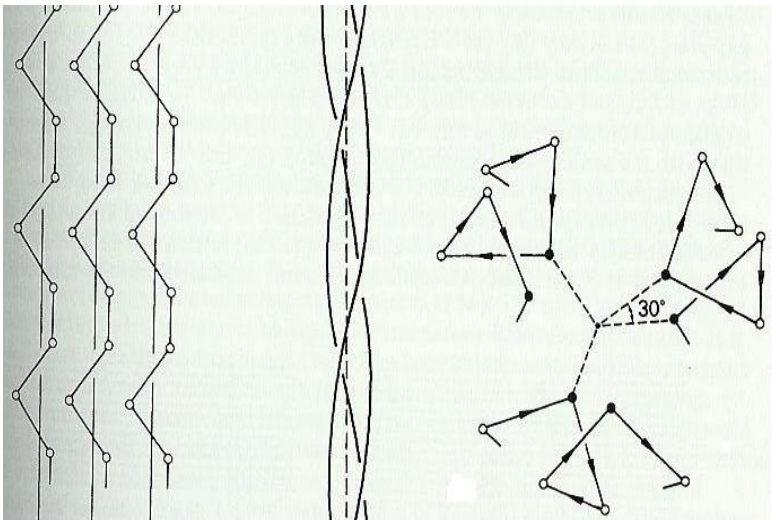

Figure 6: Structure of collagen[37]

The hierarchical structure of collagen causes it to display a characteristic tensile stress-strain curve (Figure 7). The collagen fibers are slightly 'crimped' when there is not a load placed on them. The initial uncrimping of the collagen fibers forms a toe-region on theess-strain curve where the fibers are aligning. This is followed by a linear region where the fibers themselves are loaded. Yielding usually occurs around 4% strain with failure following at approximately 8-10% strain.

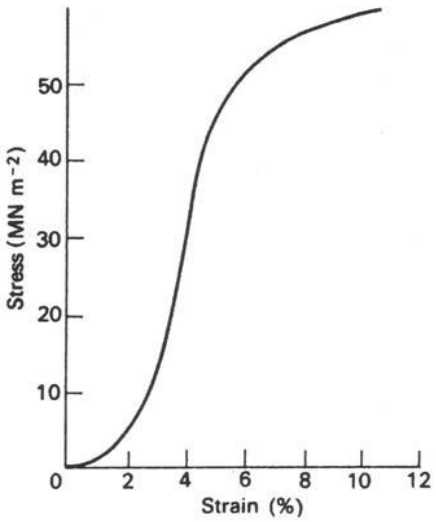

Figure 7: Tendon Stress Strain Curve Wainwright [29]

The thickness, density, and alignment of collagen fibrils vary from the articular surface, where fibrils are oriented parallel to each other and circumferentially around the meniscus, to the deep layer, where fibrils are randomly arranged as seen in Figure 3. The relationship between the properties of full-thickness fibro-cartilage and those of partial-thickness sections is unclear [38]. In other words, research is still needed to determine whether the properties of a whole meniscus are similar to that of a small slice. The compressive stiffness of cartilage is proportional to the tissue's total proteoglycan content, but varies inversely with its water content [24, 29, 39-42]. Recent theoretical contact studies have demonstrated that a significant portion (e.g. 80-95%) of contact stresses are actually supported by interstitial fluid pressurization under the majority of physiological loading conditions, hence shielding the solid matrix of cartilage from

excessive stresses and strains [43]. The ability of meniscus to withstand such high compressive loading without being crushed is due to the multiphasic nature of the tissue, and the unique combination of the related material properties of the tissue [26, 44, 45].

Towe Thesis Review

During a literature review, Towe noticed that many mechanical testing studies on meniscus utilized frozen samples, either for transport or to prepare specimens for slicing, while claiming to use only fresh samples [46]. For example, Goertzen et. al. performed tensile tests on five bovine menisci within twenty-four hours of harvest. The specimens were frozen to a microtome stage in order to slice uniform slabs for testing [47]. Lechner et. al. followed a similar procedure with thirty human, medial menisci which were tensile tested within 72 hours of slaughter. The specimens were also frozen to a microtome stage for slicing [32]. Skaggs et. al performed tensile tests but stored their bovine menisci specimens at -80° C for as long as four weeks [35]. Proctor et. al. justified performing full property testing on bovine menisci that had been stored at -20° C for up to four weeks by stating that no macroscopic changes were seen before testing [33].

The meniscus is nearly 80 percent water though, and there has been no comprehensive study on the effects freezing has on the structure or the material properties of the tissue. The purpose of the Towe study was to quantitatively measure any changes in the circumferential tensile properties of the testing menisci due to the freezing and thawing in the specimen preparation [46]. However, the study utilized a large number of slices taken from a small number of menisci which was based upon from experimental design taken from the literature review of previous research for meniscus testing [46].

Bovine meniscus is commonly the tissue of choice in studies of mechanical properties of meniscus because it is inexpensive and readily available from local slaughterhouses [16, 27, 32, 47]. However, reducing the effect of variables naturally present in the specimens can be difficult because of the source. Data regarding the age, health, diet, gender, and weight of the animals are unavailable; therefore there is a large degree of variability among menisci with respect to the mechanical properties that needs to be taken into account when designing an experiment, testing the specimens, and analyzing the resulting data. Also, the variation in the composition and structure of cartilage as depth from the proximal surface increases appears to affect the mechanical properties for each sample [48]. For instance, the compressive modulus of full thickness cartilage increases with increasing density of the fixed electrolyte charges and the thickness, density, and alignment of collagen fibrils varies with depth [48]. Therefore, the mechanical properties vary greatly from one meniscus to the next.

In order to reduce this variability, Towe chose only large, medial menisci that were pearly white in color [46]. Also, the medial meniscus is damaged or diseased much more frequently than the lateral meniscus [3]. Therefore, it is more likely that the medial meniscus will show property changes or structural damages than the lateral. Towe used 12 slices per treatment group with no control over which slices came from which meniscus [46]. The study did not find statistical significance among treatments as a result of the variability among menisci. However, the knowledge found was used to improve the experimental methods on a tissue welding study performed with Dr. Robert Kane [27]. Kane had previously seen no statistical differences between various bonding compounds. By modifying the experimental design to a repeated measures design where

every treatment and control was tested on slices from every meniscus, statistically significant differences in bonding strength of various compounds was observed [27]. Repeated measures data analysis is capable of accounting for variations from subject to subject which makes it ideal for mechanical property data analysis on specimens as varied as bovine meniscus.

Morgan Thesis Review

The research design by Towe was modified for a previous study by the author by increasing the sample size to 12 menisci per treatment group with minimum 5 slices per meniscus [49]. The mechanical properties measured and calculated for each slice from a single meniscus were then averaged to form one set of values for that meniscus. Statistical analysis was performed with ANOVA and Tukey-Kramer multiple comparisons.

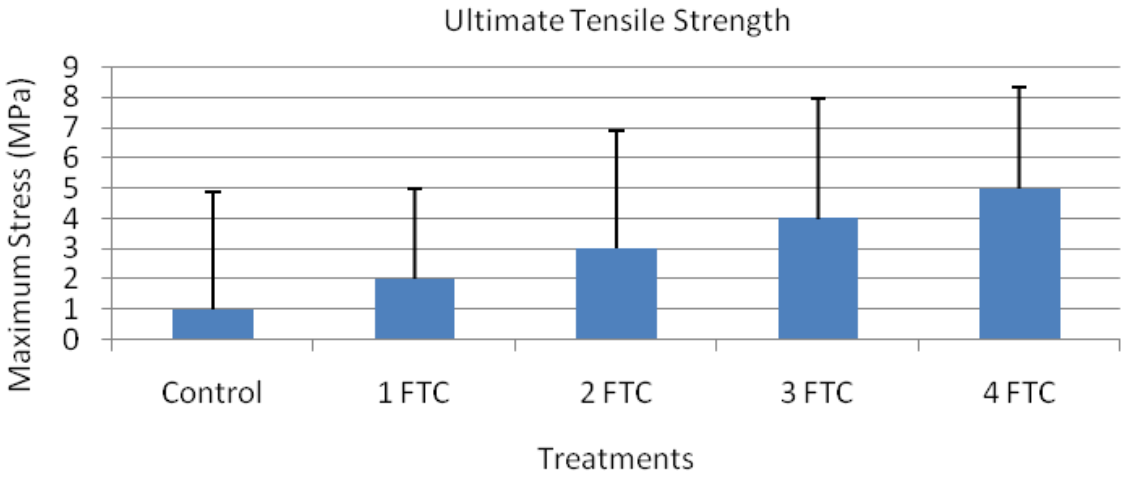

Figure 8: Max Stress Variations for Treatment Groups [49]

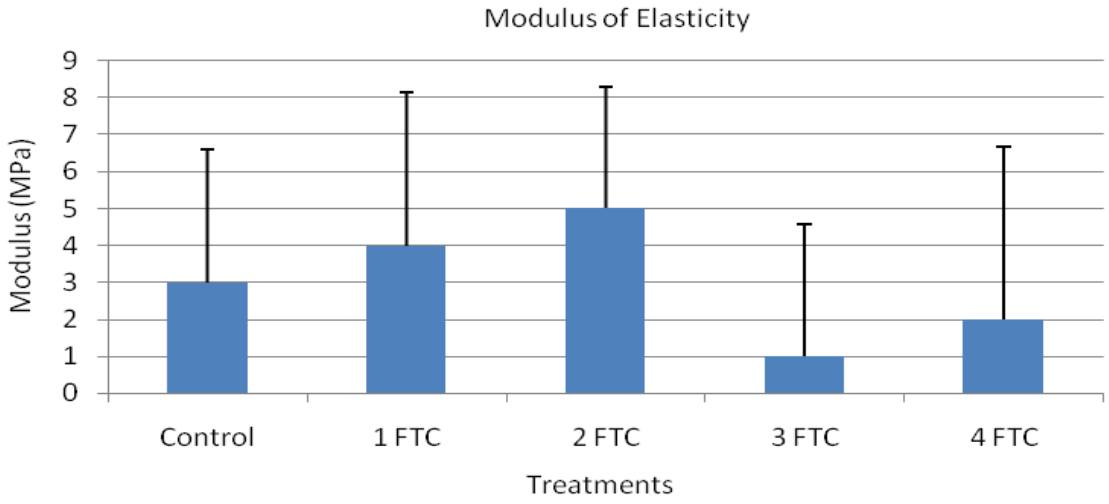

Figure 9: Modulus of Elasticity Variations for Treatment Groups [49]

Figure 8 contains the mean and standard deviation of the maximum tensile strength of the treatment groups. Similarly, Figure 9 shows the mean and standard deviation of the modulus of elasticity for the treatment groups. The study concluded that there appeared to be no effects on the circumferential tensile properties of meniscus due to freezing and thawing.

However, during specimen preparation, it was observed that the texture and compressibility of the meniscus seemed to have been altered as the number of freeze-thaw cycles increased. The texture of the control specimens was fleshy and soft, and the specimen slicing was difficult due to the rubbery nature of the menisci. Specimens that had undergone as little as two FTC's showed signs of hardening, and the ability to slice the menisci during specimen preparation was noticeably easier compared to the control group. The four FTC specimens had the consistency of a solid rubber ball and the slicing was far easier than what was required for the control specimens.

The current study was designed to observe the effects of freezing on the structure and viscoelastic properties in order to perform a comprehensive property study on the effects of repeated freezing and thawing on the mechanical properties of meniscus. In order to perform this study, a scanning electron microscope (SEM) was used to observe any structural changes, and confined compression indentation tests were used to observe the compressive visco-elastic properties.

When fibro-cartilage is loaded in uniaxial confined compression, water is forced from the tissue and permeability decreases with compressive strain [22, 38]. Since the meniscus is a visco-elastic material comprised mostly of water, freezing may cause changes in the permeability and the reaction of the meniscus to compressive strain. Therefore, in order to ensure accurate research the effects of freezing on the material properties of meniscus must be understood.

Hypotheses

The current study builds upon previous studies by Towe and Morgan in order to assess whether repeated freezing and thawing cycles affect the visco-elastic mechanical properties of the menisci [46, 49]. The hypotheses are the same as those from Towe's work. The null hypothesis was that multiple freezing thawing cycles would not significantly affect the mechanical properties of the specimens. If the null hypothesis is rejected, then the material properties of the menisci will have significantly changed.

CHAPTER TWO

Materials and Methods

Specimen Harvest and Preparation

The medial and lateral menisci have different shapes (Figure 10) in order to better conform to the femoral condyles and tibial plateau that they are attached to. This difference in shape was eliminated as a source of variability during the tensile testing portion of this study by testing only the medial meniscus. Therefore, to remain consistent with the prior studies, during the compression testing and the scanning electron microscope analysis only the medial menisci were chosen for testing again [27, 32, 33, 46, 47, 49].

Fresh bovine knees were obtained from a local slaughterhouse on the day of slaughter. Each knee was disarticulated by first severing the anterior cruciate ligament (ACL), posterior cruciate ligament (PCL), tibular collateral ligament (TCL), the fibular collateral ligament (FCL) and the patellar tendon to alloy for separation of the knee joint

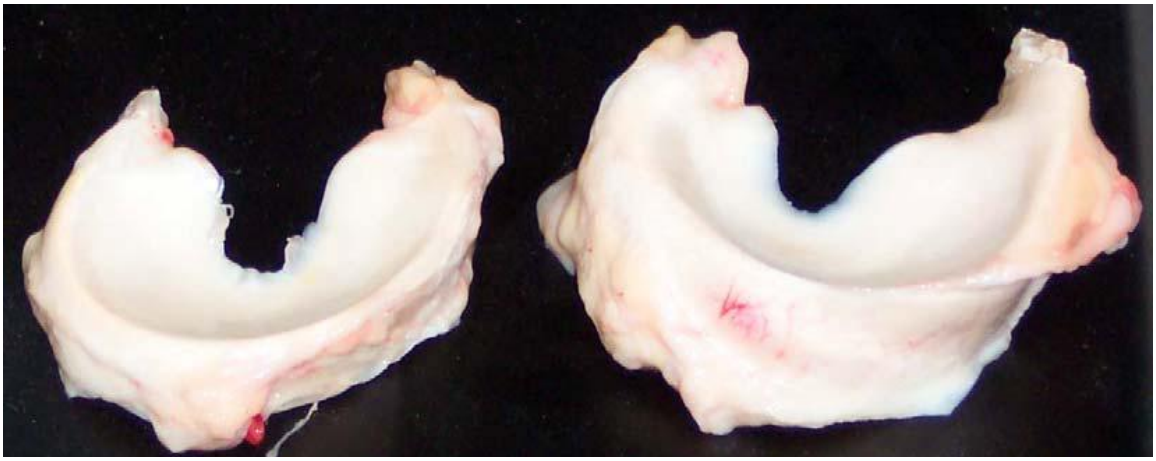

Figure 10: The medial (left) and the lateral (right) menisci from the same knee

and removal of the menisci. The femora were separated from the ligaments and menisci and completely separated from the tibia in order to facilitate easier meniscus removal. Finally, the medial meniscus was identified by its characteristic half-moon shape and by locating the vestigial fibula in order to determine if the knee was a right or left knee. The medial meniscus was carefully removed to prevent any inadvertent damage to the specimen, such as scraping or accidental cuts, that might be mistaken for structural damage due to freezing during the SEM analysis. The specimen was cleaned of any remaining ligament and soft tissue attachments. Only menisci that were large and pearly white in color were chosen for analysis. Upon visual inspection any menisci that appeared damaged (i.e. yellowed, scarred, torn) were rejected.

The menisci were then inspected for quality and the specimens that passed visual inspection were placed on gauze sponges soaked with a 0.9% saline solution (NaCl) to preserve physiological hydration level.

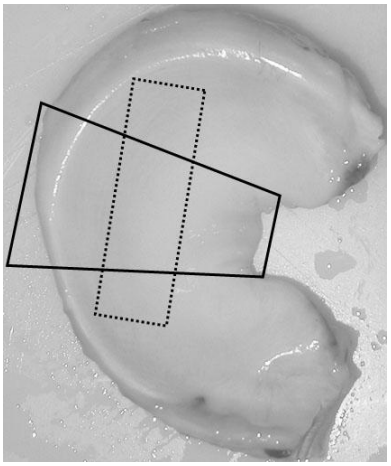

Figure 11: Meniscus Wedge Cut [27]

The horns of the meniscus were removed, and the meniscus was cleaned again of any soft tissue or ligament remnants. A wedge-shaped section was cut from the center of the meniscus where the collagen fibers are mostly parallel (Figure 11) [11, 16, 50]. A small vertical slice was cut with a scalpel (Figure 12) (from proximal surface to distal surface) along the edge of the wedge-shaped section and removed from the menisci (Figure 12) in each treatment group as a control (i.e. fresh) specimen to view under the SEM. The remainder of the wedge-shaped specimens were

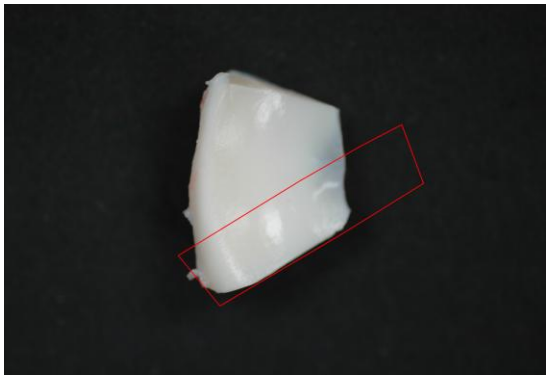

Figure 12: Wedge with SEM Slice

soaked in saline and covered with a second saline soaked gauze wrap before being placed into a plastic freezer bag for storage in a commercial freezer at -20 degrees Celsius (Arctic Air Commercial Freezer, WCI/Frigidaire Co., Minneapolis, MN). The mechanical testing specimens were randomly assigned to the control group or one of the four treatment groups and cyclically frozen and thawed for the appropriate number of FTCs. In order to gradually thaw the treated specimens, they were placed in a compact refrigerator (Kenmore, Sears Roebuck and Co., Chicago IL.) at 1.4 °C for two days. On the day of analysis, the menisci were checked to verify complete thawing by ensuring that no ice crystals were present. The specimens were kept wet throughout sample preparation to ensure hydration. A second small vertical slice (from proximal surface to distal surface) along the edge of the wedge-shaped section was cut with a scalpel from each meniscus to undergo SEM analysis after treatment. This ensures that the images for each treatment group were compared to the control images from the same specimens.

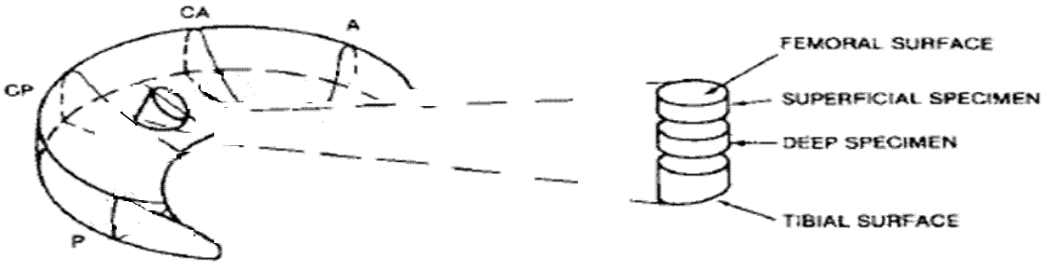

Figure 13: Meniscus layers and Plug region [33]

Comparing the control images to the matching treated images allowed for more accurate observations of any potential changes to the structure due to the FTCs.

Figure 14: Data Analysis Photo

Once the SEM slices were removed, the remaining wedge was fixed in a custom vice attached to a tri-axial base on a drill press and a one-quarter inch diameter sample plug was drilled out (Figure 13). The vice ensured that each meniscus was tightly secured to prevent movement while the plug was cut. The tri-axial base was used to carefully position each meniscus to ensure that the plug was cored out perpendicular to the proximal loading surface of each meniscus. Each meniscus was drilled completely through to obtain a full-thickness specimen and each plug was kept well hydrated with saline solution. Once the plugs were removed from each meniscus they were trimmed from the tibial side to a thickness of one-eighth of an inch. Digital photos with a ruler were taken of the thickness and diameter of each compression sample for analysis (Figure 14).

Confined Compression Testing

Confined compression test was run according to the method developed by Armstrong and Mow (Figure 15) [41]. The samples were placed in a custom-built apparatus (Figure 16),

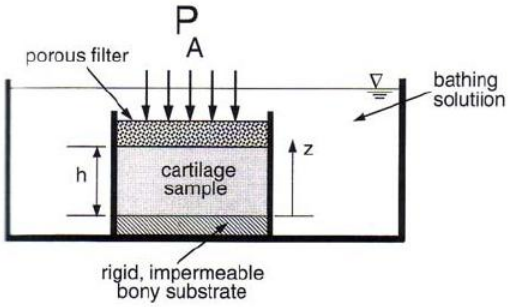

Figure 15: Confined Compression Test [2]

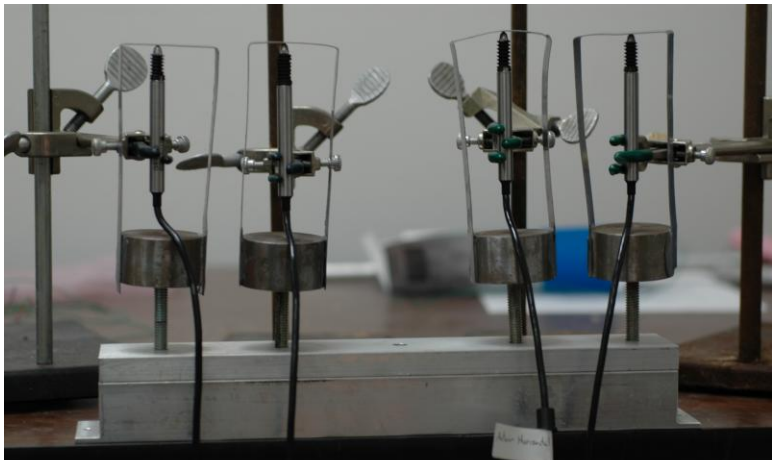

Figure 16: Confined Compression Test Apparatus

with precisely machined compression chambers, for testing. Each chamber had a diameter of one half of an inch, with a tolerance of 0.005 inches, in order to tightly confine each sample to ensure that the test is performed in confined compression. Once the samples were placed into the compression chambers, the tank was filled with saline solution to completely hydrate each sample. A quarter inch, rigid, stainless-steel filter with 50% porosity, 60 μm pore diameter, and high permeability (Texas Valve and Fitting, Dallas, TX) served as the indenter to compress the specimens through the use of steel indenters and custom built weights (Figure 17). Confined compression ensures that all loading and fluid exudation occurred in only one direction [41]. A compression force of 323 grams-force (gf) was rapidly applied and held for 20,000 seconds through the use of the custom built weights and indenters. The strain was recorded using a linear variable displacement transducer (LVDT) connected to a StrainSmart 5000 system (Vishay Products, Shelton, CT). The Strain Smart hardware was set up to collect ten strain measurements every second for 20,000 seconds or approximately five hours and thirty minutes.

Figure 17: Porous Indenter and Custom Weight

Data Analysis

Digital image analysis using Scion Image (Scion Corporation, Frederick, MD) was used to measure the specimen height and diameter from the digital photographs taken before mechanical testing. A ruler placed in the pictures was used to calibrate the software so that accurate measurements could be taken. For height, three measurements were made, one for each side of the meniscus and one down the center, so that an average could be calculated. The same method was applied to measuring the diameter with three measurements being taken from three different directions so that an average diameter could be calculated.

The Strain Smart data and the image analysis data were both imported into Microsoft Excel™ for further calculations. The diameter was used to calculate the cross sectional area (mm^2) in order to calculate the stress on each specimen. The stress and height were used in curve fitting the data to the governing differential equation (Figure 18). The unknowns, aggregate modulus (H_A) and permeability (K_0) were found through plotting the results of the creep test and performing a curve fit. An optimization curve was also plotted (Figure 19) and a correlation coefficient was calculated to compare the quality of fit of the optimized curve to the experimental data.

$$u(x_3,t) = -\frac{P_A}{H_A}\left[x_3 - \frac{2h}{\pi^2}\sum_{n=0}^{\infty}\frac{-1^n}{\left(n+\frac{1}{2}\right)^2}\sin\left[\left(n+\frac{1}{2}\right)\frac{\pi x_3}{h}\right]e^{\left[\frac{-H_A k_0}{h^2}\right]\left(n+\frac{1}{2}\right)^2\pi^2 t}\right]$$

Figure 18: Soltz Ateshian Solution [51]

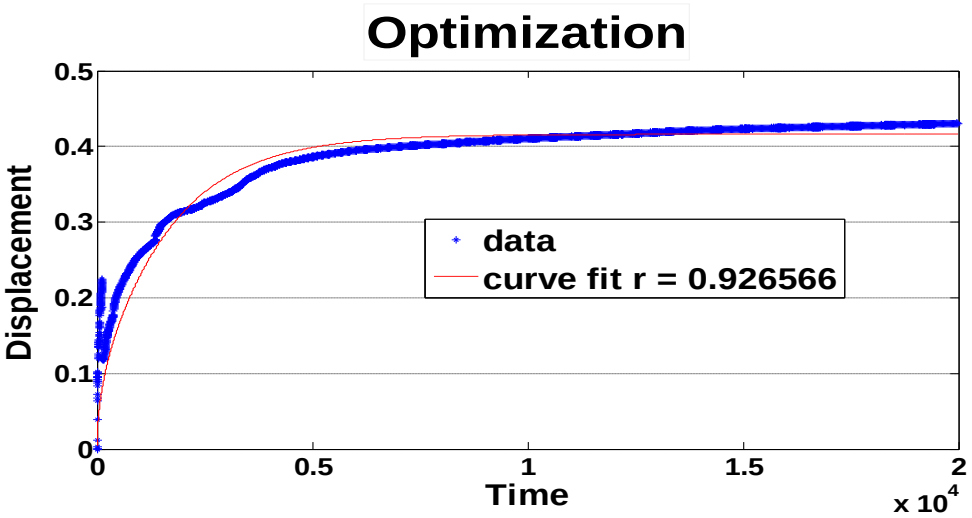

Figure 19: Optimization Plot

An Analysis of Variance (ANOVA) test was run with Tukey-Kramer multiple comparisons and with Bonferroni's Method at an $\alpha = 0.05$ in JMP (SAS Institute Inc., Cary, NC) to check for significant differences in H_A & K_0 among treatments.

CHAPTER THREE

Materials and Methods

Scanning Electron Microscopy

On the day of SEM analysis, the menisci slices were checked to verify thawing had occurred, and all slices were kept wet with saline throughout the procedure to ensure hydration. Each prepared sample was mounted on a quarter inch diameter aluminum stub in order to be viewed under the SEM. Therefore, each slice was trimmed so that the bottom of each meniscus slice could be adhered to the top of the stub and the femoral loading surface of each meniscus slice could be viewed under the microscope. The sides for each sample were not viewed to avoid mistaking scalpel damage for structural damage caused by treatment.

After trimming the slices to fit onto a stub, the trimmed samples were bathed in a series of chemical solutions to fix the tissue structure and prevent degradation of the specimen due to autolytic processes and exposure to the electron beam [52]. Each specimen was fixed for at least three hours in a solution of 2.5% glutaraldehyde and 2.5% formaldehyde in 0.1 M phosphate buffer which rapidly crosslinks the collagen. The 0.1 M phosphate buffer was then used for three separate washes of ten minutes each. Once fixation and buffering was completed, a series of ethanol washes consisting of 20%, 50%, 75%, and 95% solution for ten minutes per solution and three washes of 100% ethanol at ten minutes a piece were used to dehydrate the specimens [52].

Following dehydration, critical point drying was used to dry the specimens and prevent the structure of the menisci from collapsing, flattening, or shrinking from the passage of the receding air/water interface through the specimen [52]. The specimens were placed in a small wire-mesh basket, inserted into the critical point dryer, and bathed in 100% ethanol. Once sealed in the drying chamber, liquid carbon dioxide (CO_2) was flushed in, removing the ethanol, and starting the drying process. Warm water at 50 °C was used to warm the chamber from the outside and cause a pressure increase. The pressure was increased to greater than 1,060 psi, which is the critical point for CO_2, causing the CO_2 to sublimate. The pressure was then relieved by opening a release valve and allowing the CO_2 gas to escape. The specimens were carefully removed with forceps to ensure that they were not rehydrated or compromised in any way from moisture and oils in the hands.

Each specimen was mounted onto a stub using double-sided adhesive tape. Colloidal silver conducting paint was used to electrically connect the specimen to the stub and establish a ground for the SEM's electron beam. A sputter coater was used to coat the specimens with a thin layer of gold to prevent an excessive build-up of electrical charge while being viewed under the SEM and to coat the specimens with a conductive layer. The specimens were placed into the vacuum chamber of the scanning electron microscope (JSM-5410, JEOL Ltd., Akishima, Tokyo) at 10 kV and the structure was observed at a spot size of 8, a working distance of 25 mm, and a magnification of 1000x to look for changes or damage caused by the repeated FTC's. The control group images for each treatment group were visually inspected and compared to the FTC images with

special attention paid to comparing the 4 FTC treatment images and the 4 FTC control images.

CHAPTER FOUR

Results

Confined Compression Results

Data analysis (Table 1) revealed that the standard deviation for aggregate modulus and permeability was large for each treatment group of five menisci. The correlation coefficient data clearly shows that the governing equation developed by Soltz and Ateshian was a good fit. The average aggregate modulus for each treatment group and standard deviation shows an increase in aggregate modulus during the first two FTC's, followed by a sharp decrease on the third FTC, and an incline after the fourth

Table 1: Averages and Standard Deviations

	Aggregate Modulus	Permeability (x10-14)	R2
Control	0.329 ± 0.141	2.121 ± 2.17	0.79 ± 0.177
1 FTC	0.579 ± 0.308	9.73 ± 1.226	0.8 ± 0.248
2 FTC	0.501 ± 0.293	8.491 ± 8.401	0.905 ± 0.076
3 FTC	0.278 ± 0.122	1.168 ± 6.871	0.925 ± 0.099
4 FTC	0.404 ± 0.126	4.28 ± 4.435	0.924 ± 0.053

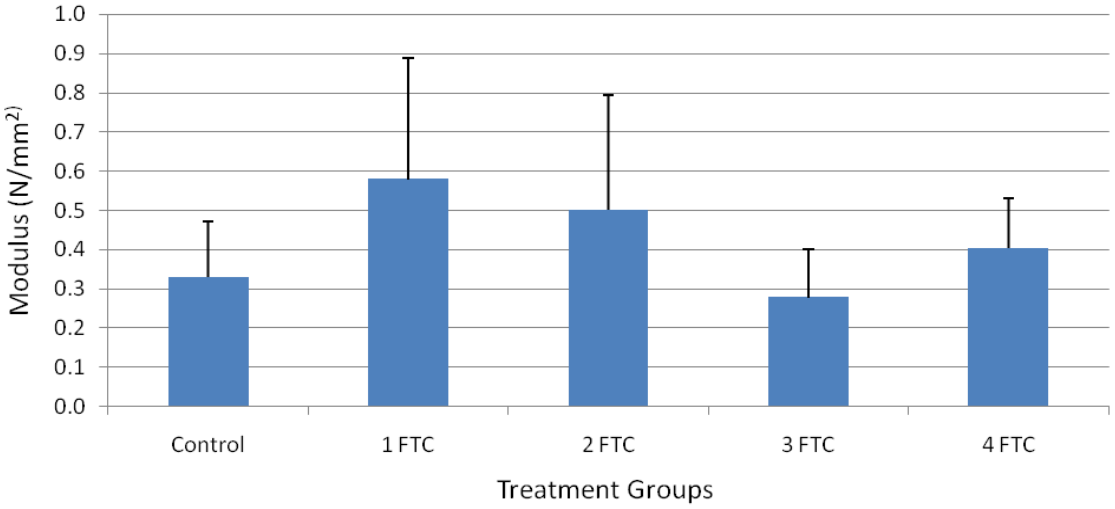

Figure 20: Aggregate Modulus

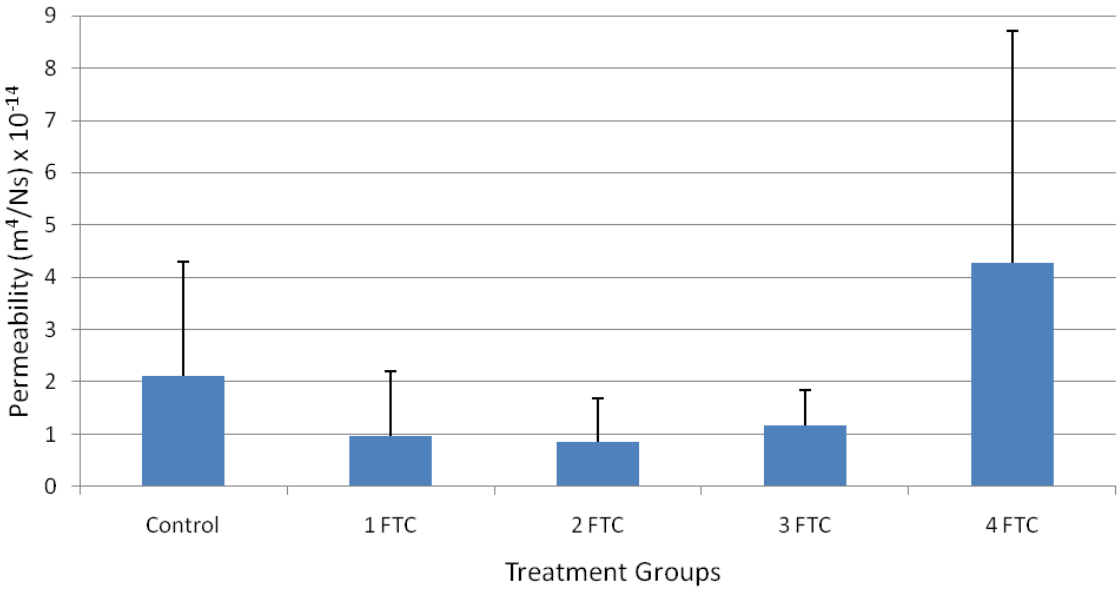

Figure 21: Permeability

FTC (Figure 20). Each treatment group has a higher aggregate modulus than the control except for the 3 FTC treatment group. The average permeability data for each treatment group and standard deviation (Figure 21) revealed the control group's average permeability is greater than the 1, 2, and 3 FTC treatment groups. The 4 FTC group shows a large jump in permeability when compared to the other treatment groups. Even with the large standard deviation, this is a noticeable change.

An ANOVA test with significance set at α=0.05 was performed to compare the treatment groups to check for significant property variations in aggregate modulus and permeability values. The p-value for the ANOVA of the aggregate modulus was 0.2027 which indicates that no statistically significant differences were found between the treatment groups for aggregate modulus. The p-value for the permeability ANOVA was 0.1505 which also indicates that no statistically significant differences were found between the permeability values. Since the ANOVA testing did not find significant

differences at $\alpha=0.05$, further multiple comparisons testing was not run. Even though the 4 FTC permeability average is large, the 4 FTC treatment group is not statistically different from the others.

SEM Results

After 1 FTC treatment, specimens showed (Figure 22) long ridges that appear to be the circumferential collagen fibers. The entire surface is rough and uneven with clear valleys between the fibers. There are also bulges and pock marks on the surface. A matching control specimen (Figure 23) that was not treated with an FTC was harvested from the same group of menisci as the treated specimens. The surface of the control has a smoother appearance and smaller grooves with no valleys present. The bulges and pock marks seen in Figure 22 are also not present.

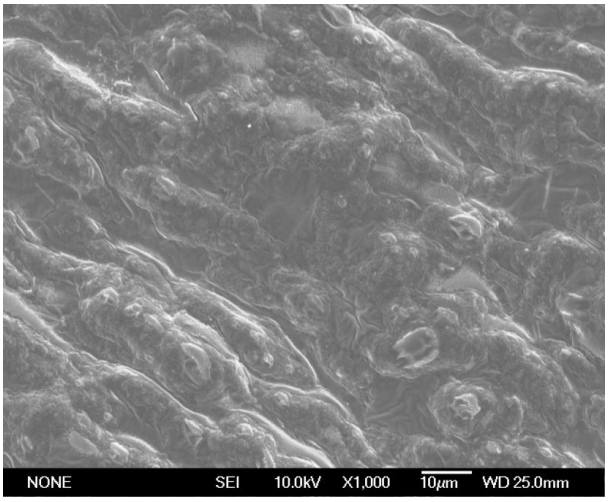

Figure 22: 1st Specimen, 1 FTC Treated

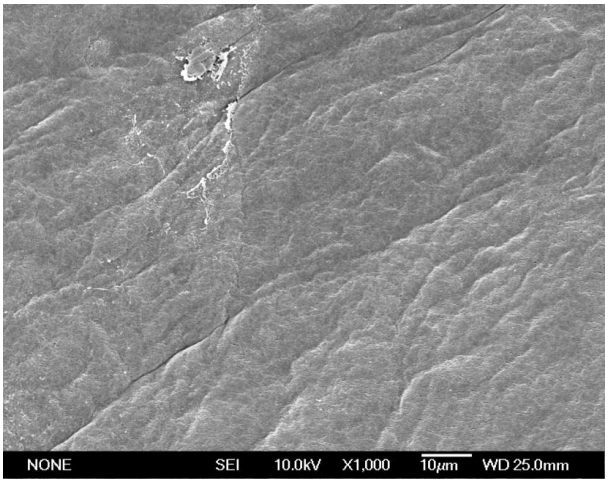

Figure 23: Control Specimen 1 for 1 FTC group

After 2 FTC treatment, specimens still clearly have deep grooves associated with the circumferential collagen fibers (Figure

24). However, there appears to be fiber degradation at the surface. Loose fibers and fiber remains are scattered throughout the entire image of the meniscus. The bulges and pock marks from the 1 FTC image are no longer present and the surface appears smoother than the specimen seen in Figure 22. The matching 2 FTC control image (Figure 25) is similar to the 2 FTC treated image but with a smoother surface and smaller fiber remains. The deeper grooves in the 2 FTC treated specimen are not present in the control specimen.

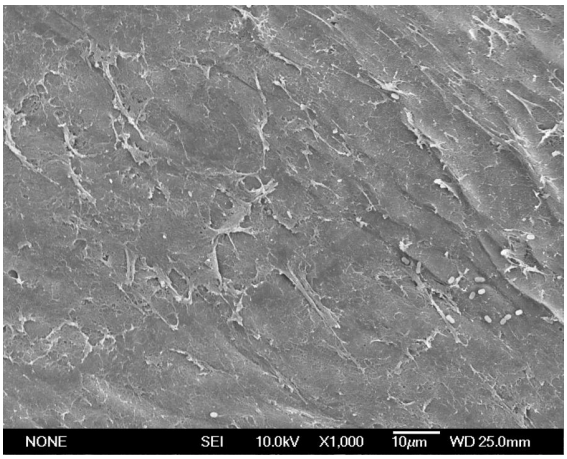

Figure 24: 1st Specimen, 2 FTC Treated

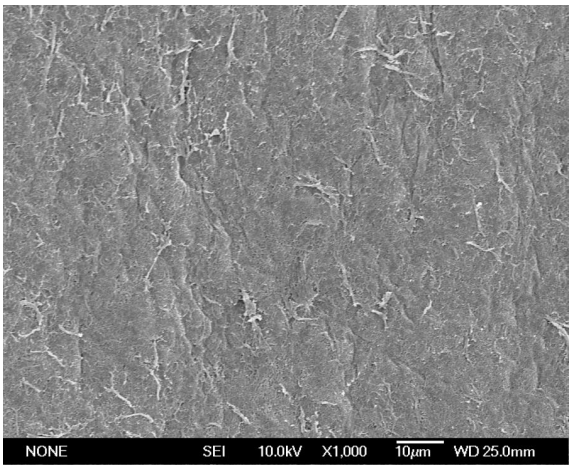

Figure 25: Control Specimen 1 for 2 FTC group

After 3 FTC treatment, the specimen (Figure 26) has even larger and deeper grooves running through its surface and the texture continues to appear rough. Fewer loose fibers are present at the surface as compared to Figure 24. The specimen does not have any bulges or pock marks like the 1 FTC specimen.

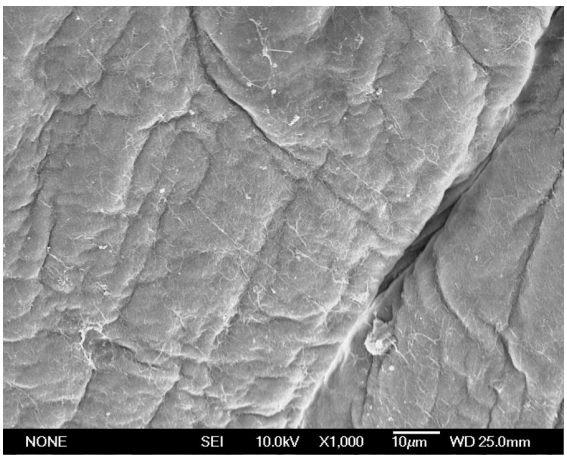

Figure 26: 1st Specimen, 3 FTC Treated

A control specimen for the 3 FTC treatment group (Figure 27) shows similarities compared to the previous images of control specimens. The surface texture still appears smooth but more flat than the previous images, and the specimen has very short grooves. A large quantity of fiber remains appears on the surface similar to Figure 25.

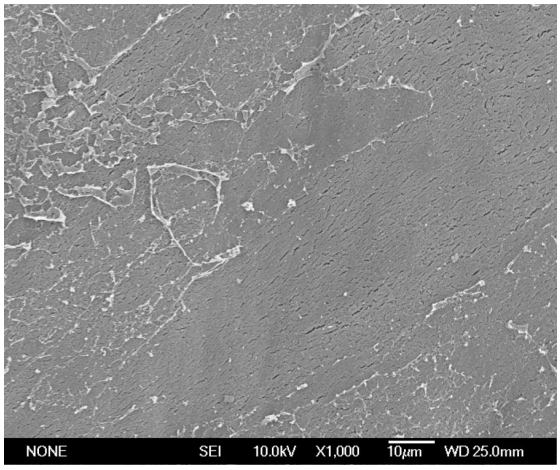

Figure 27: Control Specimen 1 for 3 FTC group

Finally, after the 4 FTC treatment, the specimens still show the long, deep grooves and the surface still appears grainy and rough (Figure 28). A matching control specimen from the 4 FTC group (Figure 29) had a surface that is smoother and more flat than the treated specimens. Also, there are fewer fiber remains at the surface of this control specimen when compared to Figures 25 and 27.

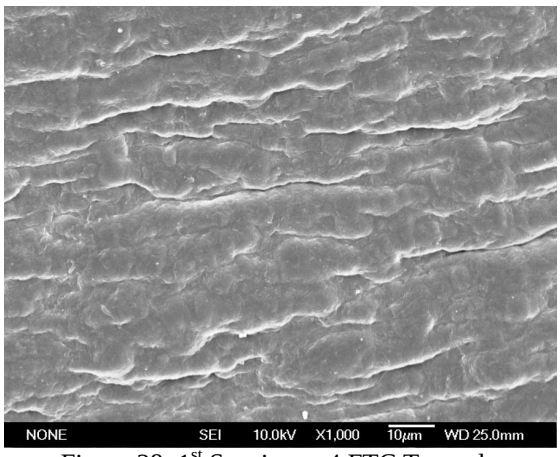

Figure 28: 1st Specimen, 4 FTC Treated

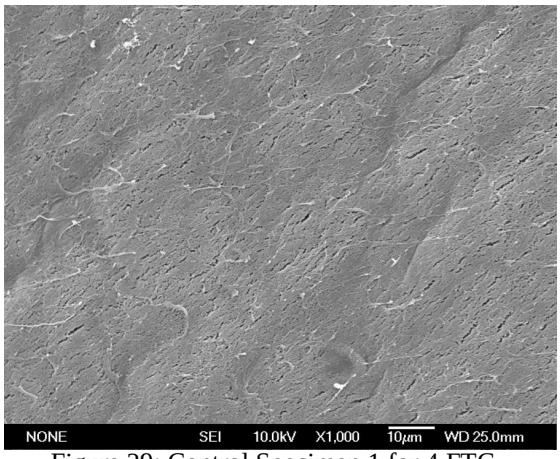

Figure 29: Control Specimen 1 for 4 FTC

Confined Compression Conclusions

The study utilized a small sample size of only five specimens per treatment group. The previous study by Towe indicated that large variability between animals exists for menisci and can affect the results of the study [46]. The small sample size reduces the statistical power of the experiment and any potential changes in the material properties could be masked by the variability present and the low statistical power.

This was a pilot study to observe the effects of repeated freezing and thawing on the viscoelastic properties of bovine meniscus. As with the pilot study of circumferential tensile properties, an additional study with an increase in the number of specimens per treatment group should be undertaken in an effort to reduce the inherent variability found in working with meniscus. The increase in the number of specimens may reveal property changes due to freezing that are masked by the variability and the low statistical power due to small sample size. Also, a stress relaxation study should occur at the same time as the creep study so that both sets of data can be compared to each other and ensure that accurate testing is occurring [2].

A number of improvements should also be made to the creep experiment to increase the repeatability of the data. First, an improved loading mechanism may reduce the noise and provide for better data acquisition. Also, the triaxial base used in drilling cores for the confined compression testing should be modified to ensure that specimen plugs are drilled more exactly perpendicular to the proximal surface of each meniscus. Finally, a slicing device could be developed to more accurately trim each specimen plug so that the heights for each specimen are more uniform.

SEM Conclusions

Due to the meniscus consisting of nearly 80% water, scanning electron microscopy may not be the ideal choice of equipment for viewing changes to the structure. Specimens must undergo a lengthy preparation consisting of numerous chemical washes with fixation agents, buffer solutions, and dehydrants. Also, drying and sputter coating are necessary to prepare the specimens for viewing. Even though the current study's specimens were dehydrated using ethanol, which is less caustic than acetone, the other commonly used dehydrating agent, changes to the structure from the fixatives and other chemical washes as well as the critical point drying can not be accounted for. However, each specimen was prepared exactly the same for viewing so general characteristics and potential changes due to repeated freezing and thawing can be noted.

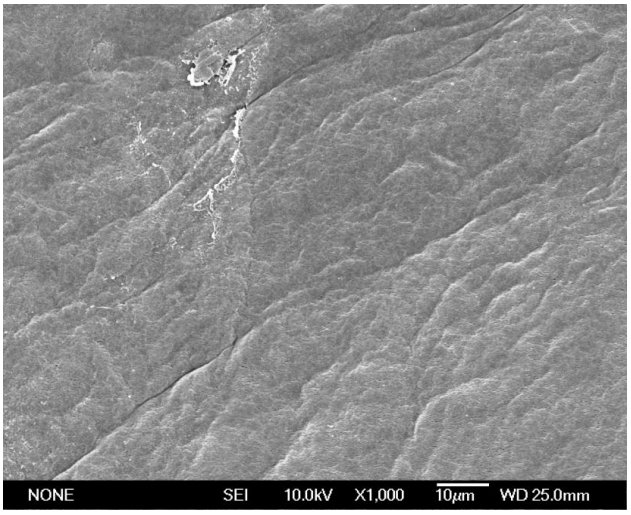

Figure 30: Control Specimen 1 for 1 FTC group

Control images from each treatment group show similar characteristics, which is expected since they were prepared the same and were not treated with FTC's. Each

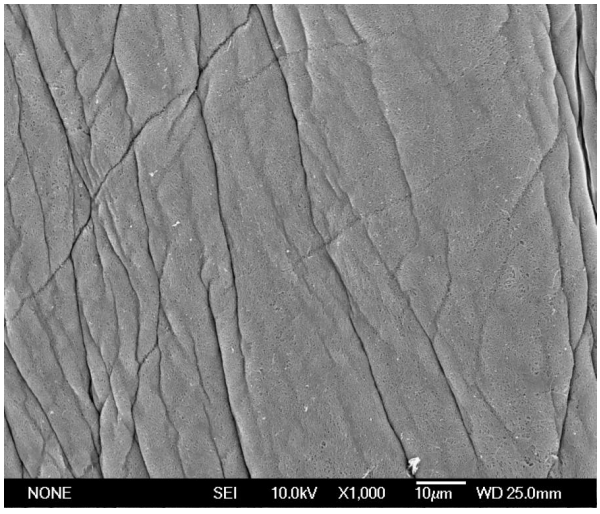

Figure 31: Control Specimen 2 for 3 FTC group

treated SEM specimen had a matching control specimen from the same area that was not exposed to FTC's. A typical control image from the 1 FTC control group (Figure 30) shows a surface with heavy grooves, distinguishing the larger circumferential collagen fibers, along with lighter areas that appear to be the radial tie fibers that connect the circumferential fibers together. There does not appear to be any noticeable damage to the overall structure and surface of the control specimens. However, there is variability from specimen to specimen in the size, depth, and number of the grooves. A control image from the 3 FTC treatment group (Figure 31) has longer, thicker, and deeper grooves when compared to the 1 FTC treatment group (Figure 30). The visual variability between specimens appears to be pre-treatment and based upon the animal that the sample was taken from. Unfortunately, this makes it difficult to also differentiate potential changes due to repeated freezing and thawing from natural variability.

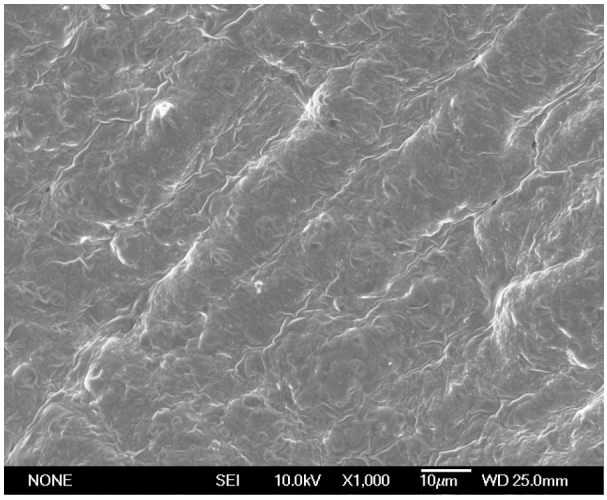

Figure 32: 2nd Specimen, 1 FTC Treated

Comparing the images of the control samples to the treated samples does indicate that the structure of the treated samples is being affected by the treatment. An image from the 1 FTC treatment group (Figure 32) shows large valleys and an extremely textured surface when compared to the control images. These deep valleys can also be seen in the 3 FTC treatment group (Figure 33). A potential cause of this phenomenon could be the repeated freezing and thawing for the treatment groups. The meniscus is mostly water

and the freezing causes the fluid to expand and contract in the gaps between the collagen fibers. The expansion and contraction may cause the spacing between the circumferential collagen fibers to increase and cause the radial tie fibers to stretch and deform. The stretching and deforming of the radial fibers may cause structural damage between the circumferential fibers which could leave the large grooves seen in the images (Figure 34). However, the dehydration and drying for SEM viewing could offer an alternative since biological tissue often shrinks when drying occurs.

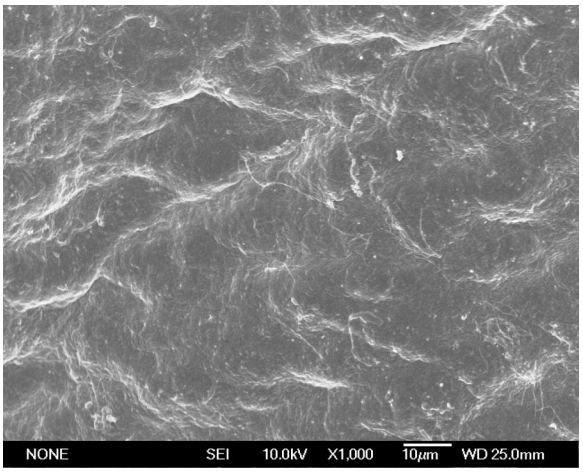

Figure 33: 3rd Specimen, 3 FTC Treated

Unfortunately, the fixation of the tissue and the vacuum necessary for SEM operation which requires all of the moisture to be removed makes it difficult to know exactly what is causing the structural changes. However, comparing the control images to the treated does appear to show that structural changes are taking place due to treatment since the control specimens are smoother. The treated specimens on the other hand, have larger grooves and the texture appears rougher and pitted.

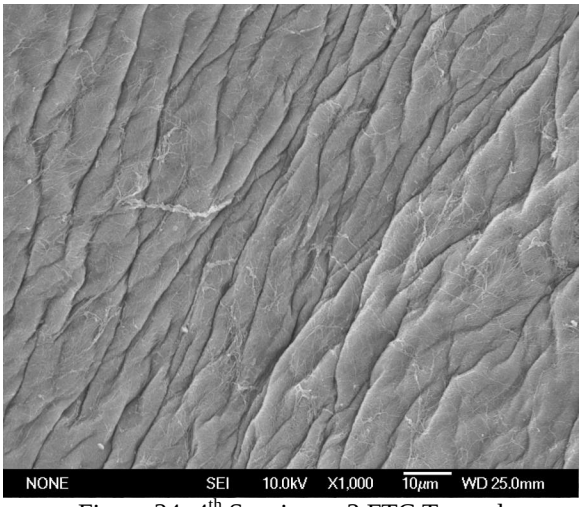

Figure 34: 4th Specimen, 3 FTC Treated

Future Work

In order to validate the data acquired from the confined compression creep test, Mow et. al. recommend calculating stress relaxation curves based on the aggregate modulus and permeability calculated for each specimen [2]. A stress-relaxation experiment should be performed using the same experimental model and stress-relaxation curves should be calculated from the experimental data. The theoretical curves using the aggregate modulus and permeability from the creep experiment should be compared to the experimental curves derived from the stress-relaxation tests. If both curves closely match, the experimental values of aggregate modulus and permeability are validated. However, if the curves do not match, both the creep and stress-relaxation tests need to be reexamined for errors.

An environmental scanning electron microscope can be used to view meniscus samples that were not fixed and dehydrated. Viewing new specimens with this type of SEM could make it clearer as to whether repeated freezing and thawing or SEM preparation caused the changes in the structure seen in the current study. Unfortunately, it is often difficult to capture clear environmental SEM images.

Larger sample sizes are needed to reduce the masking effects of the variability between menisci. Increasing the number of specimens within each treatment group may show statistically significant changes to the visco-elastic properties from the repeated freezing and thawing. Also, better loading mechanisms to rapidly apply the weights during the creep test could be used to improve data acquisition.

APPENDICES

APPENDIX A

SEM Images

1 FTC: Control 1

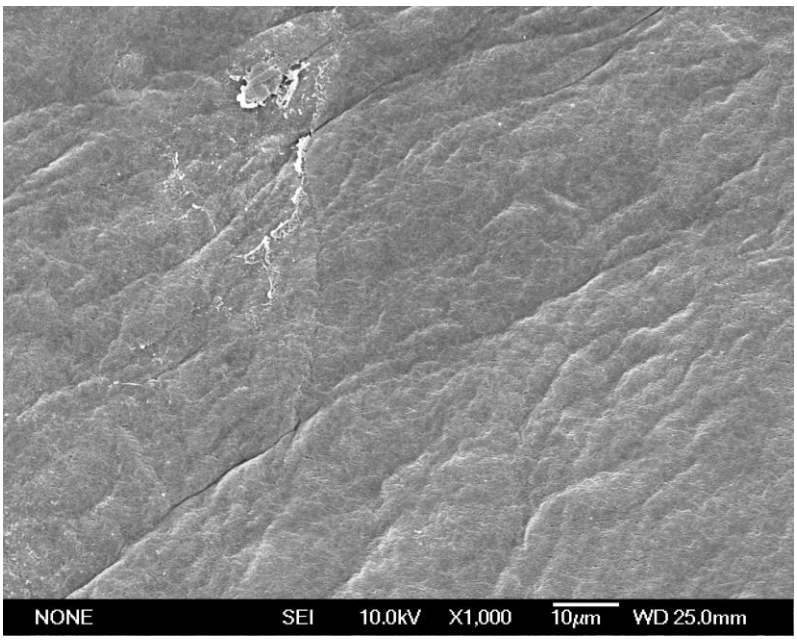

1 FTC: 1

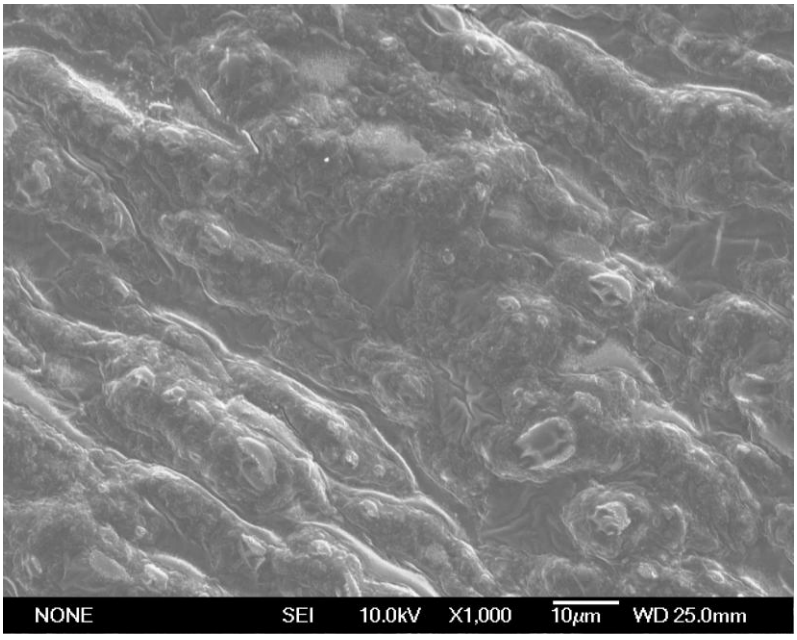

1 FTC: Control 2

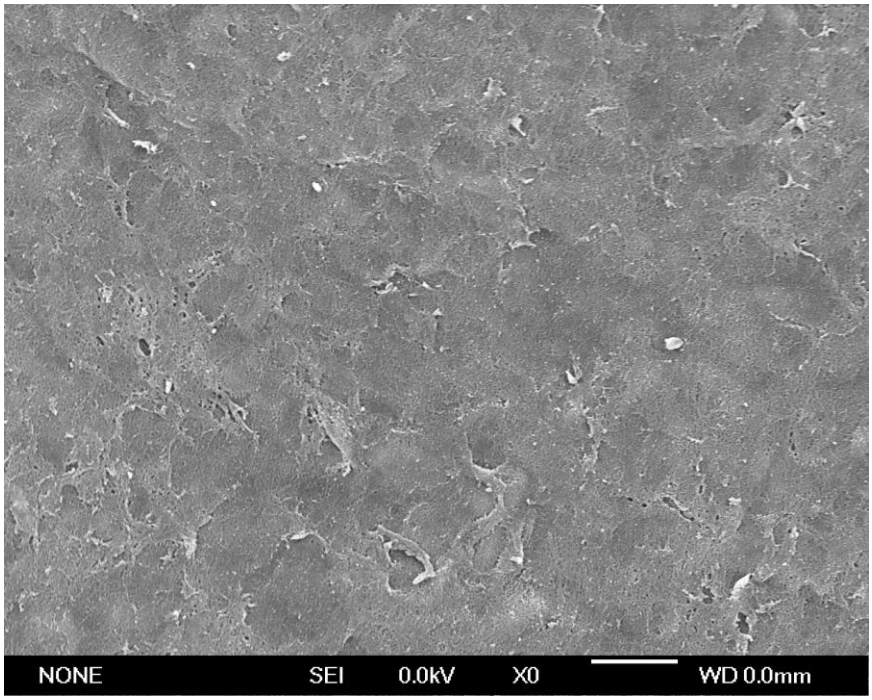

1 FTC: 2

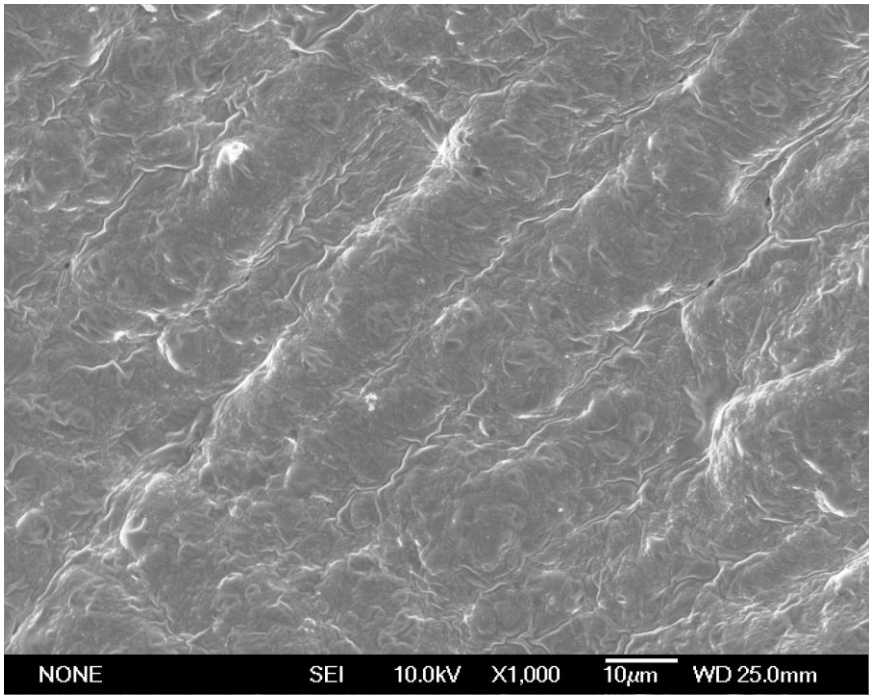

1 FTC: Control 3

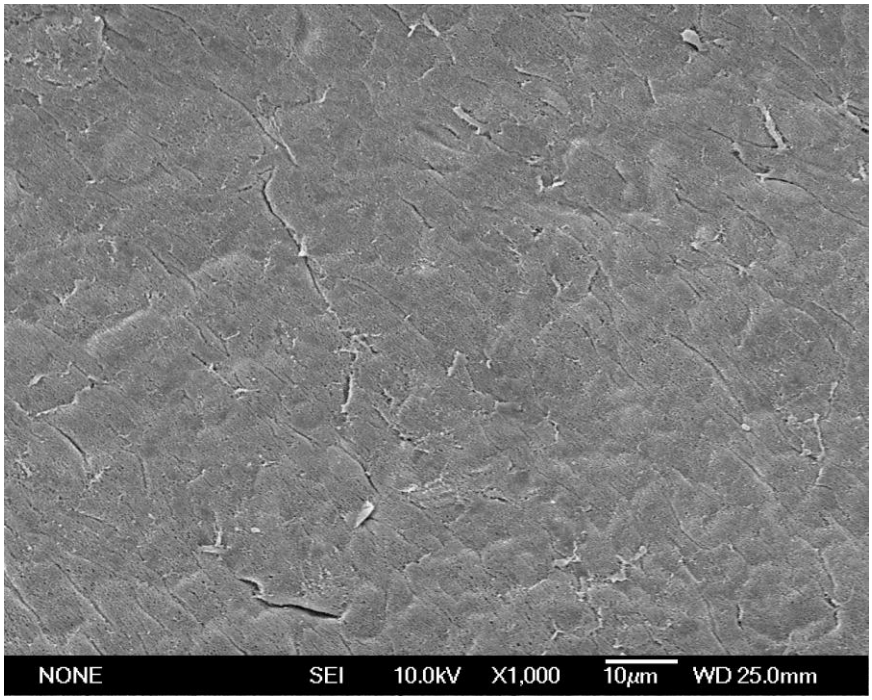

1 FTC: 3

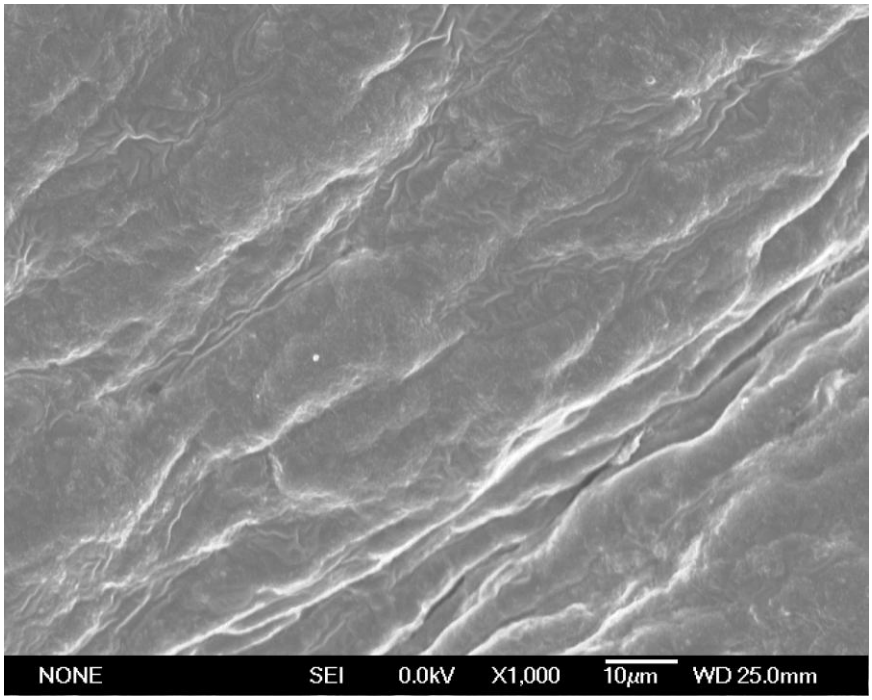

1 FTC: Control 4

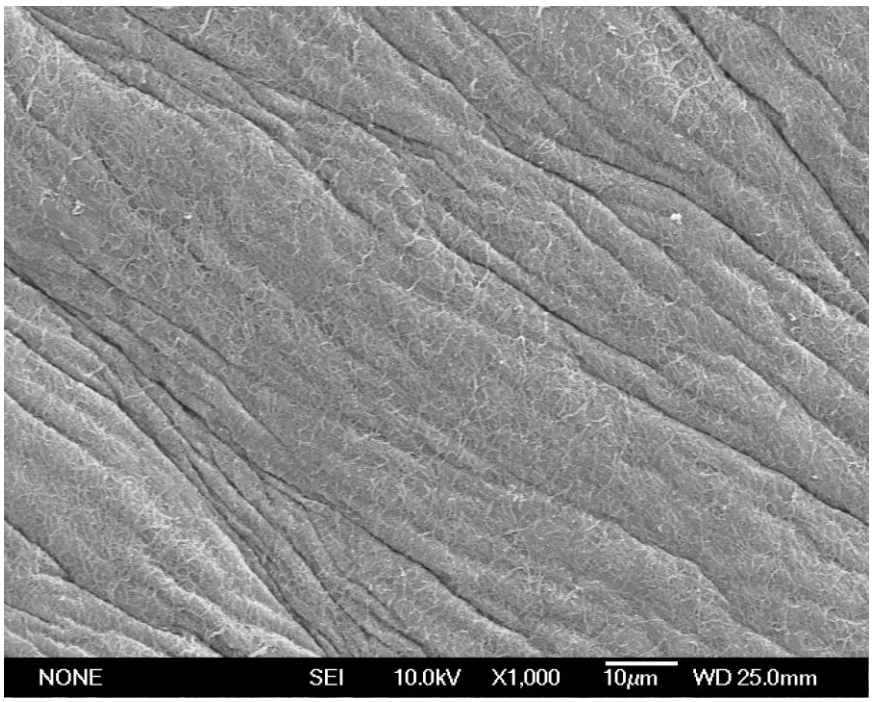

1 FTC: 4

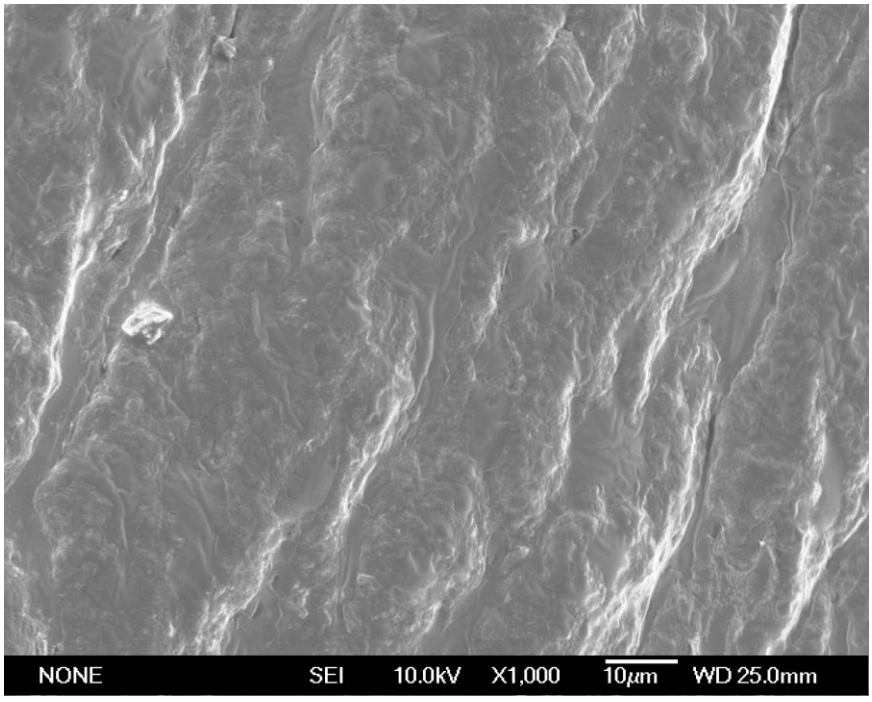

1 FTC: Control 5

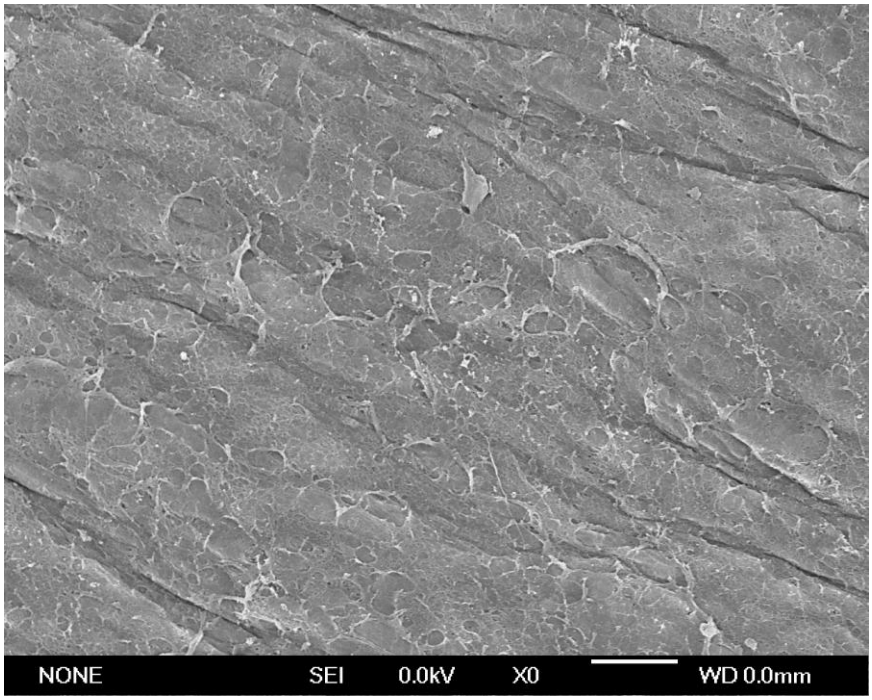

1 FTC: 5

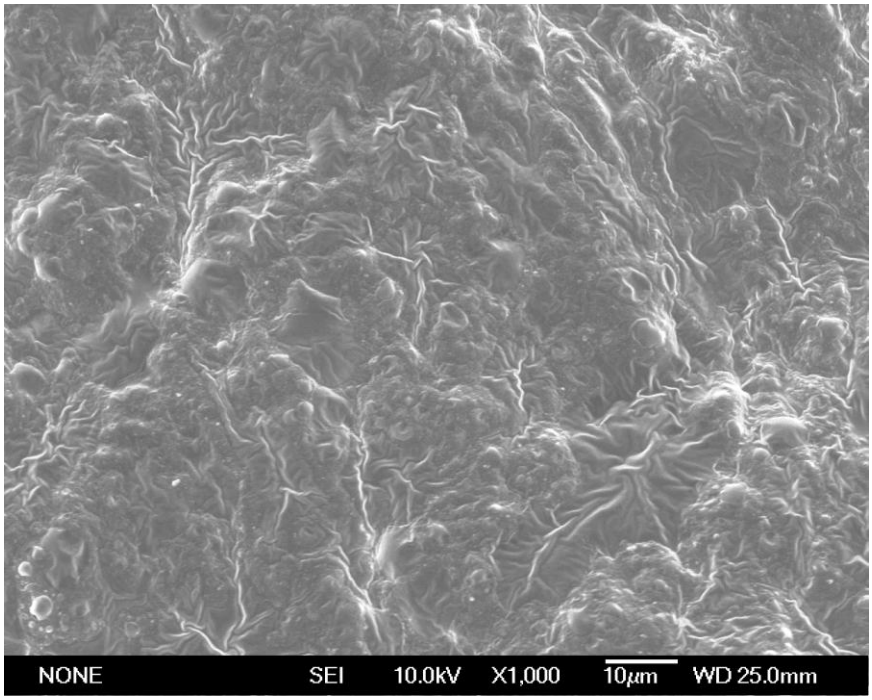

2 FTC: Control 1

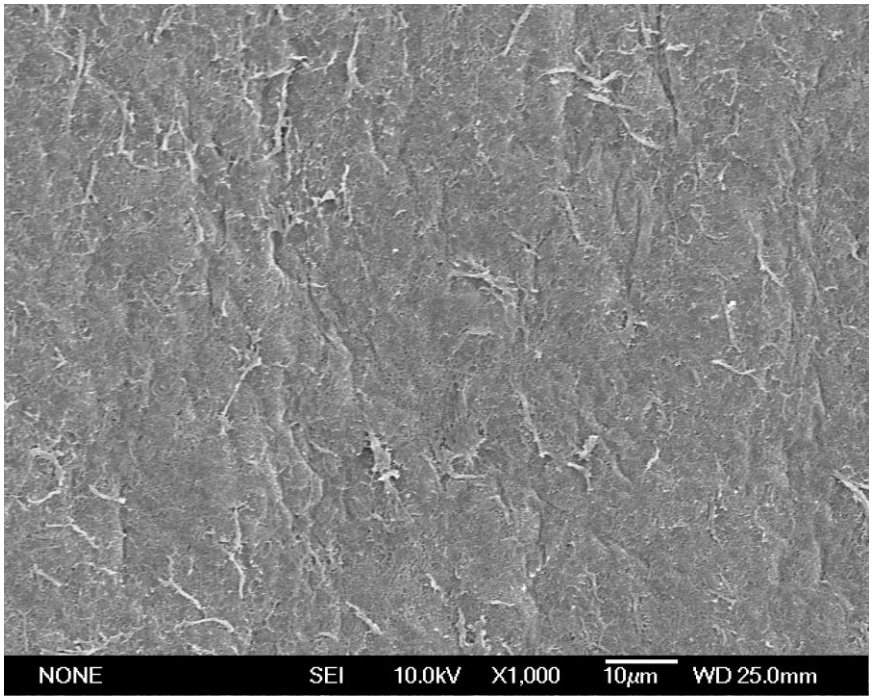

2 FTC: 1

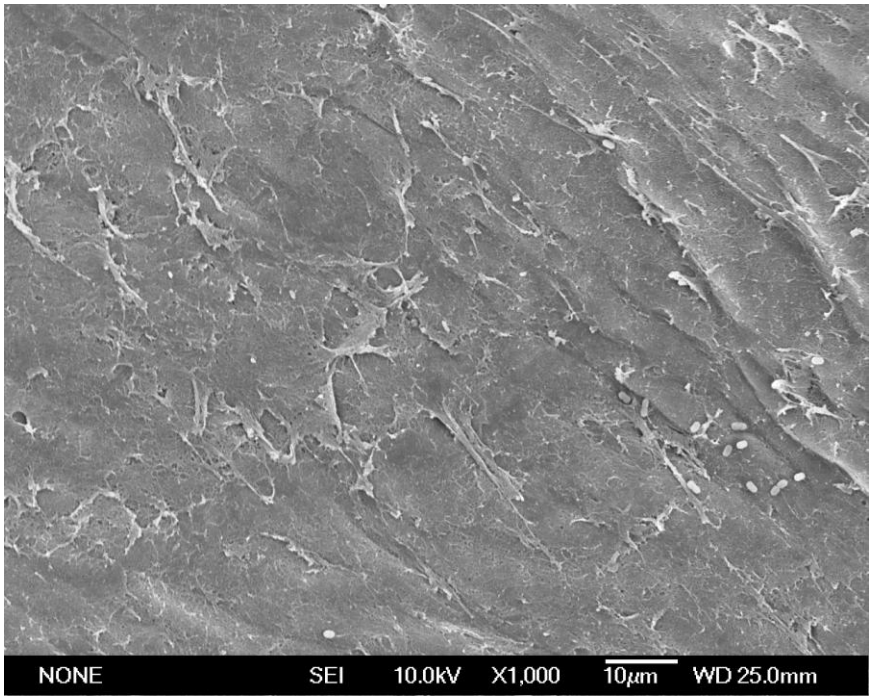

2 FTC: Control 2

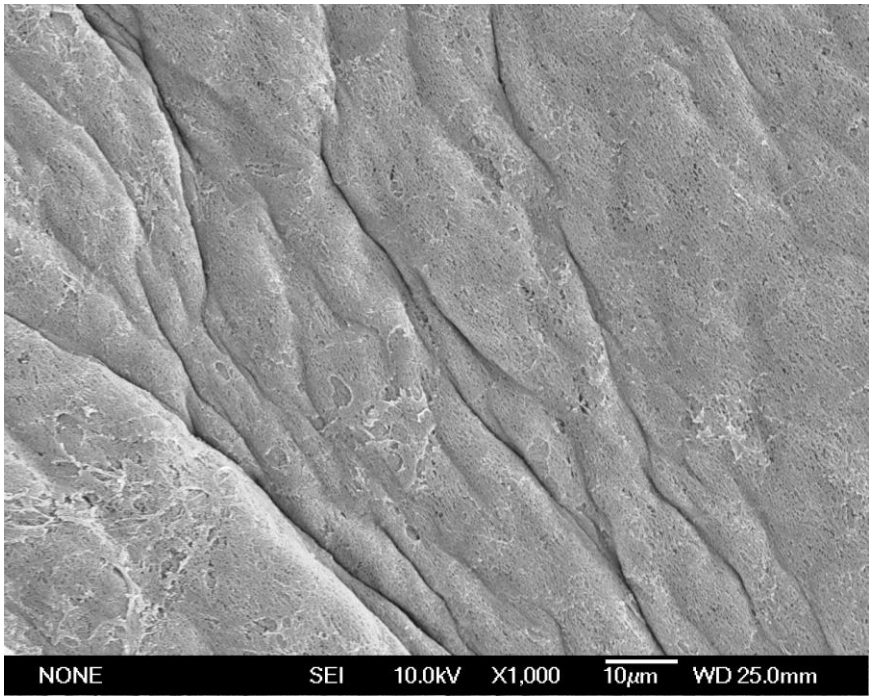

2 FTC: 2

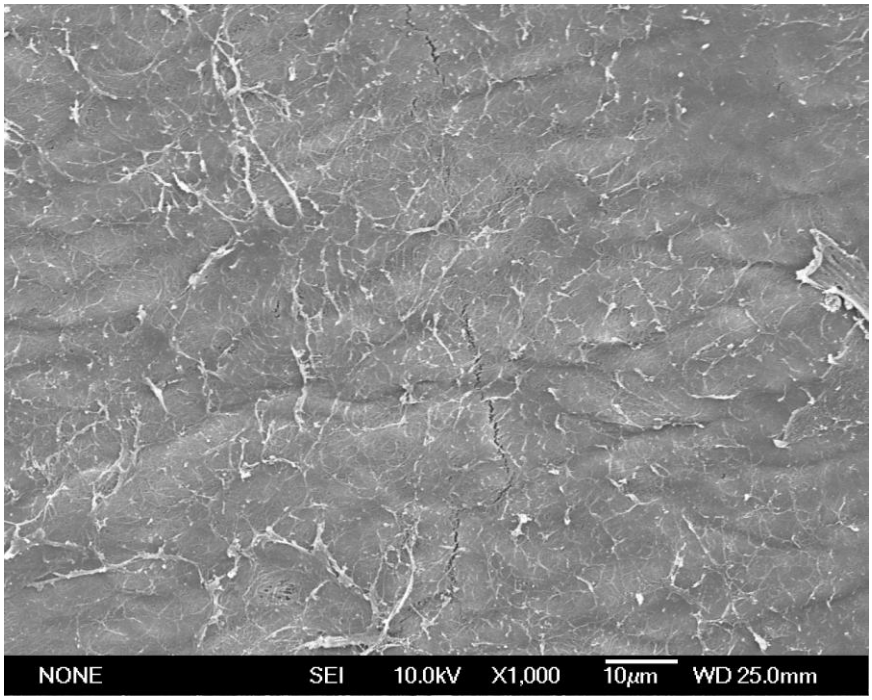

2 FTC: Control 3

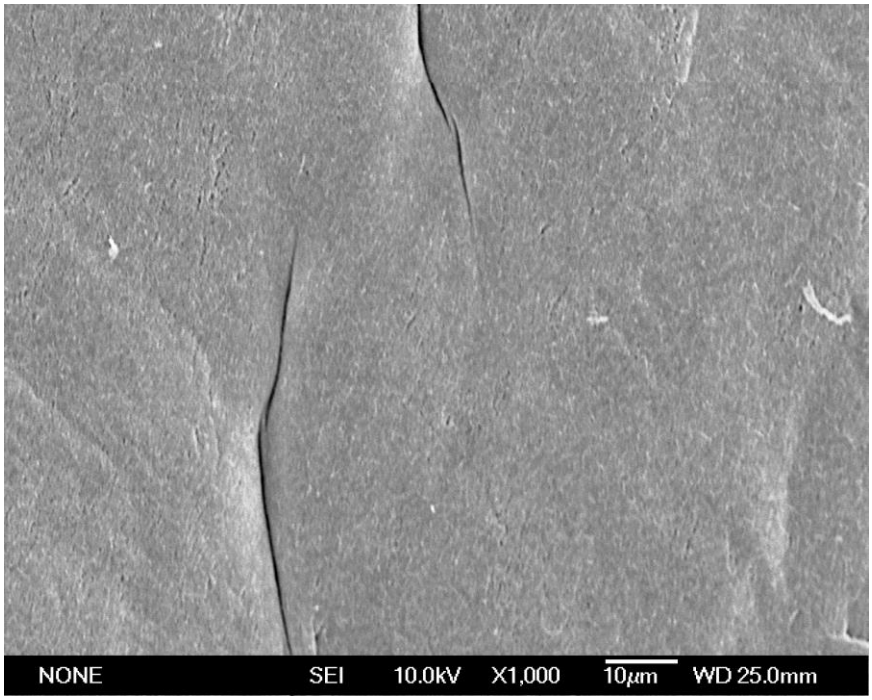

2 FTC: 3

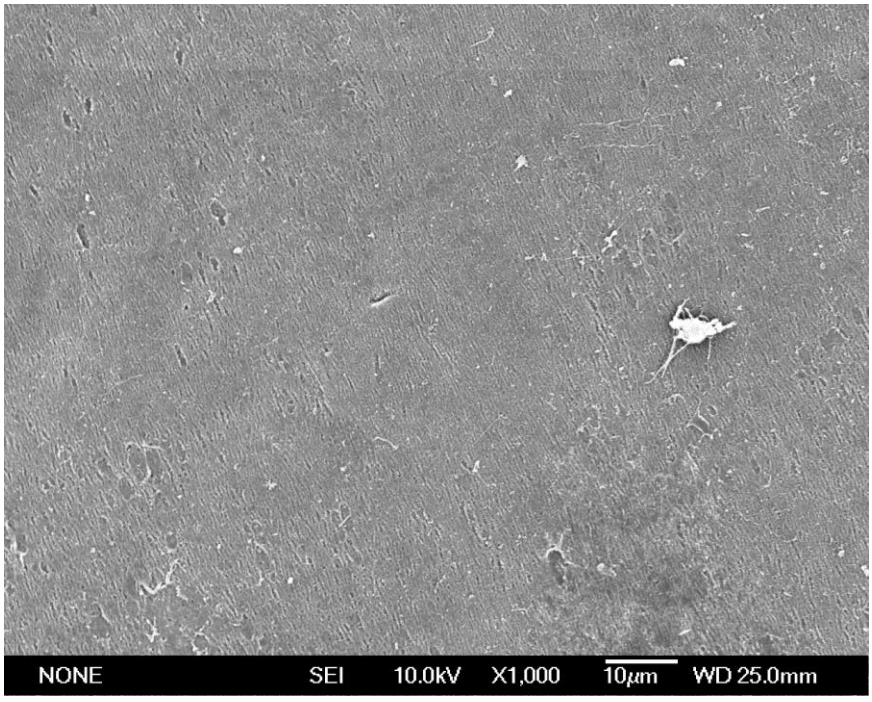

2 FTC: Control 4

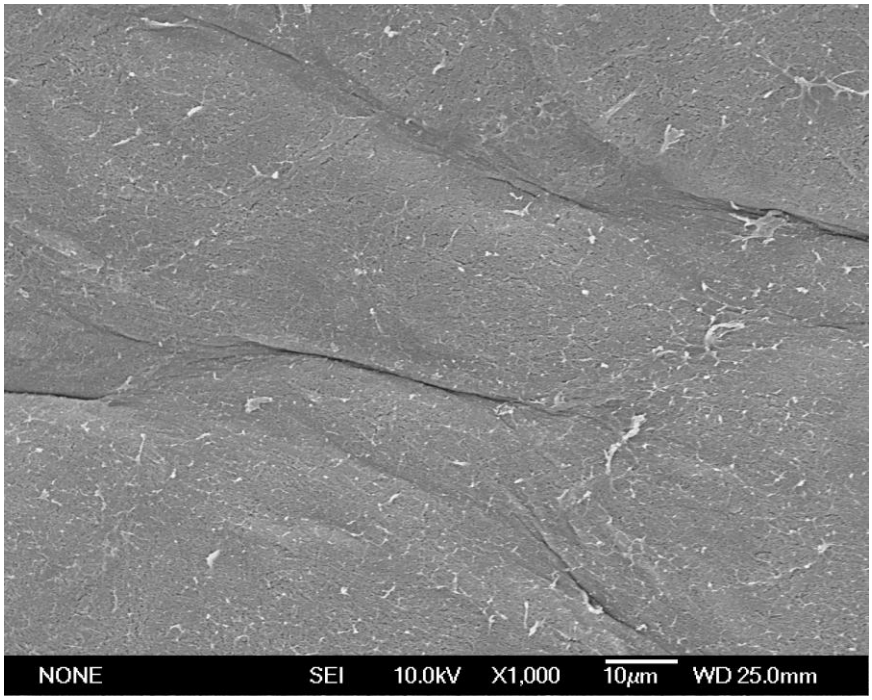

2 FTC: 4

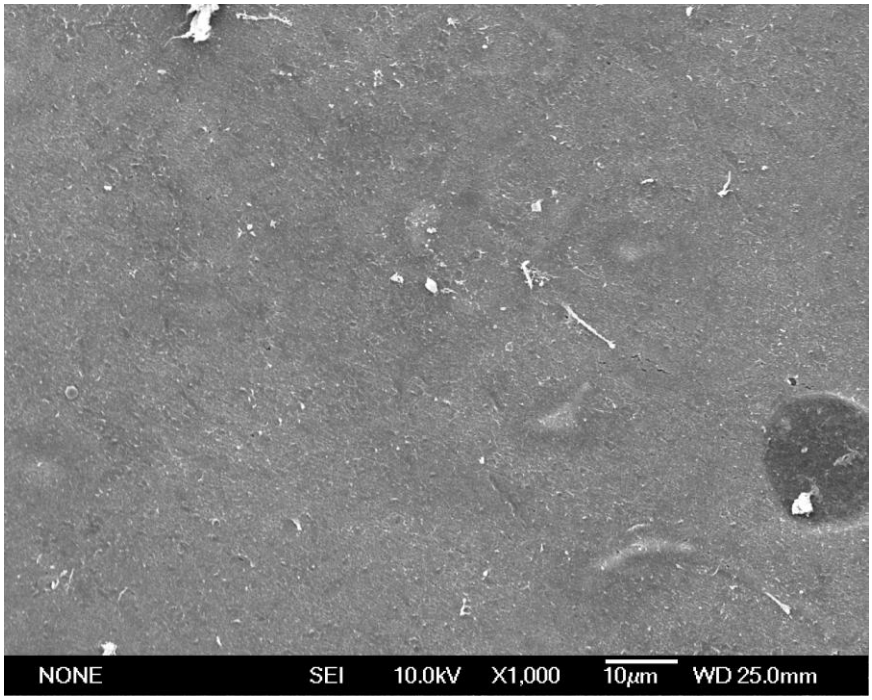

2 FTC: Control 5

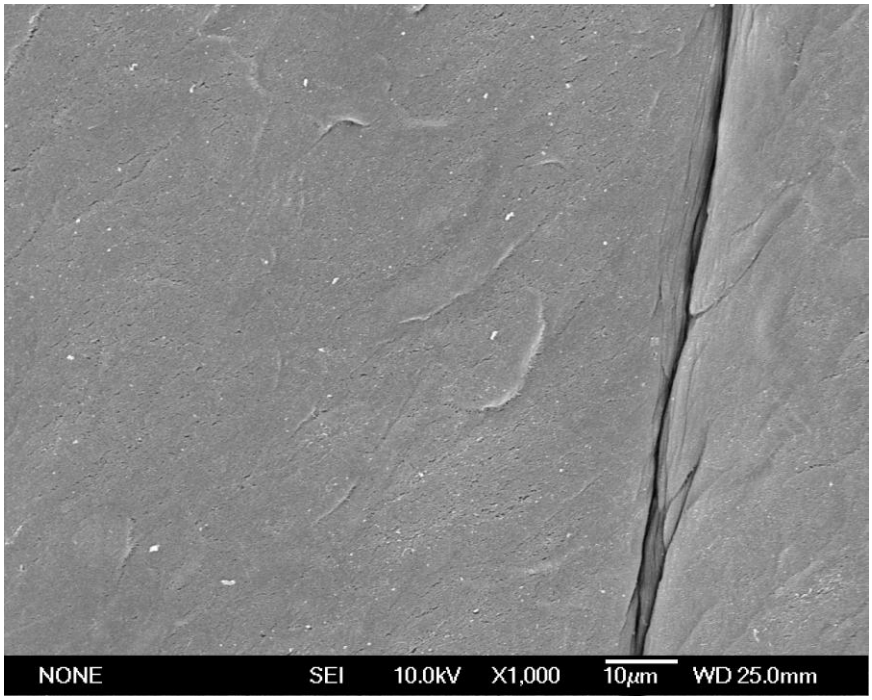

2 FTC: 5

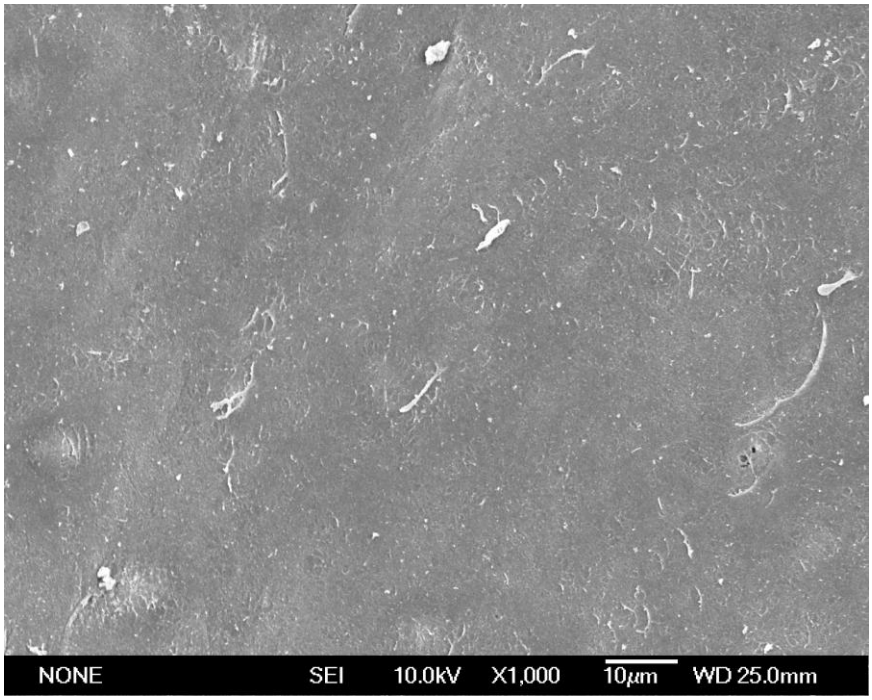

3 FTC: Control 1

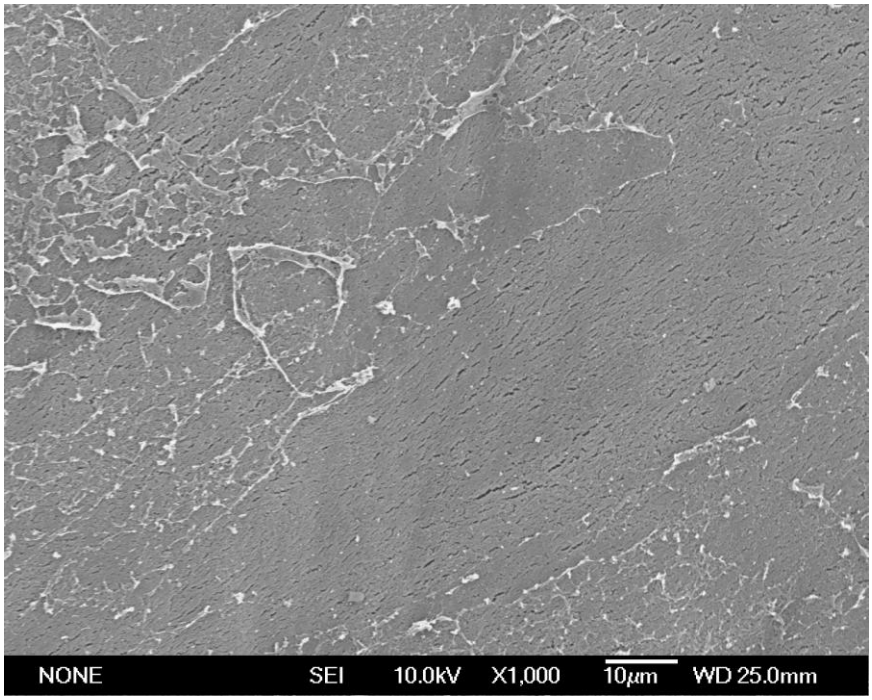

3 FTC: 1

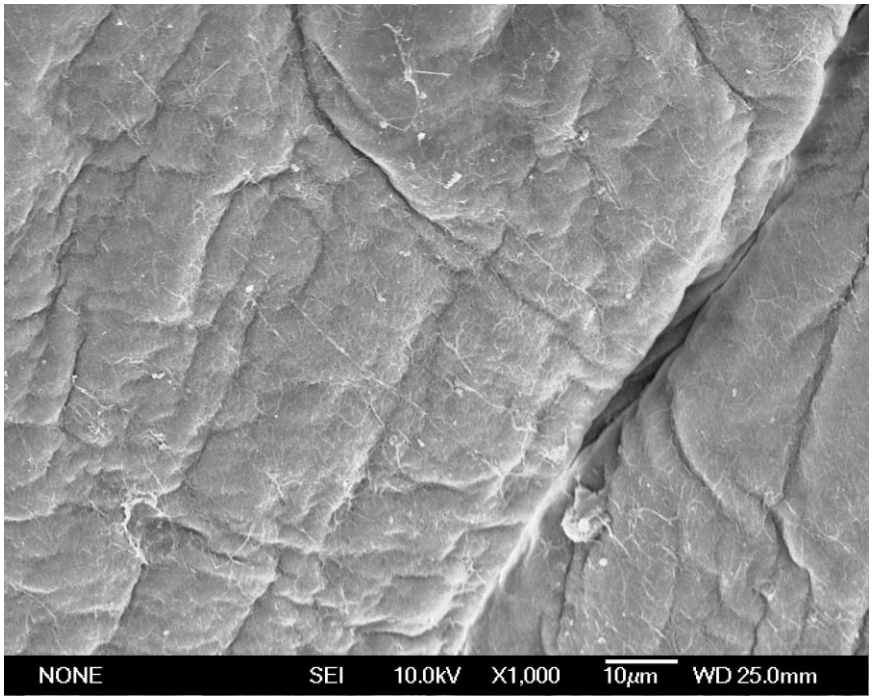

3 FTC: Control 2

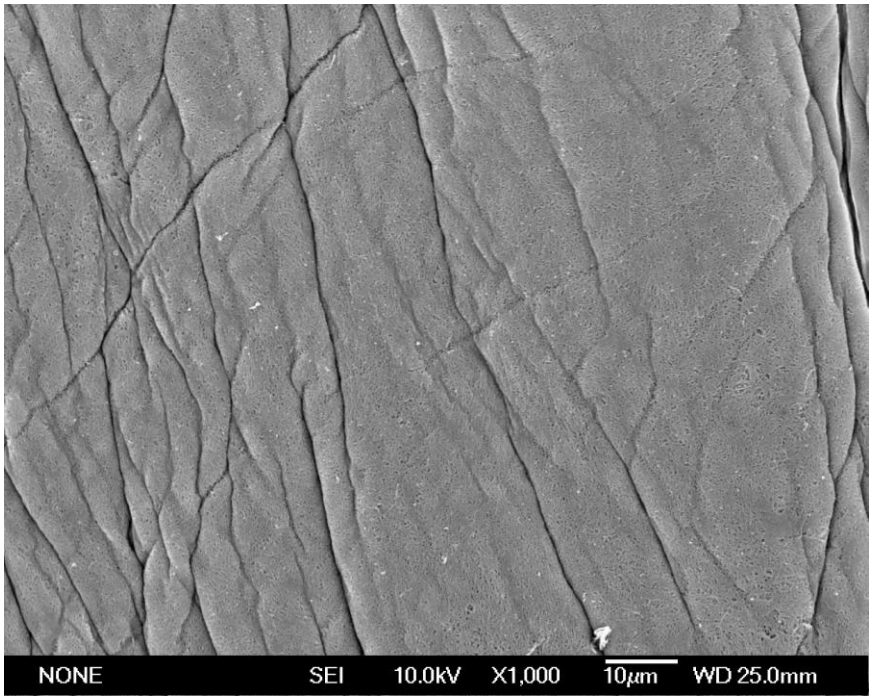

3 FTC: 2

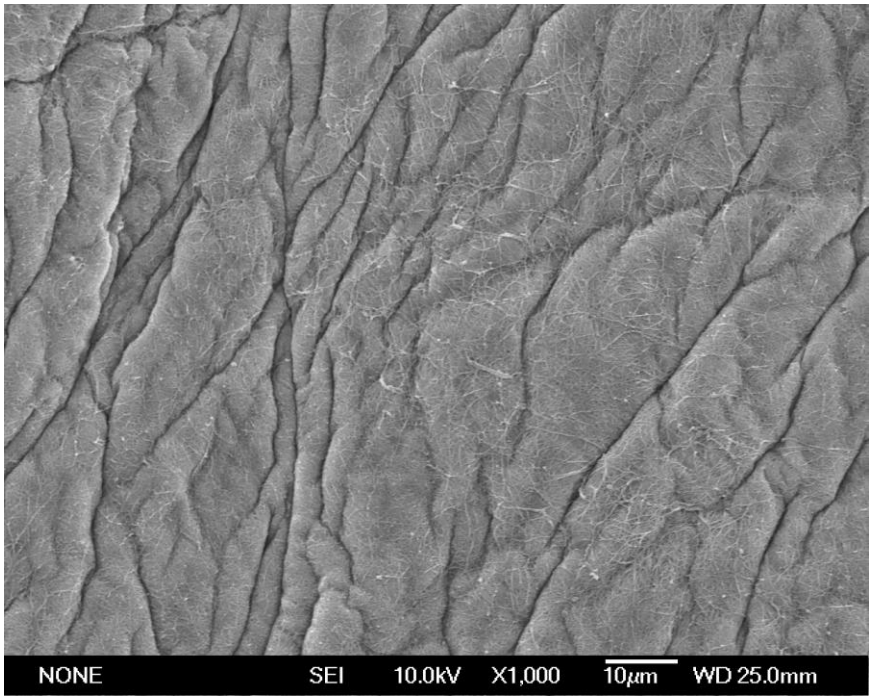

3 FTC: Control 3

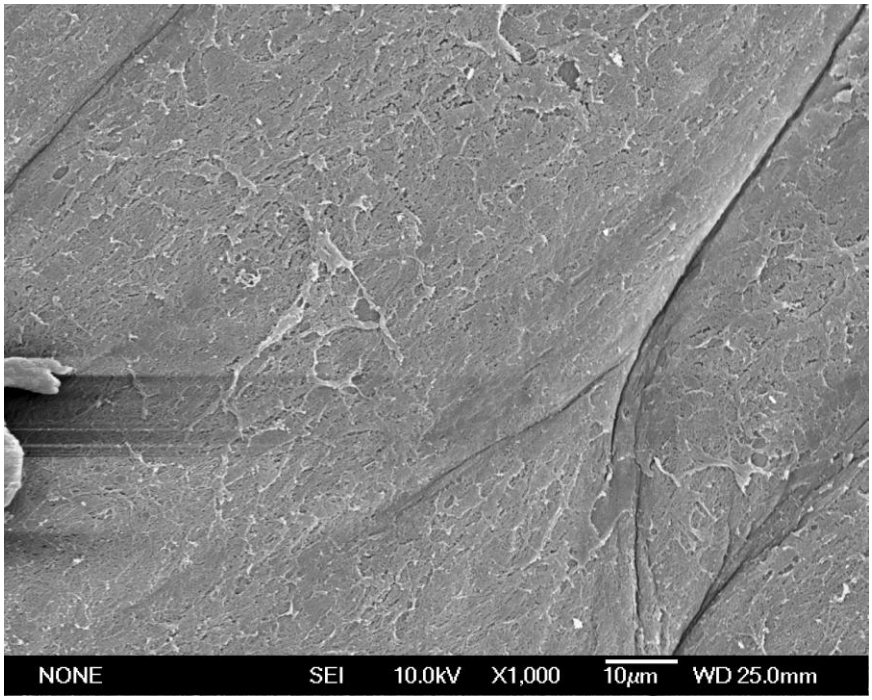

3 FTC: 3

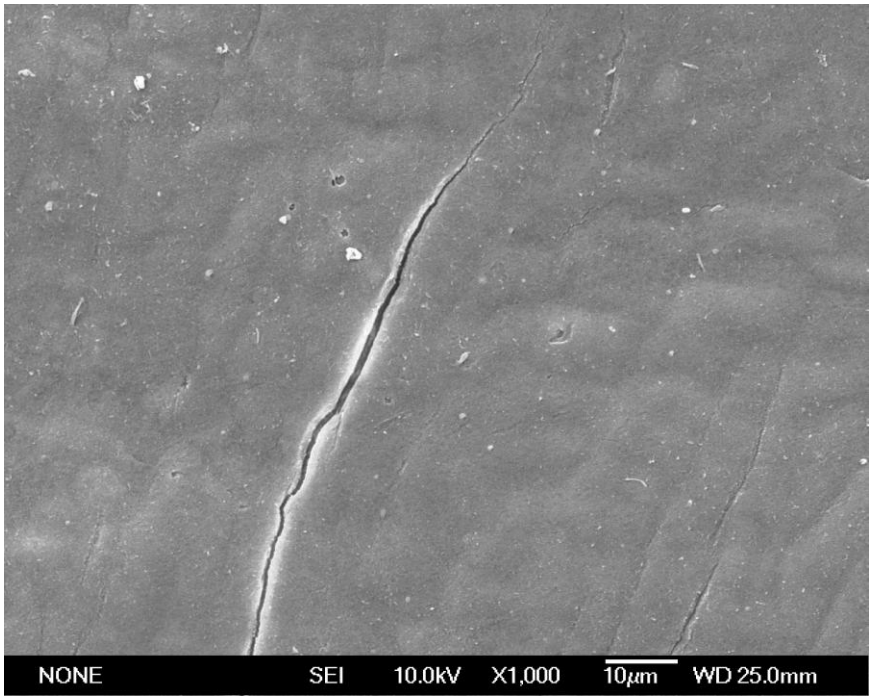

3 FTC: Control 4

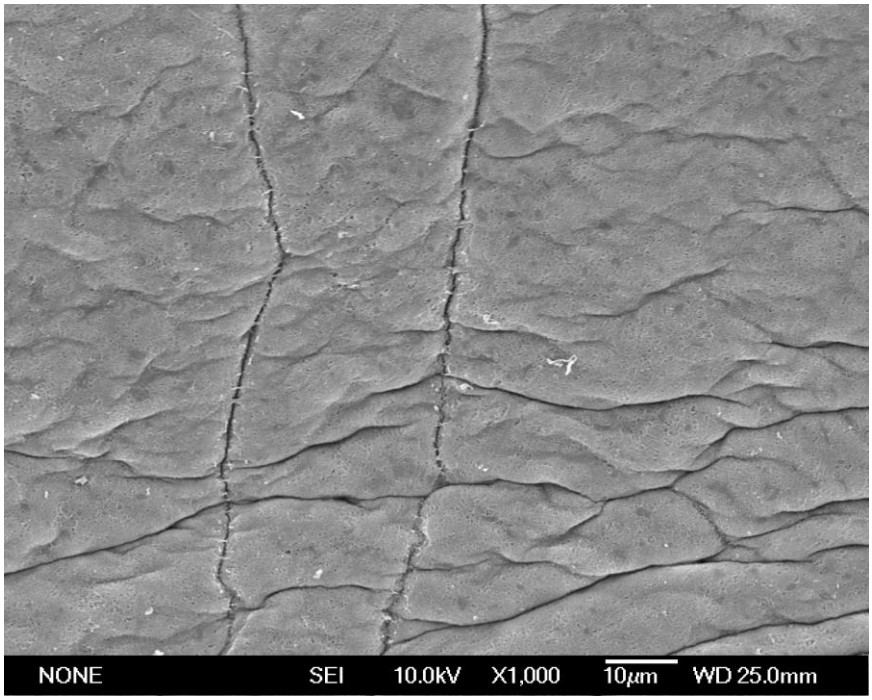

3 FTC: 4

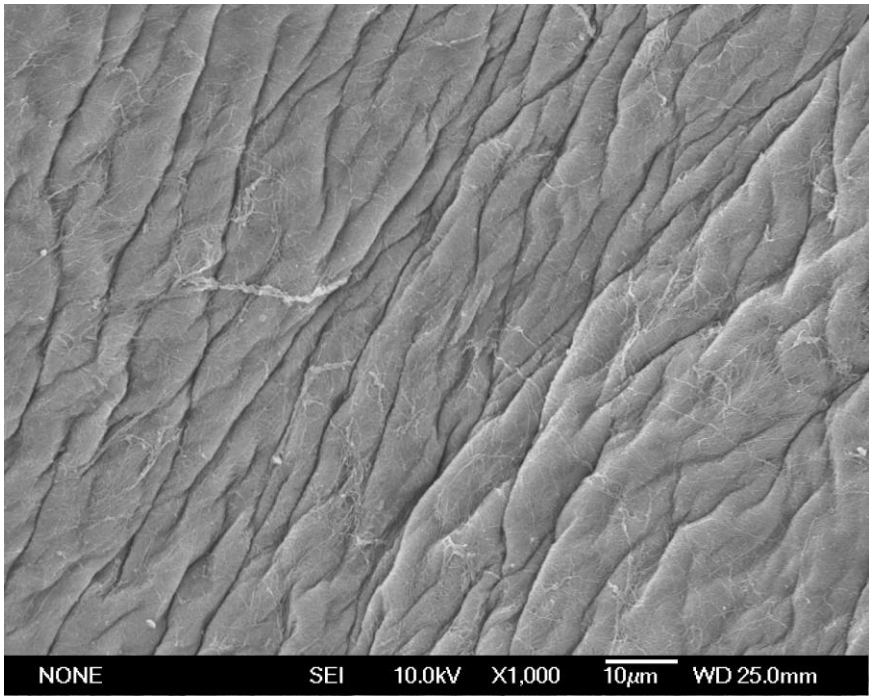

3 FTC: Control 5

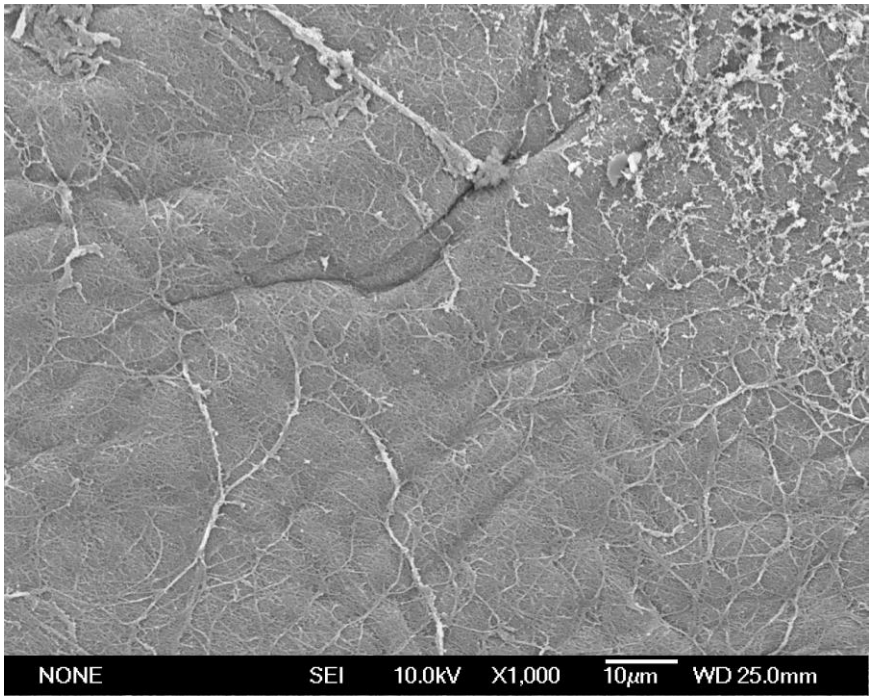

3 FTC: 5

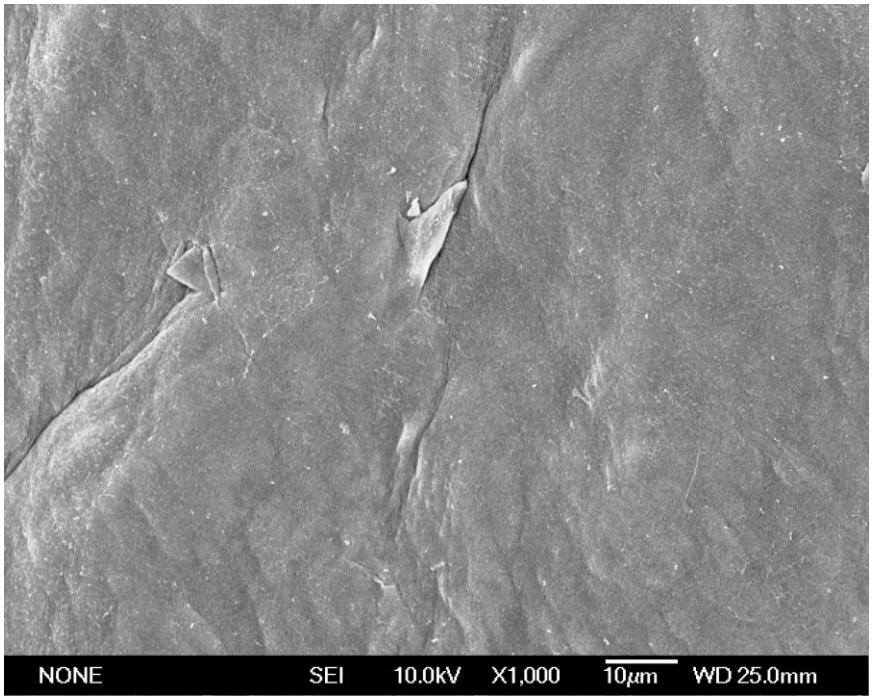

4 FTC: Control 1

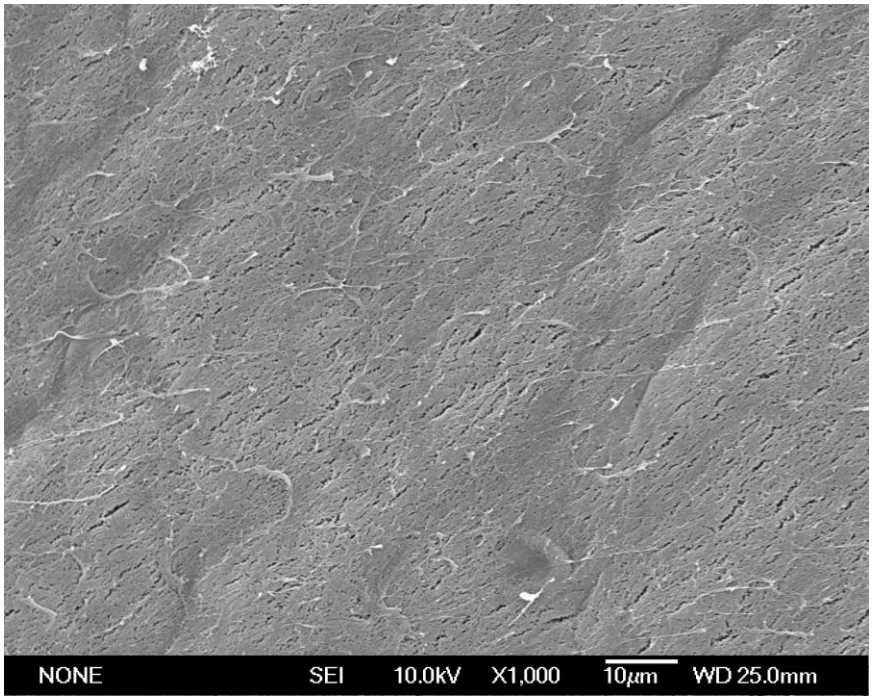

4 FTC: 1

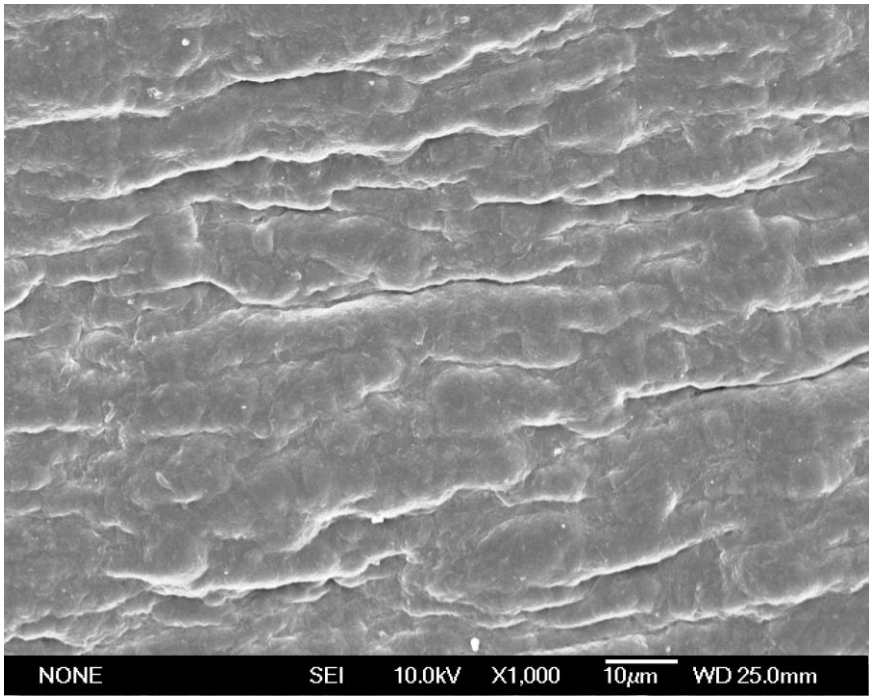

4 FTC: Control 2

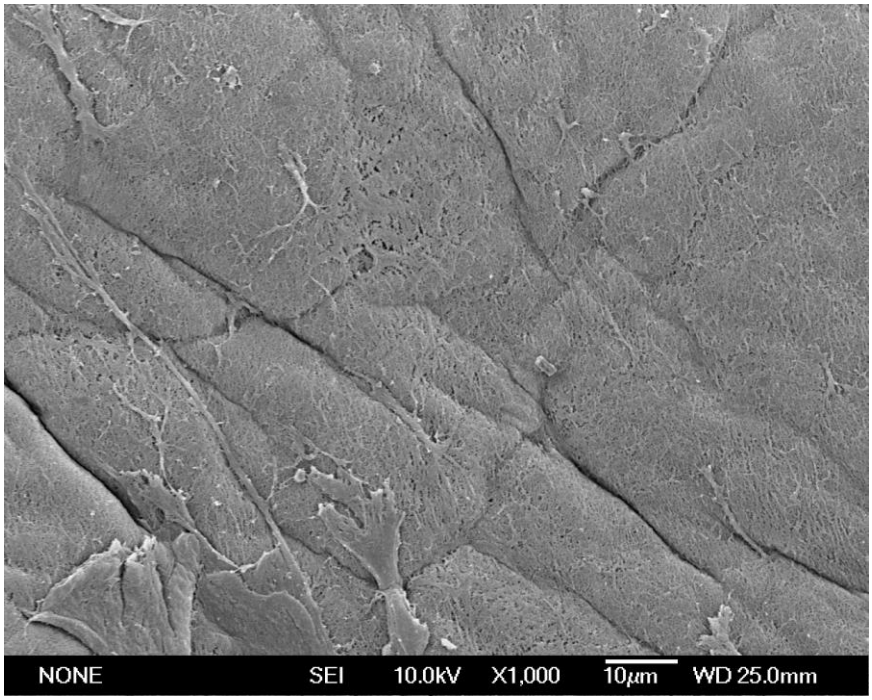

4 FTC: 2

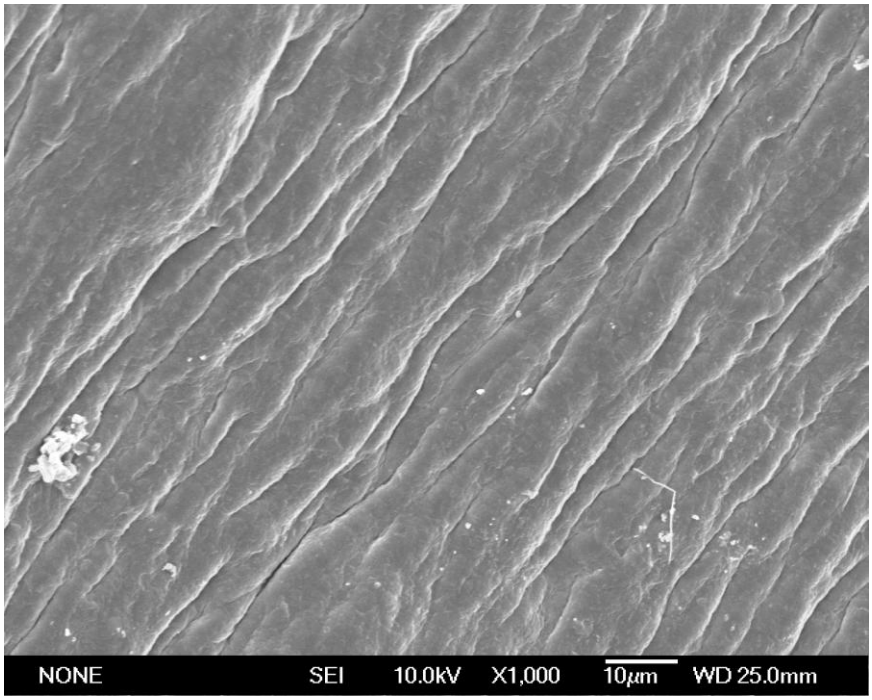

4 FTC: Control 3

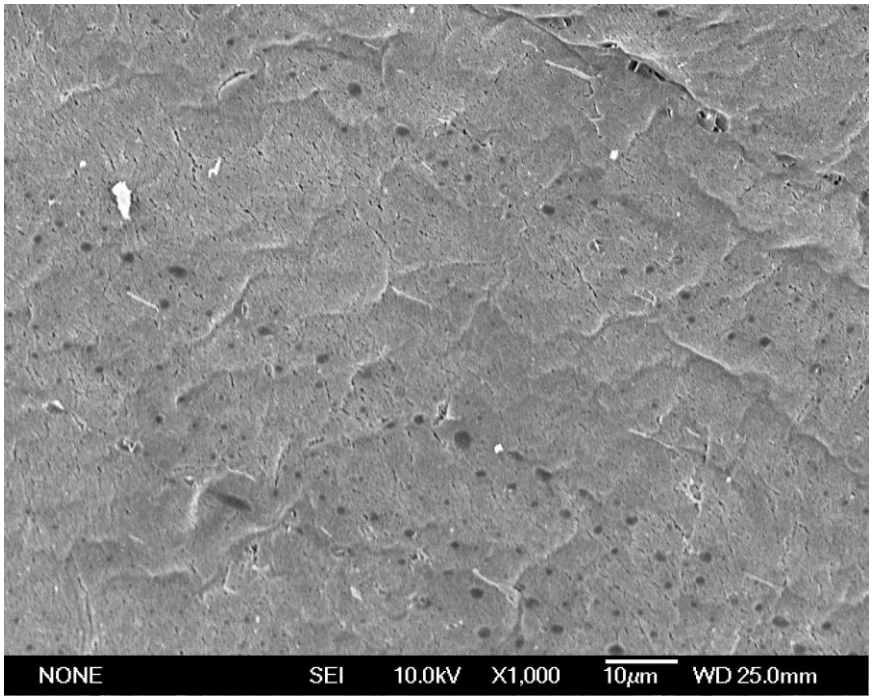

4 FTC: 3

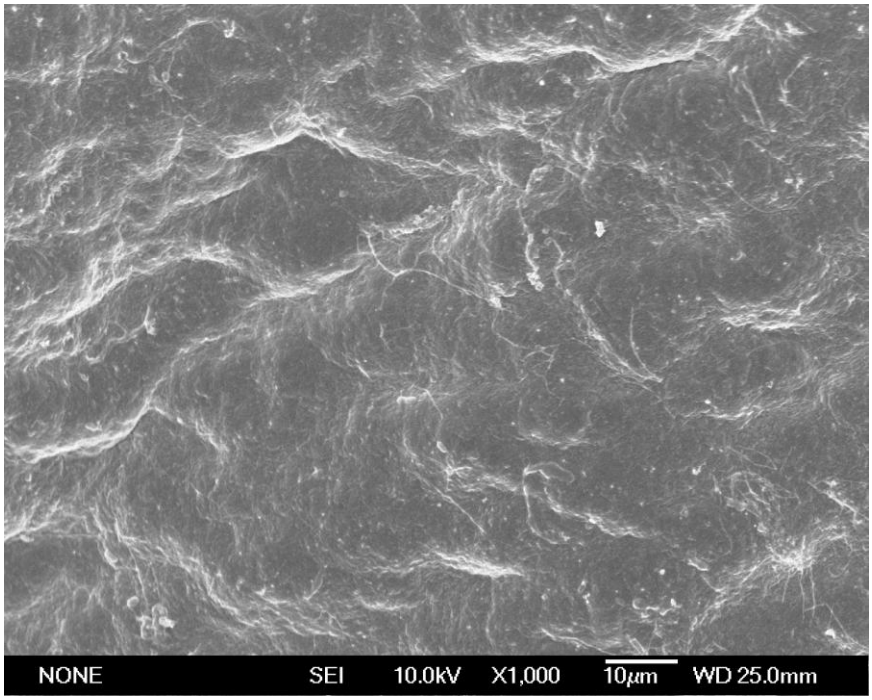

4 FTC: Control 4

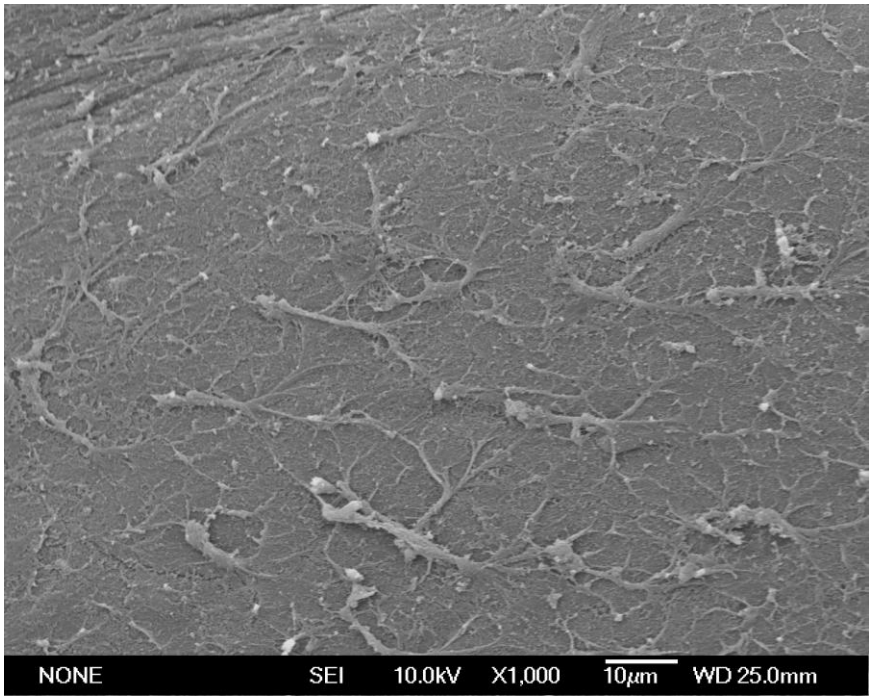

4 FTC: 4

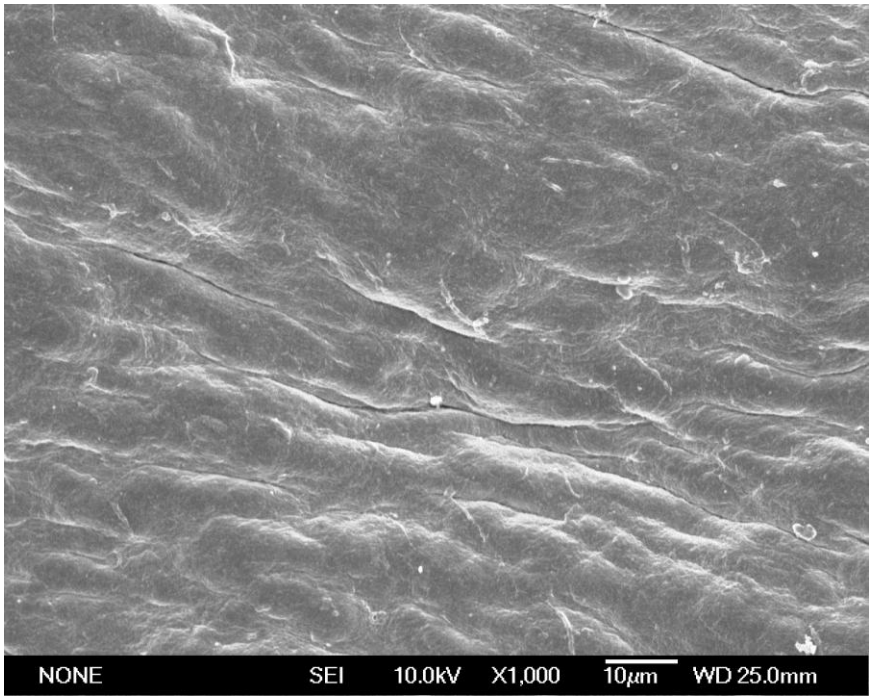

4 FTC: Control 5

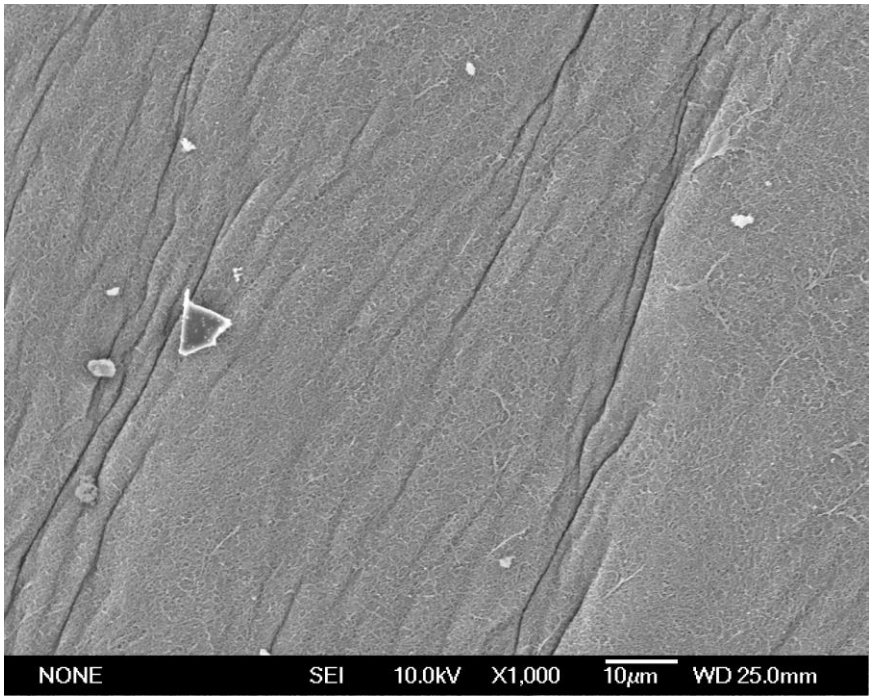

4 FTC: 5

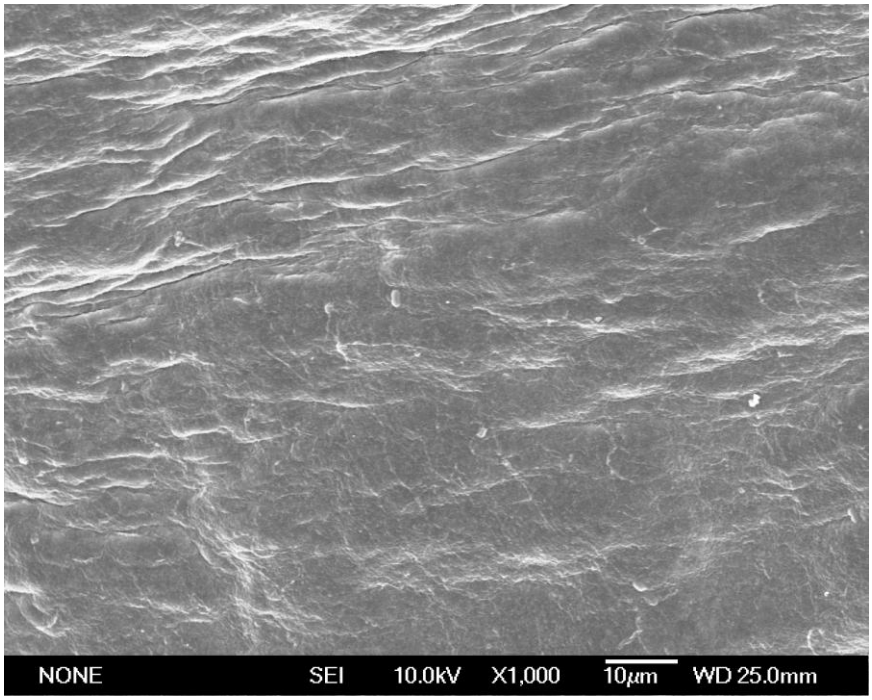

APPENDIX B

Matlab Code

```
function [H, K, r] = DataAnalysis(E)

E = E';   %transpose matrices

t = E(1,:);   %assign t to first column of time data
u = E(2,:);   %assign u to second column of displacement data

P = -0.058081; h= 3.333;    %Constants: P = stress in MPa, h = height
of specimen in mm
%Hao = -P * h / mean(u(length(u)-300:length(u)))   %looks at steady
state of data and chooses an appropriate start

clear estimates1
clear model1
[estimates1, model1] = disfit(t,u);

H = estimates1(1)    % Aggregate Modulus N/mm^2
K = estimates1(2)    % Permeability  mm^4/Ns

[sse, sst, FittedCurve] = model1(estimates1);

o2 = 1;
while ((o2 <= length(t)))
        corr3(o2) = 1 - (sum((FittedCurve(o2:length(t)) -
u(o2:length(t))).^2) / sum((u(o2:length(t))-
mean(u(o2:length(t)))).^2));
        o2 = o2+1;
end

[VAL12,POS12]=max(corr3,[],2)

plot(E(1,:), E(2,:), '*')   % data plot
hold on
plot(E(1,:), FittedCurve, 'r')   % curve fit plot
r = 1 - sse/sst;    % correlation coefficient

xlabel('Time')
ylabel('Displacement')
title('Optimization')
legend('data', sprintf('curve fit r = %f', r))
hold off

function [estimates, model] = disfit(t, u)
```

```
start_point = [.377 7.8e-4];    % initial guesses for Modulus and
Permeability
model = @biphasic;
estimates = fminsearch(model,start_point);

function [SSE, SST, CurveFit] = biphasic(in)

P = -0.058081;   %stress MPa
a = in(1);      %modulus value
b = in(2);      % permeability value
h = 3.333;        %height mm

CurveFit = (-P / a * (h-(2*h/pi^2)*((((-1)^1 / (1 + 0.5)^2) * sin((1 +
0.5)*(pi * h/h)) * exp(-a*b / (h^2) *(1+0.5)^2 * pi^2 * t))+(((-1)^2 /
(2 + 0.5)^2) * sin((2 + 0.5)*(pi * h/h)) * exp(-a*b / (h^2) *(2+0.5)^2
* pi^2 * t))+(((-1)^3 / (3 + 0.5)^2) * sin((3 + 0.5)*(pi * h/h)) *
exp(-a*b / (h^2) *(3+0.5)^2 * pi^2 * t))+(((-1)^4 / (4 + 0.5)^2) *
sin((4 + 0.5)*(pi * h/h)) * exp(-a*b / (h^2) *(4+0.5)^2 * pi^2 *
t))+(((-1)^0 / (0 + 0.5)^2) * sin((0 + 0.5)*(pi * h/h)) * exp(-a*b /
(h^2) *(0+0.5)^2 * pi^2 * t))+(((-1)^5 / (5 + 0.5)^2) * sin((5 +
0.5)*(pi * h/h)) * exp(-a*b / (h^2) *(5+0.5)^2 * pi^2 * t))+(((-1)^6 /
(6 + 0.5)^2) * sin((6 + 0.5)*(pi * h/h)) * exp(-a*b / (h^2) *(6+0.5)^2
* pi^2 * t))+(((-1)^7 / (7 + 0.5)^2) * sin((7 + 0.5)*(pi * h/h)) *
exp(-a*b / (h^2) *(7+0.5)^2 * pi^2 * t))+(((-1)^8 / (8 + 0.5)^2) *
sin((8 + 0.5)*(pi * h/h)) * exp(-a*b / (h^2) *(8+0.5)^2 * pi^2 *
t))+(((-1)^9 / (9 + 0.5)^2) * sin((9 + 0.5)*(pi * h/h)) * exp(-a*b /
(h^2) *(9+0.5)^2 * pi^2 * t))+(((-1)^10 / (10 + 0.5)^2) * sin((10 +
0.5)*(pi * h/h)) * exp(-a*b / (h^2) *(10+0.5)^2 * pi^2 * t))+(((-1)^11
/ (11 + 0.5)^2) * sin((11 + 0.5)*(pi * h/h)) * exp(-a*b / (h^2)
*(11+0.5)^2 * pi^2 * t))+(((-1)^12 / (12 + 0.5)^2) * sin((12 + 0.5)*(pi
* h/h)) * exp(-a*b / (h^2) *(12+0.5)^2 * pi^2 * t))+(((-1)^13 / (13 +
0.5)^2) * sin((13 + 0.5)*(pi * h/h)) * exp(-a*b / (h^2) *(13+0.5)^2 *
pi^2 * t))+(((-1)^14 / (14 + 0.5)^2) * sin((14 + 0.5)*(pi * h/h)) *
exp(-a*b / (h^2) *(14+0.5)^2 * pi^2 * t))+(((-1)^15 / (15 + 0.5)^2) *
sin((15 + 0.5)*(pi * h/h)) * exp(-a*b / (h^2) *(15+0.5)^2 * pi^2 *
t))+(((-1)^16 / (16 + 0.5)^2) * sin((16 + 0.5)*(pi * h/h)) * exp(-a*b /
(h^2) *(16+0.5)^2 * pi^2 * t))+(((-1)^17 / (17 + 0.5)^2) * sin((17 +
0.5)*(pi * h/h)) * exp(-a*b / (h^2) *(17+0.5)^2 * pi^2 * t))+(((-1)^18
/ (18 + 0.5)^2) * sin((18 + 0.5)*(pi * h/h)) * exp(-a*b / (h^2)
*(18+0.5)^2 * pi^2 * t))+(((-1)^19 / (19 + 0.5)^2) * sin((19 + 0.5)*(pi
* h/h)) * exp(-a*b / (h^2) *(19+0.5)^2 * pi^2 * t))+(((-1)^20 / (20 +
0.5)^2) * sin((20 + 0.5)*(pi * h/h)) * exp(-a*b / (h^2) *(20+0.5)^2 *
pi^2 * t)))));

SSE = sum( (CurveFit - u).^2);
SST = sum( (u - mean(u)).^2);
end
end
end
```

APPENDIX C

Optimization Curves

Control 1

>> [H, K, r] = DataAnalysis(Control1)

H =

0.2929

K =

0.0113

VAL12 =

0.8136

POS12 =

1

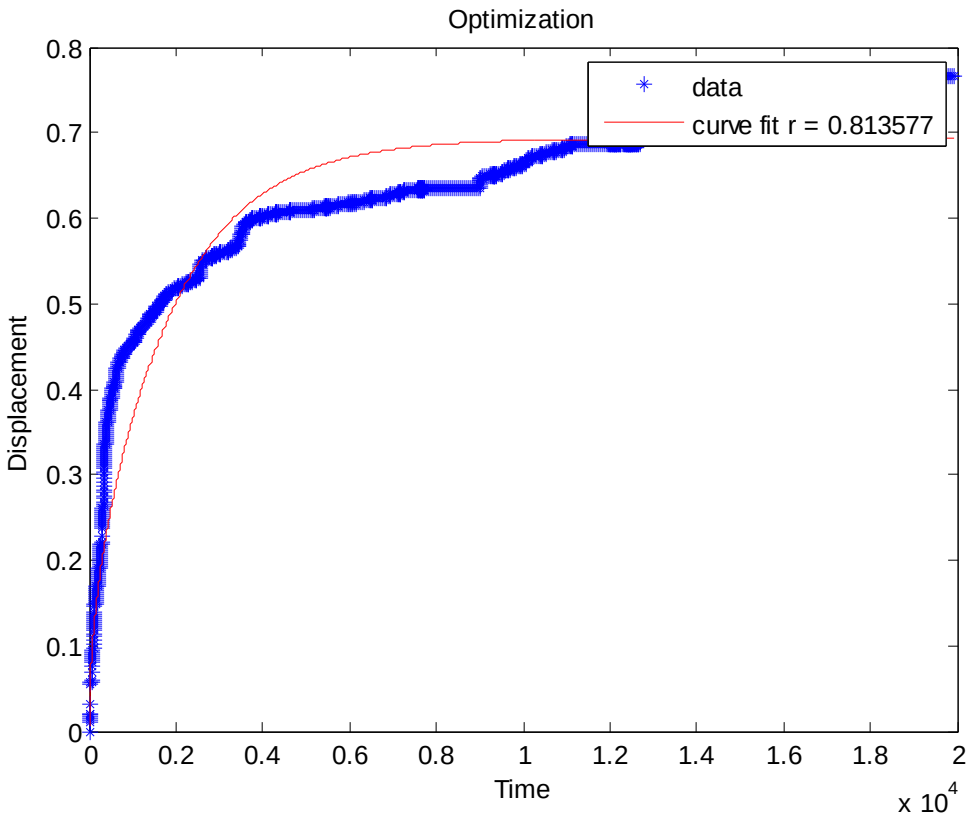

H =

0.2929

K =

0.0113

r =

0.8136

Control 2

>> [H, K, r] = DataAnalysis(Control2)

H =

0.4137

K =

0.0037

VAL12 =

0.8973

POS12 =

41

H =

0.4137

K =

0.0037

r =

0.8933

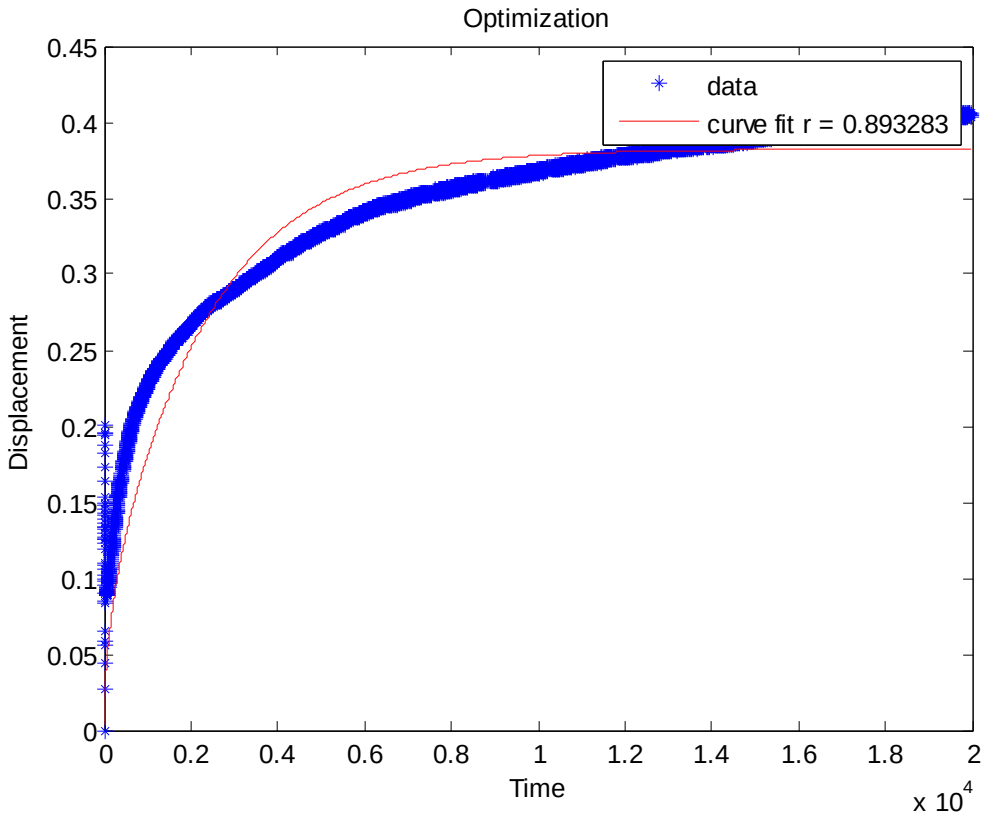

Control 3

>> [H, K, r] = DataAnalysis(Control3)

H =

0.5281

K =

0.0527

VAL12 =

0.4945

POS12 =

1

H =

0.5281

K =

0.0527

r =

0.4945

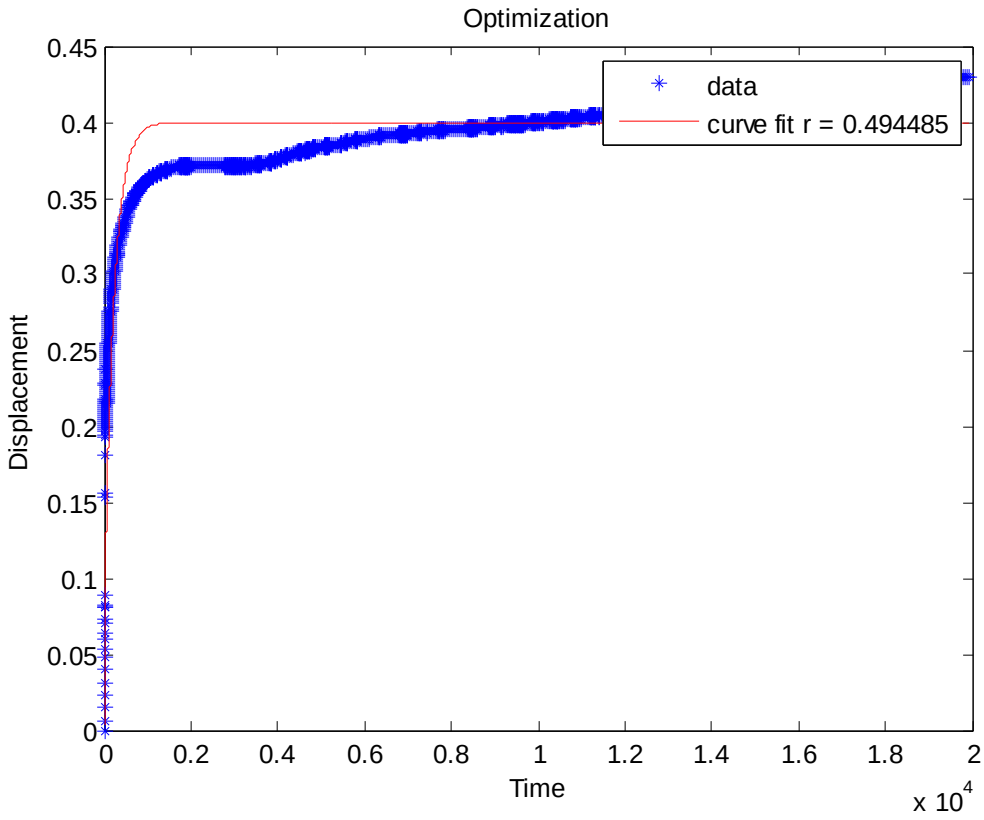

Control 4

```
>> [H, K, r] = DataAnalysis(Control4)

H =

    0.2324

K =

    0.0333

VAL12 =

    0.7960

POS12 =

     1

H =

    0.2324

K =

    0.0333

r =

    0.7960
```

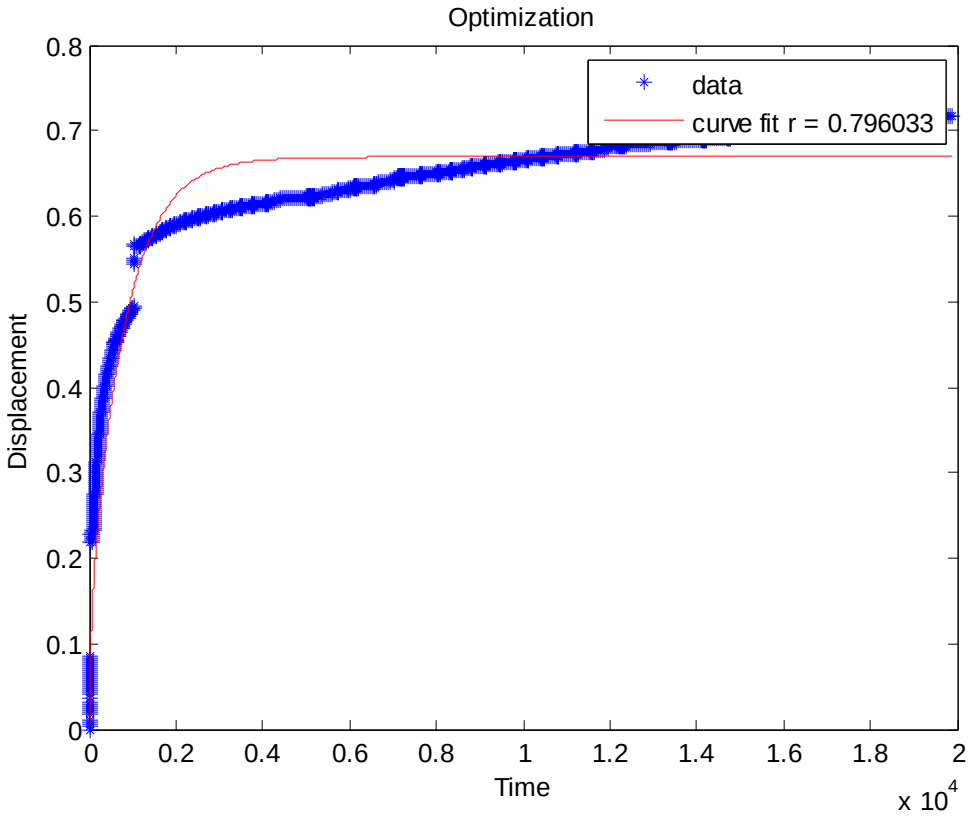

Control 5

```
>> [H, K, r] = DataAnalysis(Control5)

H =

    0.1789

K =

    0.0152

VAL12 =

    0.9547

POS12 =

     1

H =

    0.1789

K =

    0.0152

r =

    0.9547
```

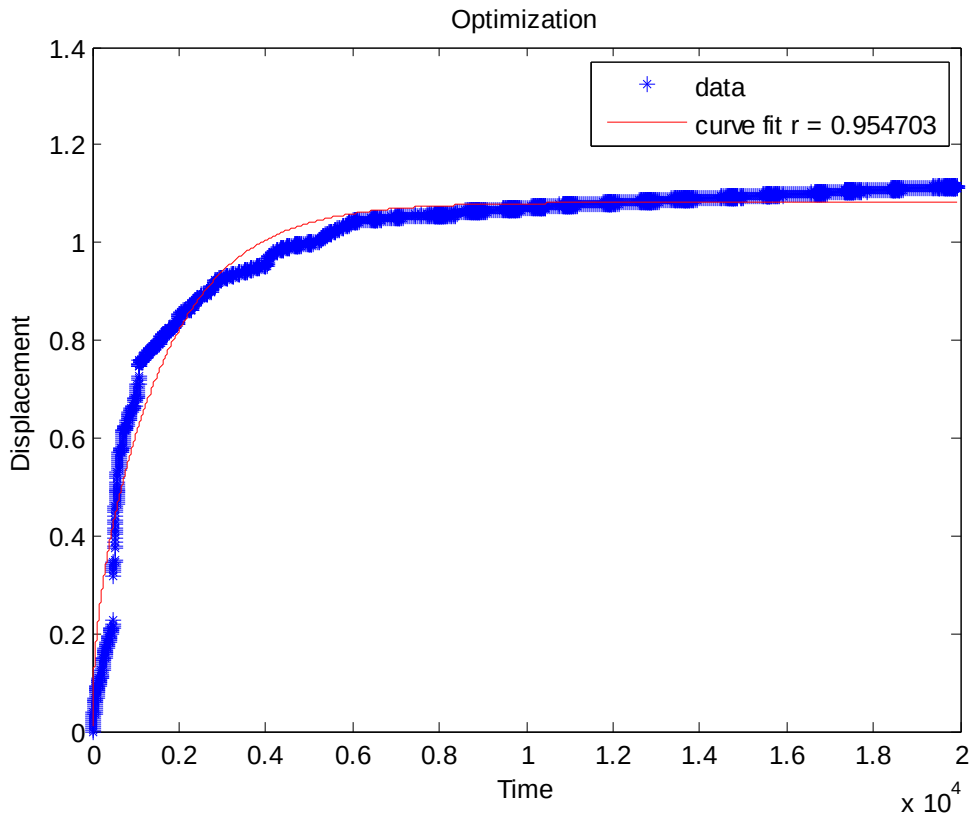

1 FTC-1

```
>> [H, K, r] = DataAnalysis(OneFTC1)

H =

    0.4610

K =

    0.0074

VAL12 =

    0.9413

POS12 =

   114

H =

    0.4610

K =

    0.0074

r =

    0.9266
```

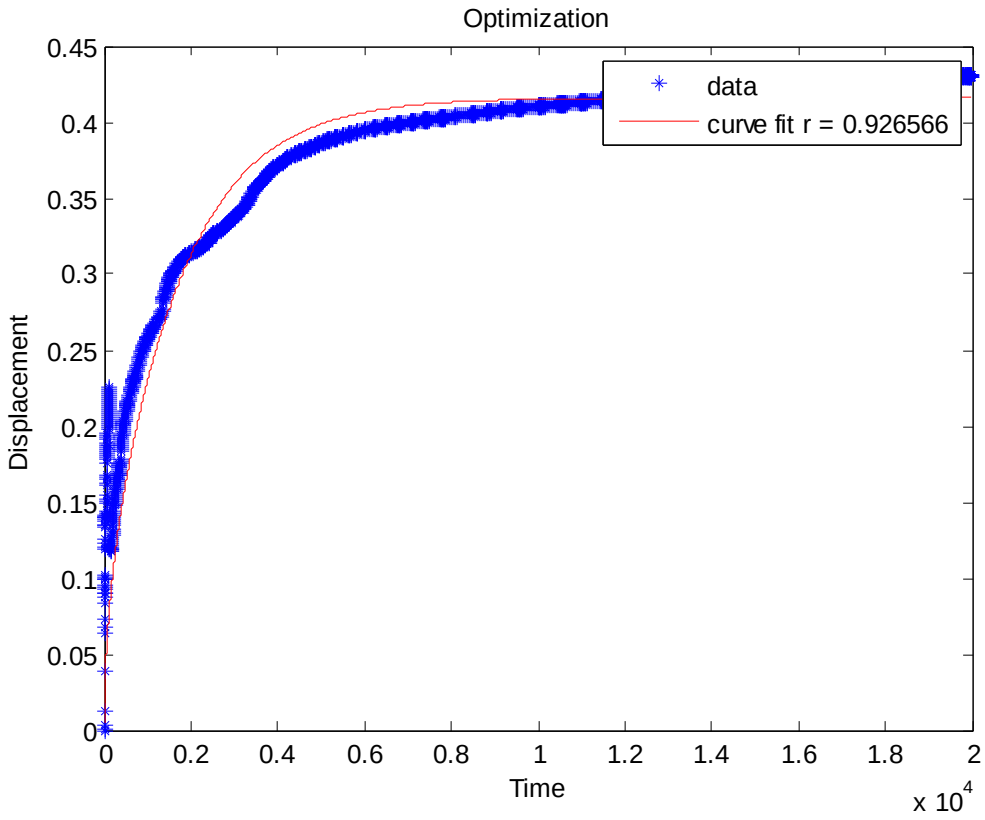

1 FTC-2

>> [H, K, r] = DataAnalysis(OneFTC2)

H =

0.7224

K =

4.2685e-004

VAL12 =

0.9664

POS12 =

3357

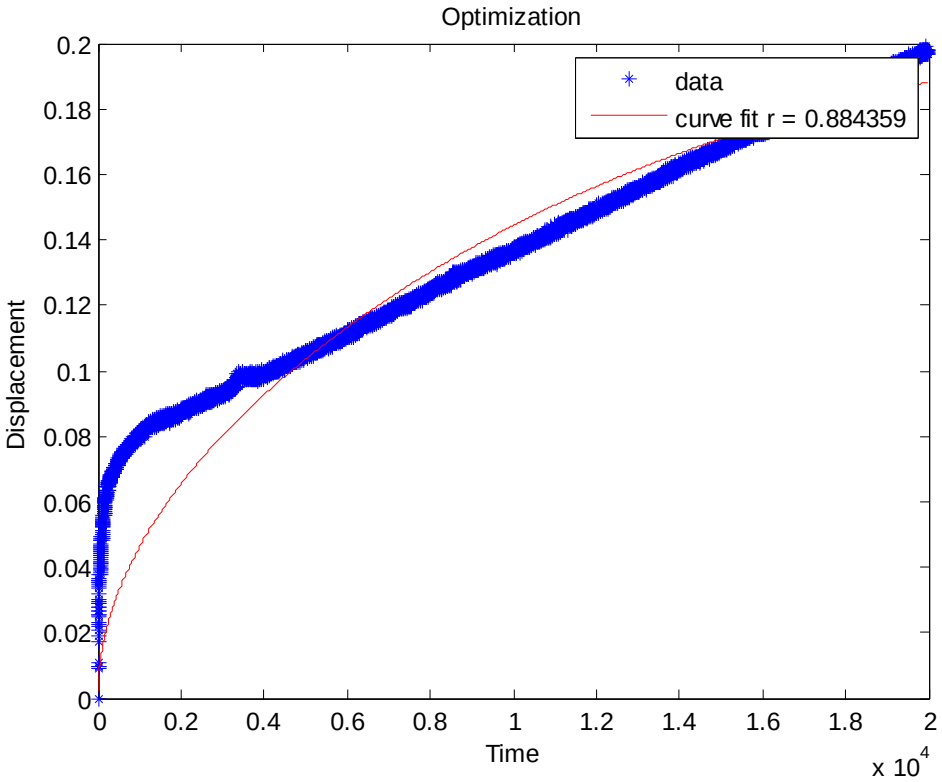

H =

0.7224

K =

4.2685e-004

r =

0.8844

1 FTC-3

>> [H, K, r] = DataAnalysis(OneFTC3)

H =

1.0080

K =

7.2121e-004

VAL12 =

0.9593

POS12 =

1

H =

1.0080

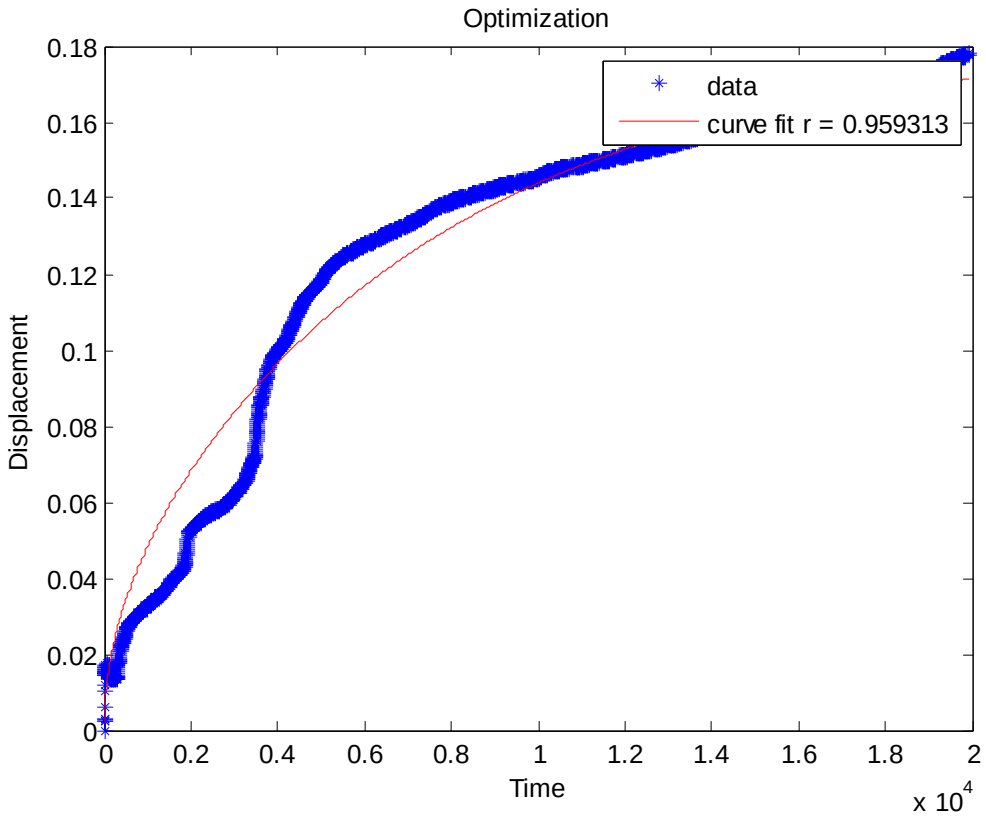

K =

7.2121e-004

r =

0.9593

1 FTC-4

```
>> [H, K, r] = DataAnalysis(OneFTC4)

H =

    0.2147

K =

    0.0304

VAL12 =

    0.8665

POS12 =

     1

H =

    0.2147

K =

    0.0304

r =

    0.8665
```

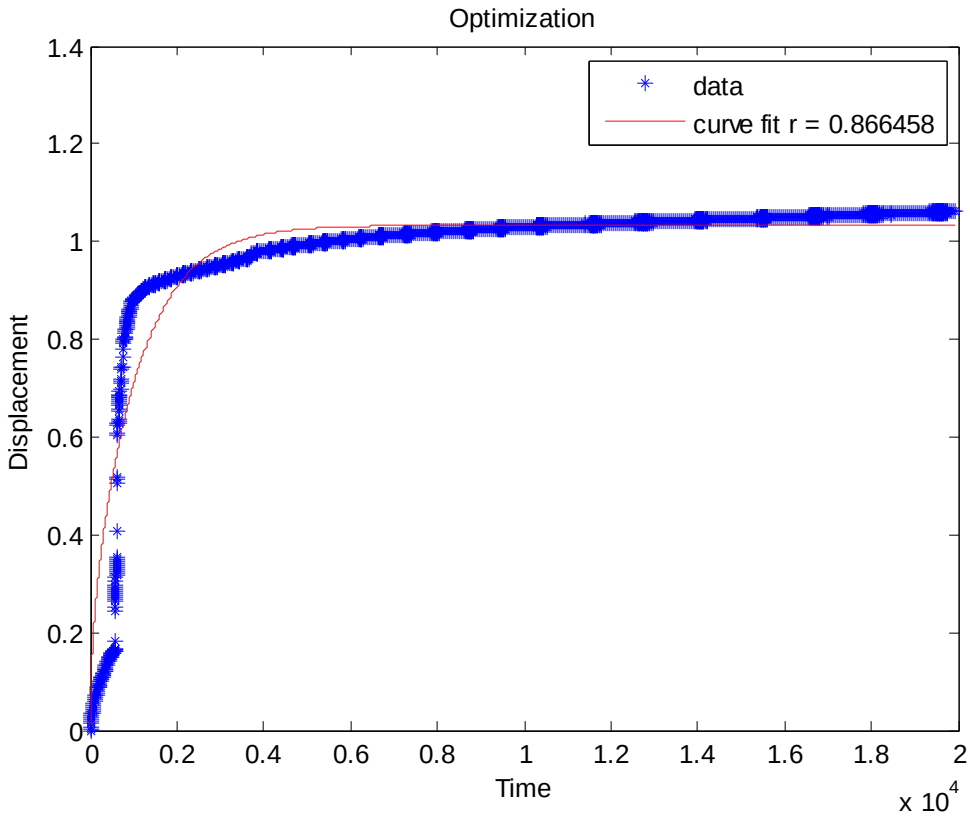

1 FTC-5

```
>> [H, K, r] = DataAnalysis(OneFTC5)

H =

    0.5782

K =

    0.0072

VAL12 =

    0.3609

POS12 =

     1

H =

    0.5782

K =

    0.0072

r =

    0.3609
```

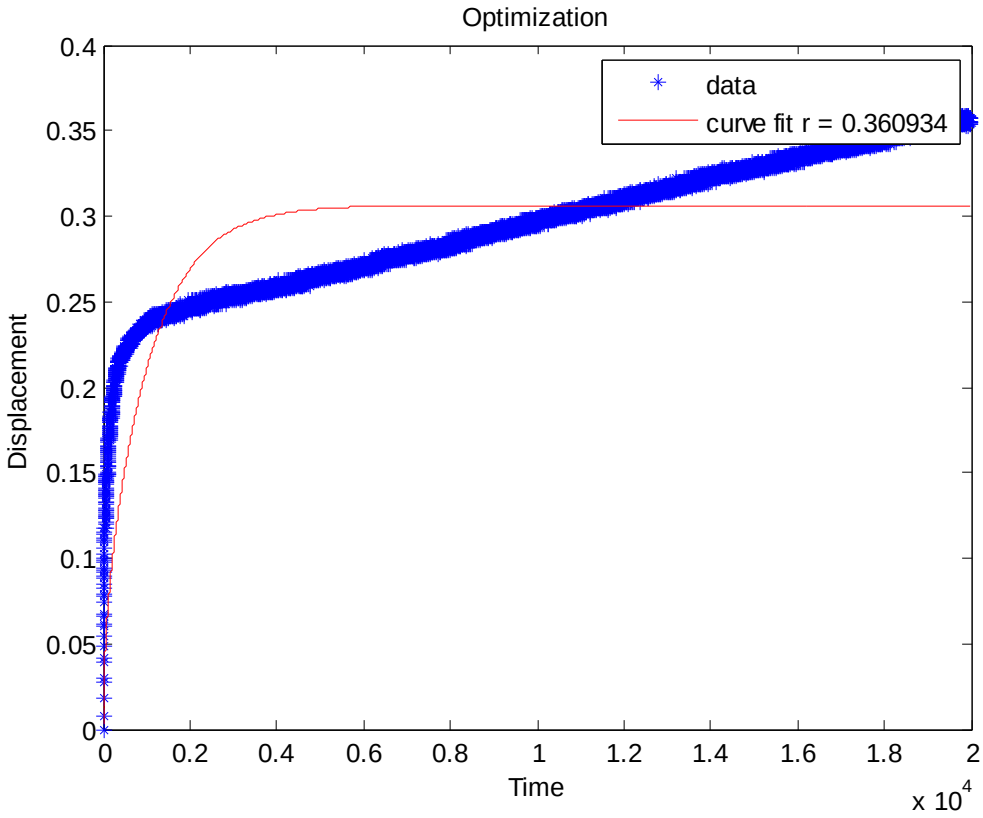

2 FTC-1

>> [H, K, r] = DataAnalysis(TwoFTC1)

H =

0.7222

K =

1.5386e-004

VAL12 =

0.9377

POS12 =

2522

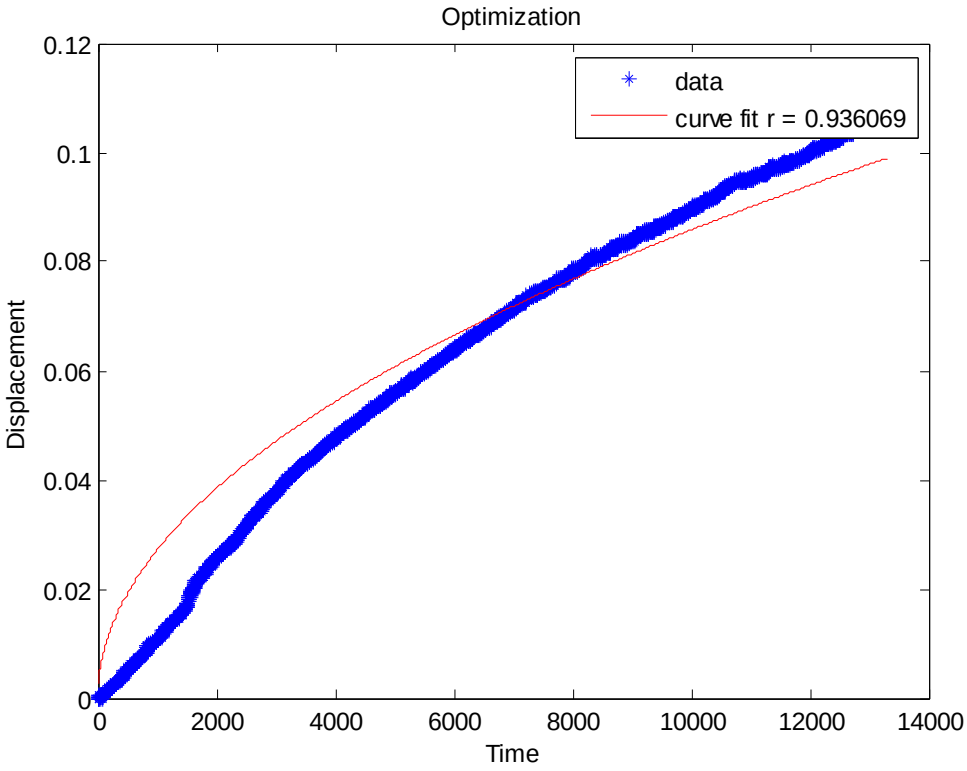

H =

0.7222

K =

1.5386e-004

r =

0.9361

2 FTC-2

```
>> [H, K, r] = DataAnalysis(TwoFTC2)

H =

    0.8380

K =

    0.0024

VAL12 =

    0.9291

POS12 =

        1636

H =

    0.8380

K =

    0.0024

r =

    0.8714
```

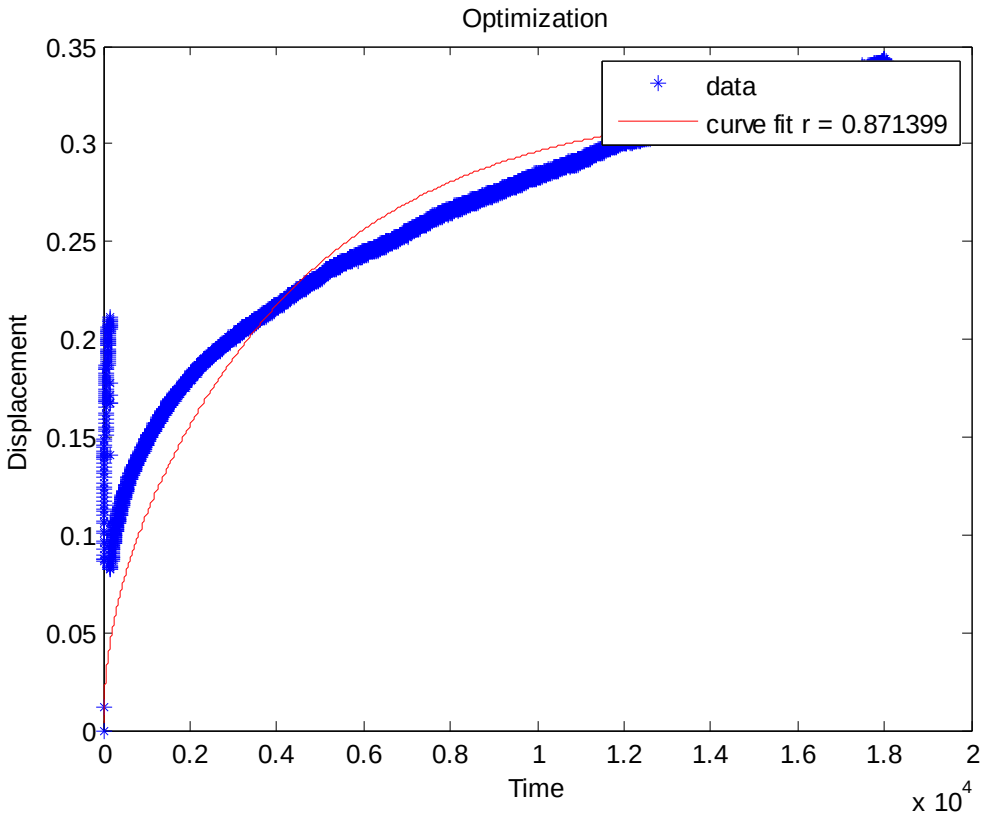

2 FTC-3

```
>> [H, K, r] = DataAnalysis(TwoFTC3)

H =

    0.1814

K =

    0.0142

VAL12 =

    0.9478

POS12 =

     1

H =

    0.1814

K =

    0.0142

r =

    0.9478
```

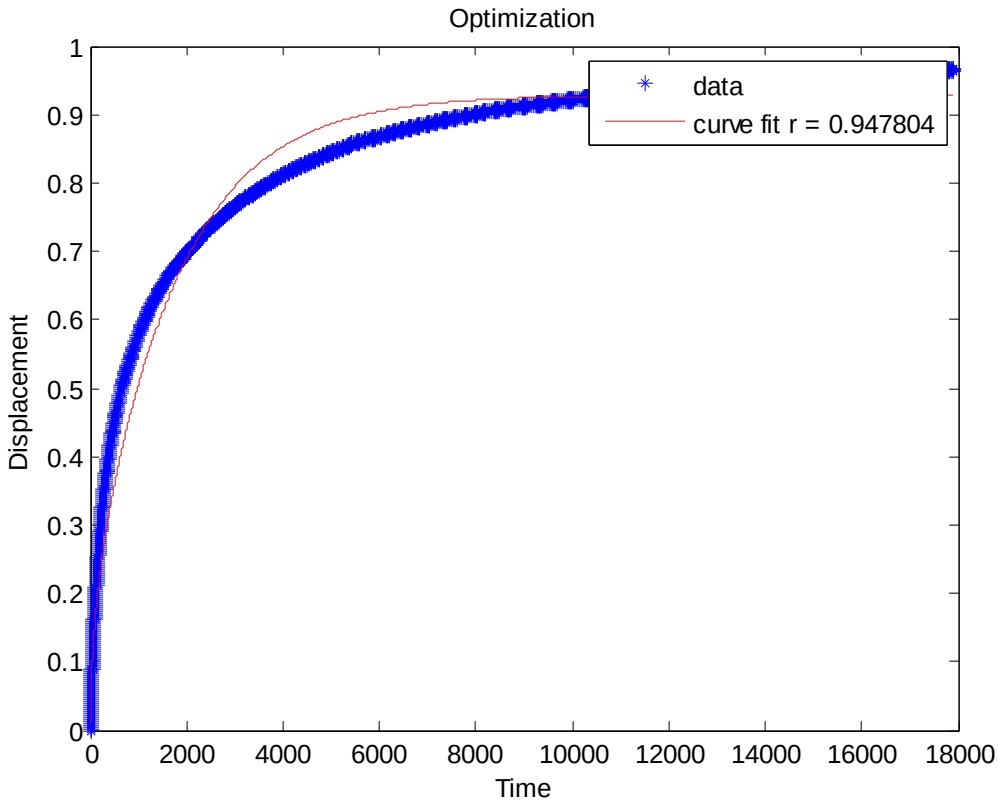

2 FTC-4

```
>> [H, K, r] = DataAnalysis(TwoFTC4)

H =

    0.5400

K =

    0.0056

VAL12 =

    0.7895

POS12 =

     1

H =

    0.5400

K =

    0.0056

r =

    0.7895
```

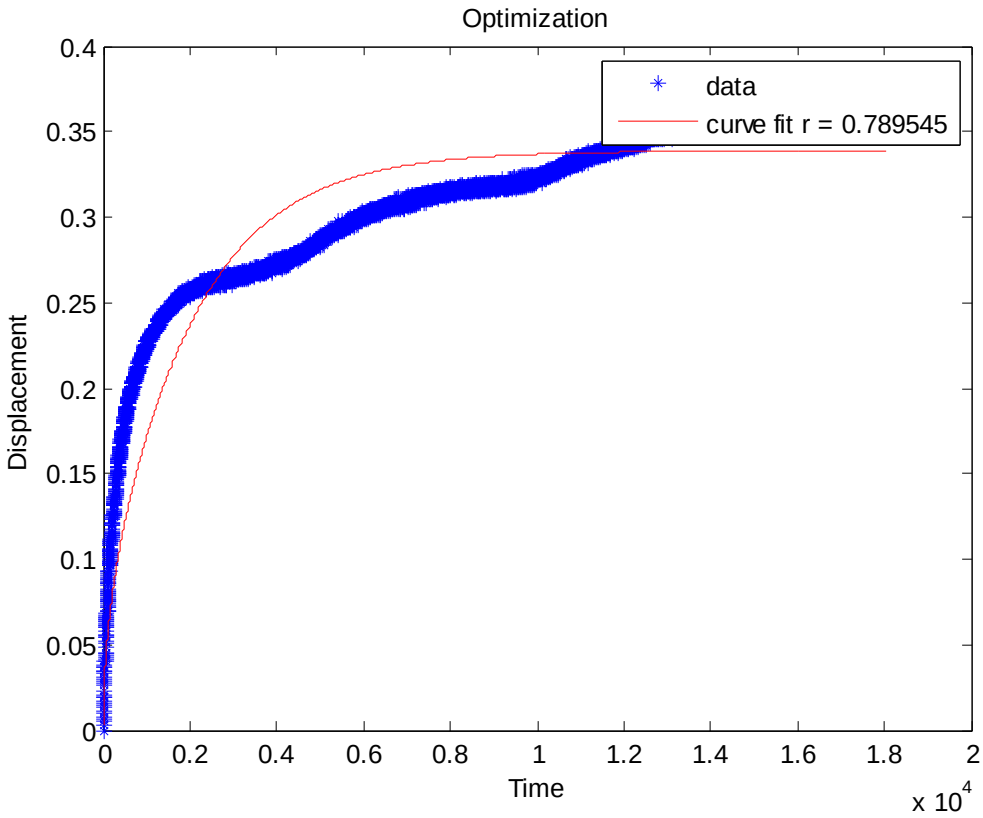

2 FTC-5

```
>> [H, K, r] = DataAnalysis(TwoFTC5)

H =

    0.2243

K =

    0.0201

VAL12 =

    0.9796

POS12 =

     1

H =

    0.2243

K =

    0.0201

r =

    0.9796
```

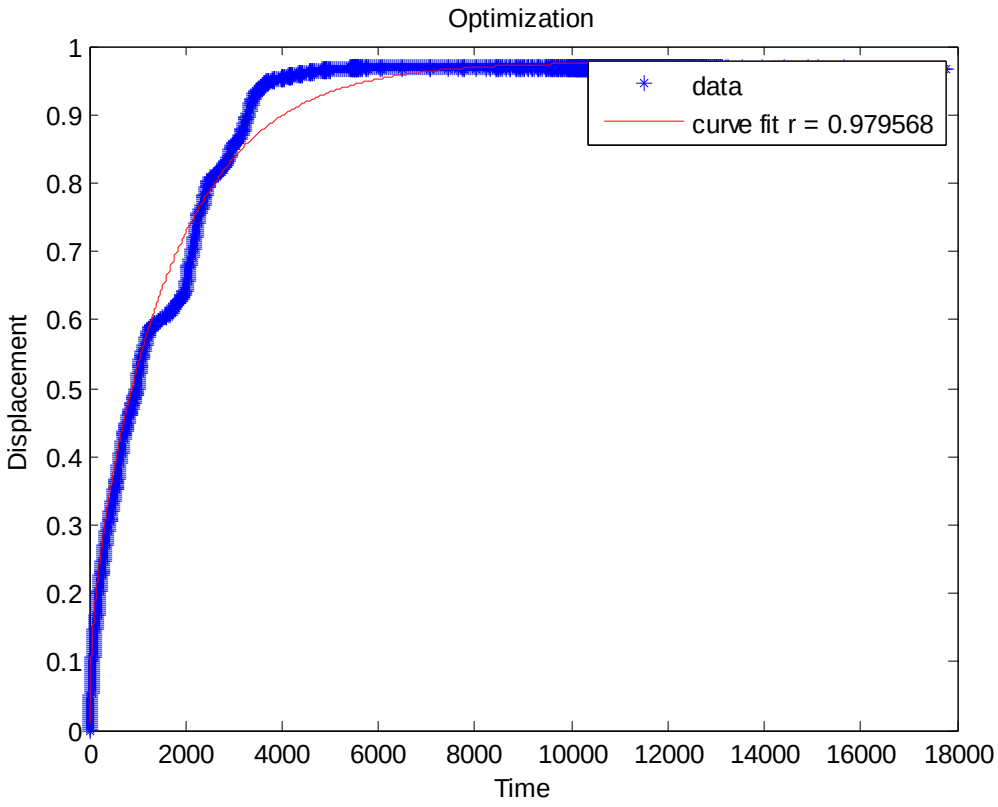

3 FTC-1

>> [H, K, r] = DataAnalysis(ThreeFTC1)

H =

0.0795

K =

0.0061

VAL12 =

0.9448

POS12 =

1

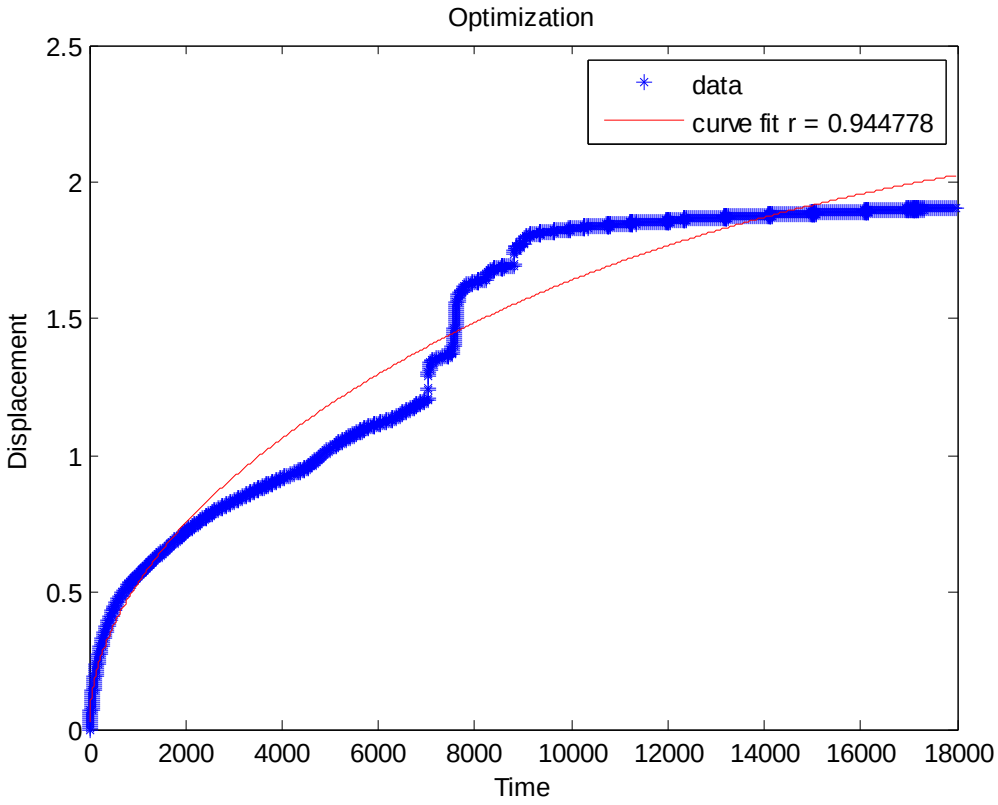

H =

0.0795

K =

0.0061

r =

0.9448

3FTC-2

```
>> [H, K, r] = DataAnalysis(ThreeFTC2)

H =

    0.2989

K =

    0.0162

VAL12 =

    0.9897

POS12 =

     1

H =

    0.2989

K =

    0.0162

r =

    0.9897
```

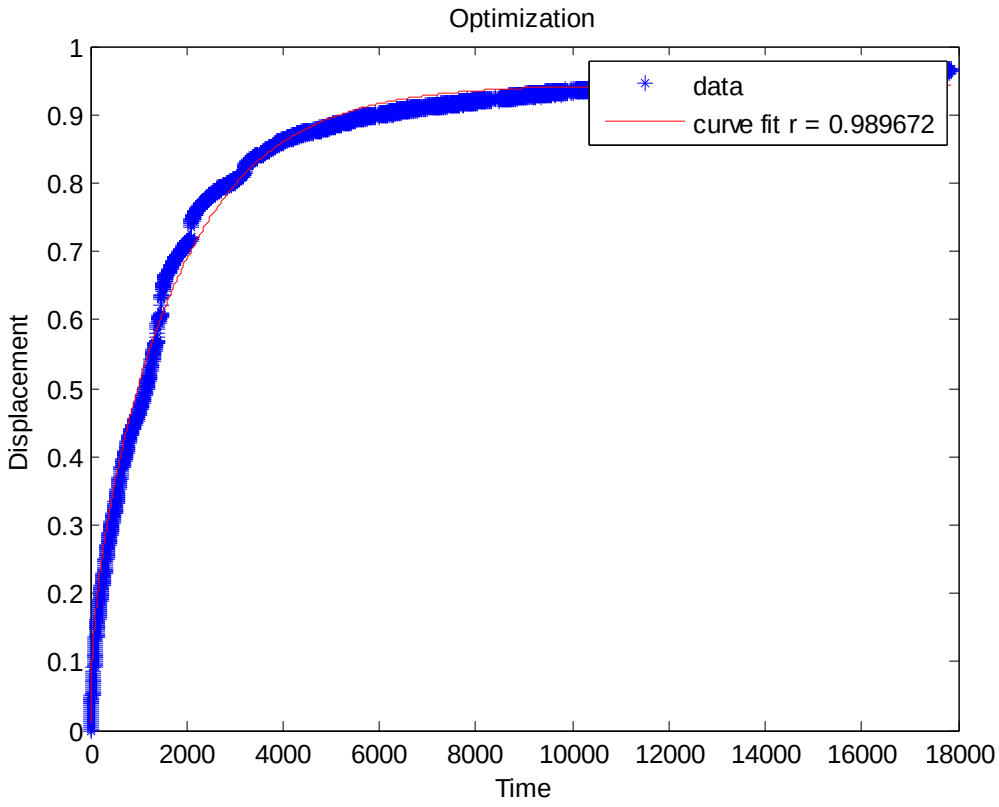

3 FTC-3

```
>> [H, K, r] = DataAnalysis(ThreeFTC3)

H =

    0.2984

K =

    0.0158

VAL12 =

    0.9801

POS12 =

     1

H =

    0.2984

K =

    0.0158

r =

    0.9801
```

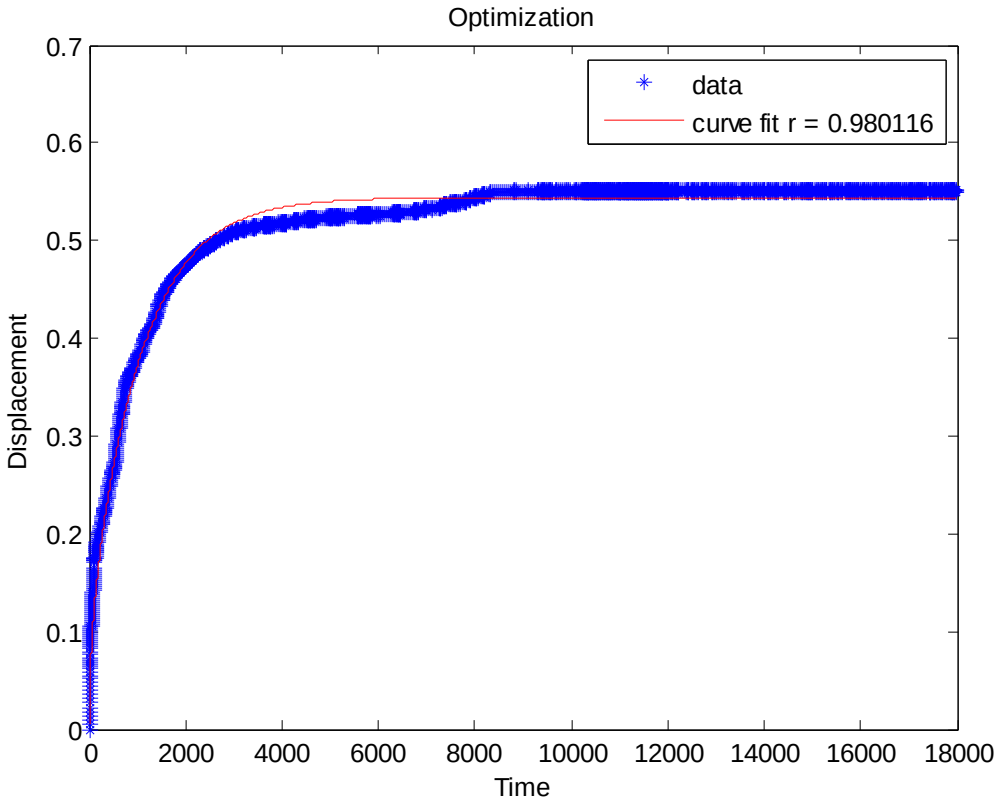

3 FTC-4

```
>> [H, K, r] = DataAnalysis(ThreeFTC4)

H =

    0.4138

K =

    0.0165

VAL12 =

    0.9603

POS12 =

     1

H =

    0.4138

K =

    0.0165

r =

    0.9603
```

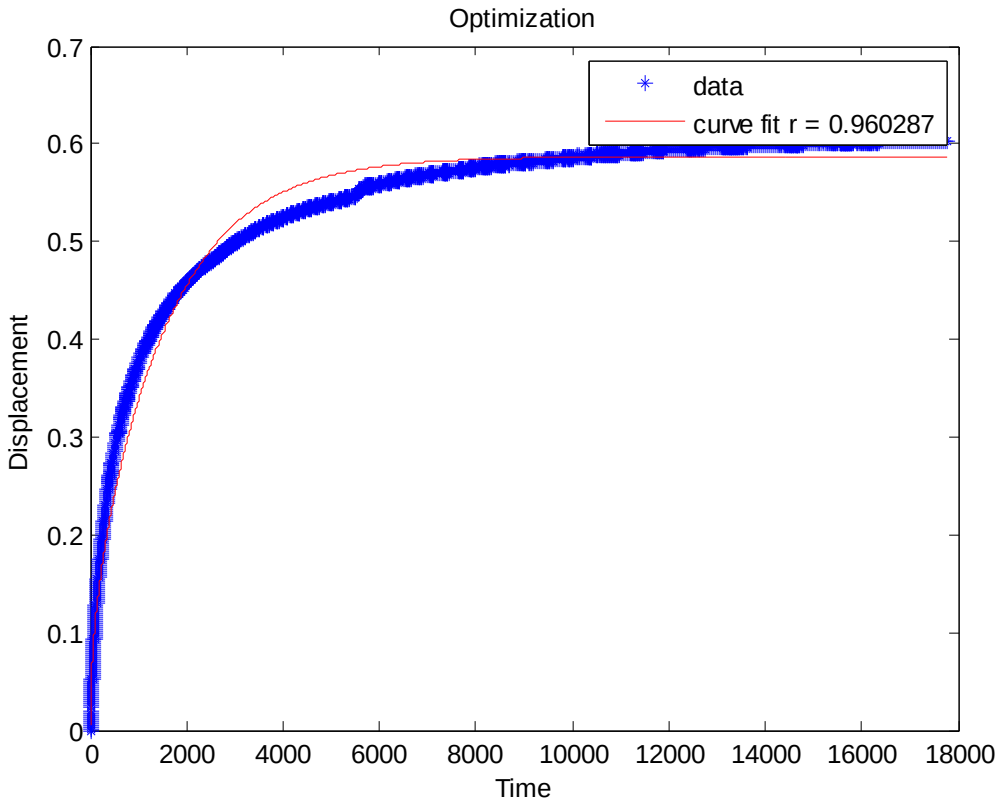

3 FTC-5

```
>> [H, K, r] = DataAnalysis(ThreeFTC5)

H =

    0.2977

K =

    0.0093

VAL12 =

    0.7518

POS12 =

     1

H =

    0.2977

K =

    0.0093

r =

    0.7518
```

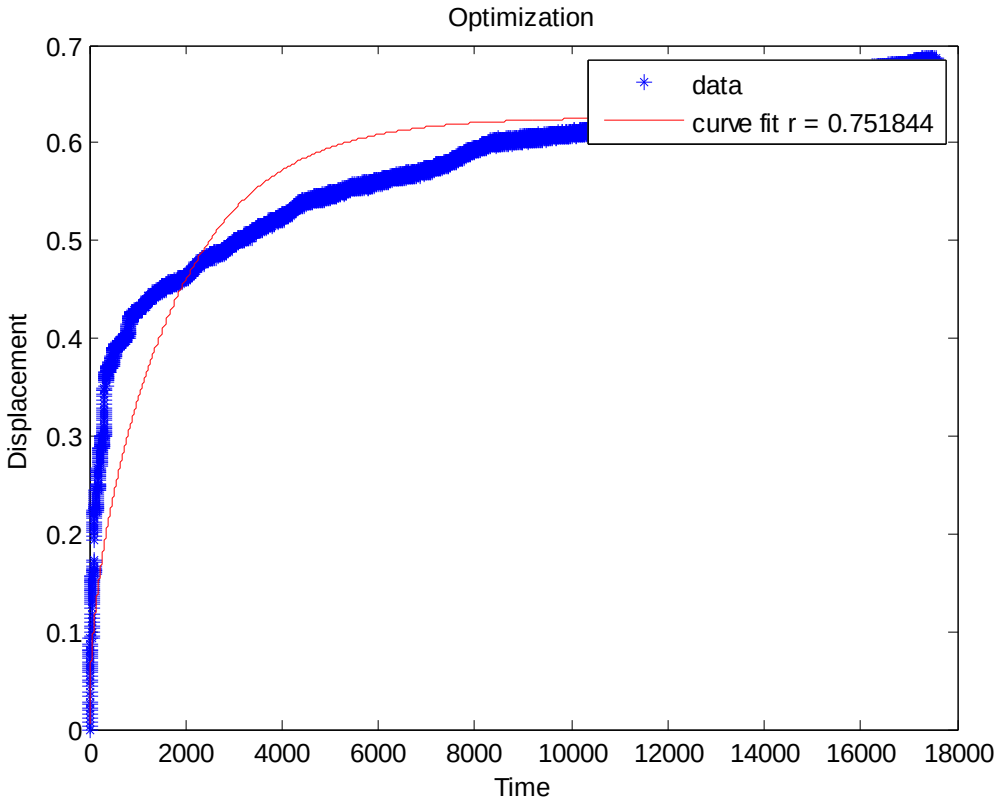

4 FTC-1

```
>> [H, K, r] = DataAnalysis(FourFTC1)

H =

    0.3116

K =

    0.0050

VAL12 =

    0.9866

POS12 =

     1

H =

    0.3116

K =

    0.0050

r =

    0.9866
```

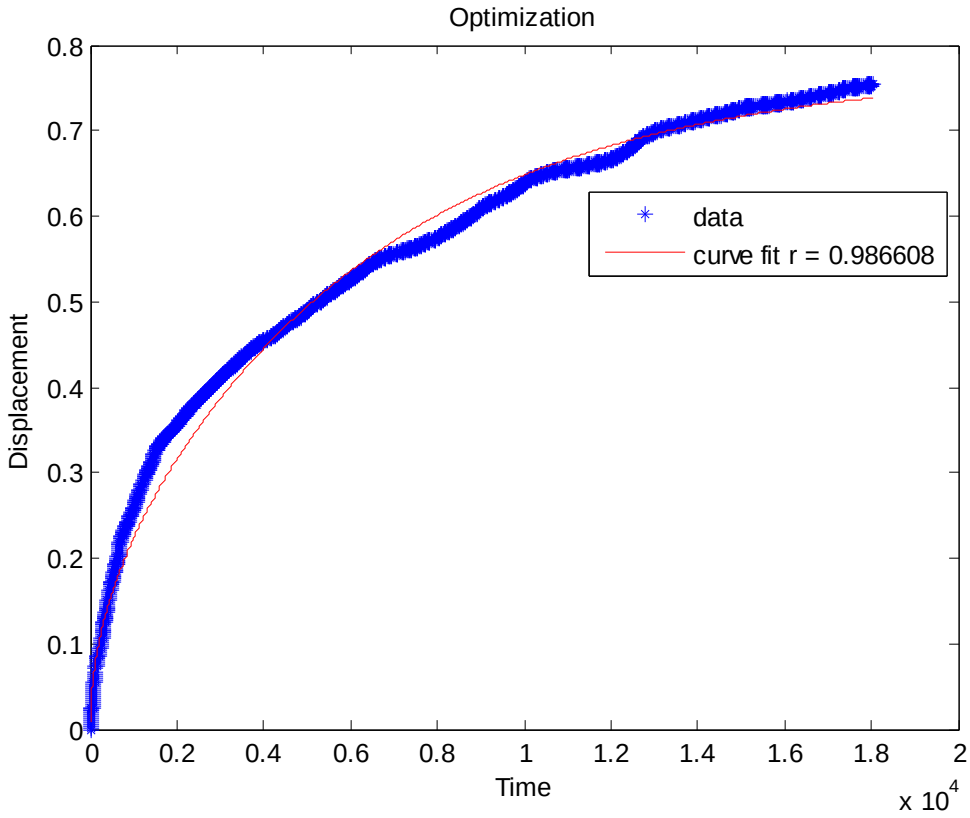

4 FTC-2

>> [H, K, r] = DataAnalysis(FourFTC2)

H =

0.2325

K =

0.0185

VAL12 =

0.8962

POS12 =

1

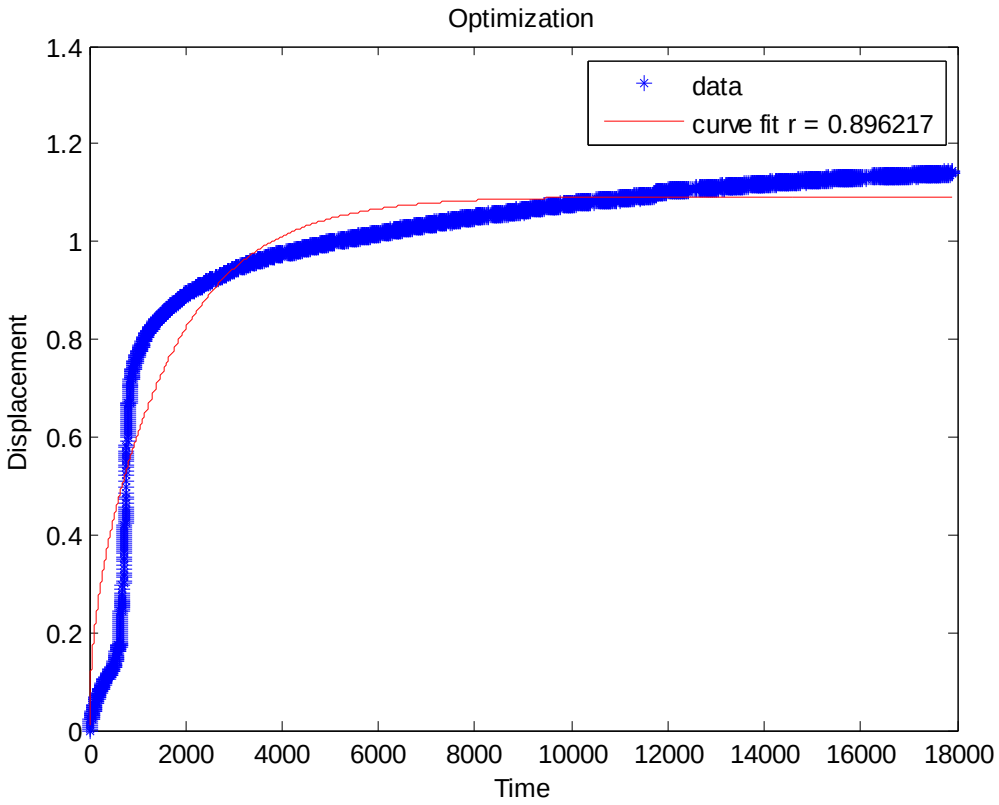

H =

0.2325

K =

0.0185

r =

0.8962

4 FTC-3

```
>> [H, K, r] = DataAnalysis(FourFTC3)

H =

    0.5296

K =

    0.0969

VAL12 =

    0.8599

POS12 =

     1

H =

    0.5296

K =

    0.0969

r =

    0.8599
```

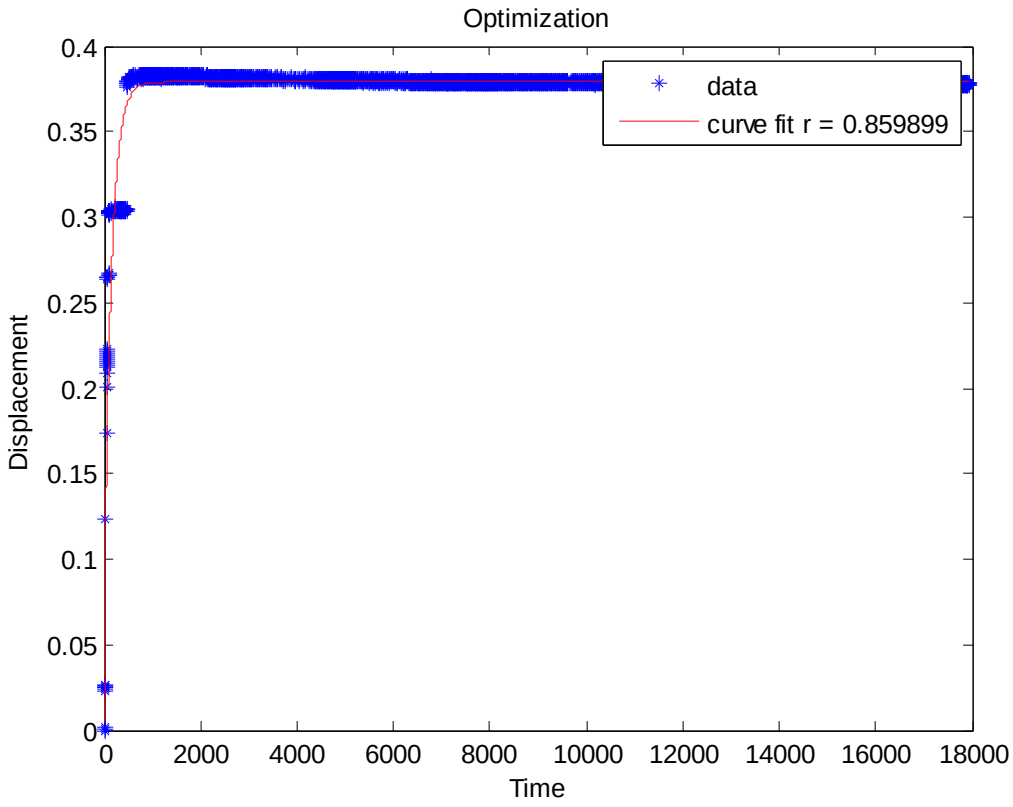

4 FTC-4

```
>> [H, K, r] = DataAnalysis(FourFTC4)

H =

    0.4781

K =

    0.0848

VAL12 =

    0.9814

POS12 =

    64

H =

    0.4781

K =

    0.0848

r =

    0.9703
```

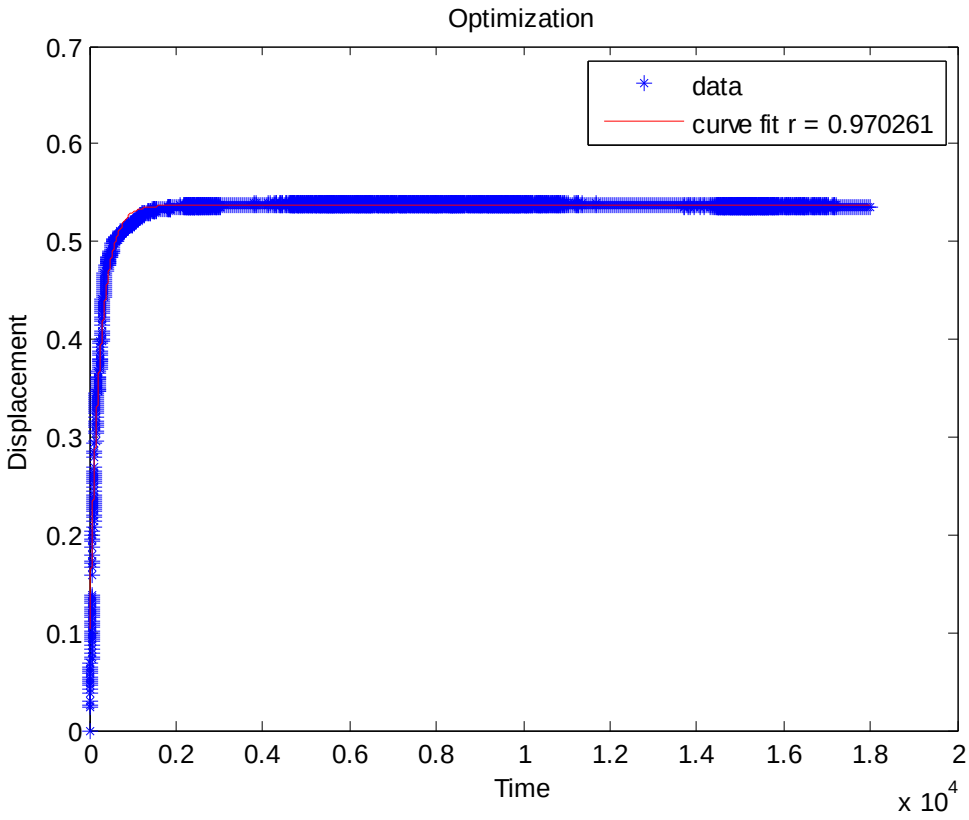

4 FTC-5

```
>> [H, K, r] = DataAnalysis(FourFTC5)

H =

    0.4674

K =

    0.0088

VAL12 =

    0.9101

POS12 =

   762

H =

    0.4674

K =

    0.0088

r =

    0.9093
```

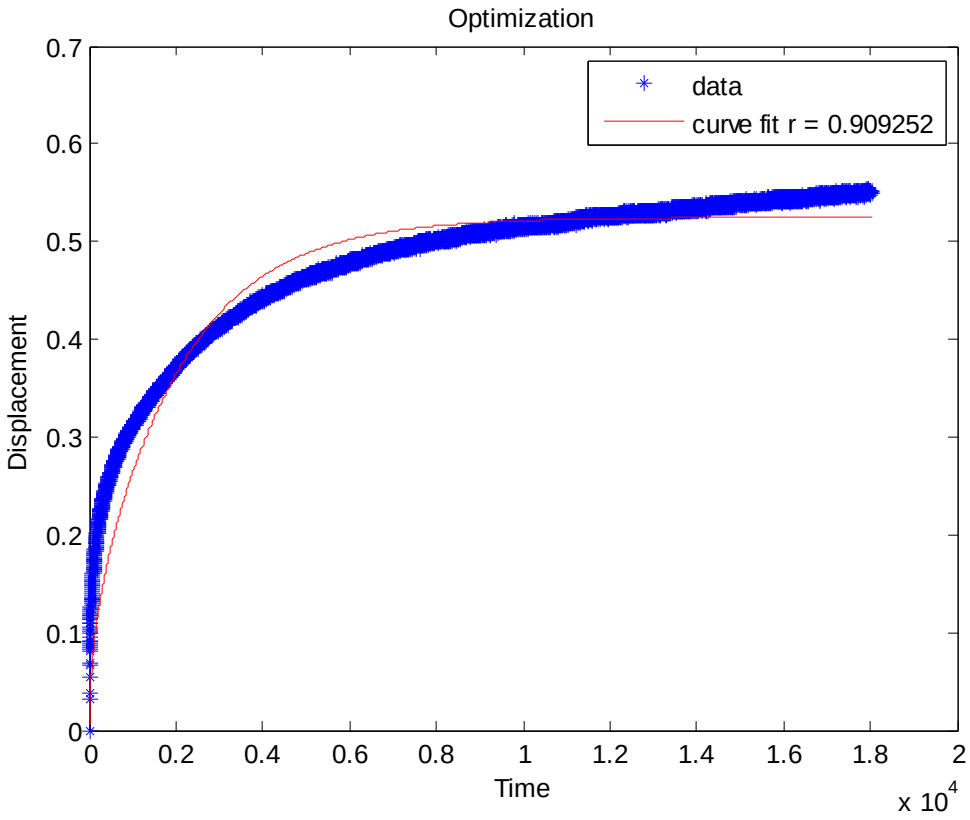

APPENDIX D

ANOVA

Oneway Analysis of Aggregate Modulus By Treatment Group

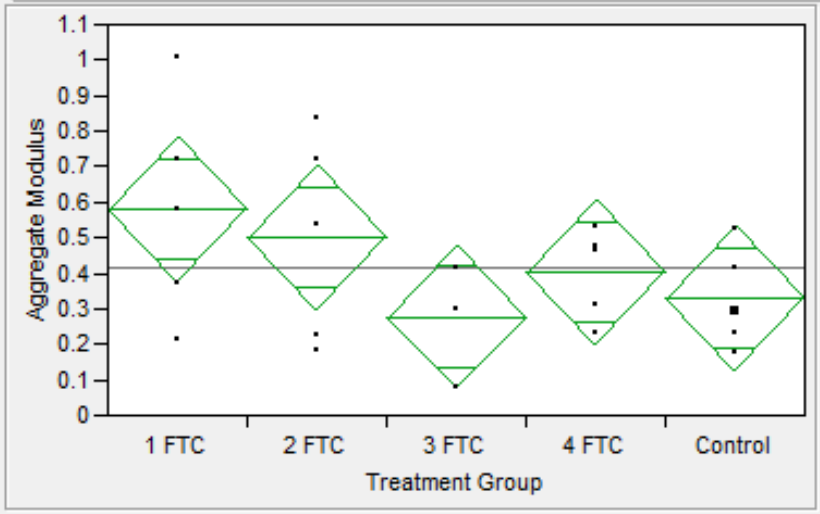

Oneway Anova

Summary of Fit

Rsquare	0.247304
Adj Rsquare	0.096765
Root Mean Square Error	0.214999
Mean of Response	0.418256
Observations (or Sum Wgts)	25

Analysis of Variance

Source	DF	Sum of Squares	Mean Square	F Ratio	Prob > F
Treatment Group	4	0.3037490	0.075937	1.6428	0.2027
Error	20	0.9244928	0.046225		
C. Total	24	1.2282418			

Means for Oneway Anova

Level	Number	Mean	Std Error	Lower 95%	Upper 95%
1 FTC	5	0.579400	0.09615	0.37883	0.77997
2 FTC	5	0.501180	0.09615	0.30061	0.70175
3 FTC	5	0.277660	0.09615	0.07709	0.47823
4 FTC	5	0.403840	0.09615	0.20327	0.60441
Control	5	0.329200	0.09615	0.12863	0.52977

Std Error uses a pooled estimate of error variance

Oneway Analysis of Permeability By Treatment Group

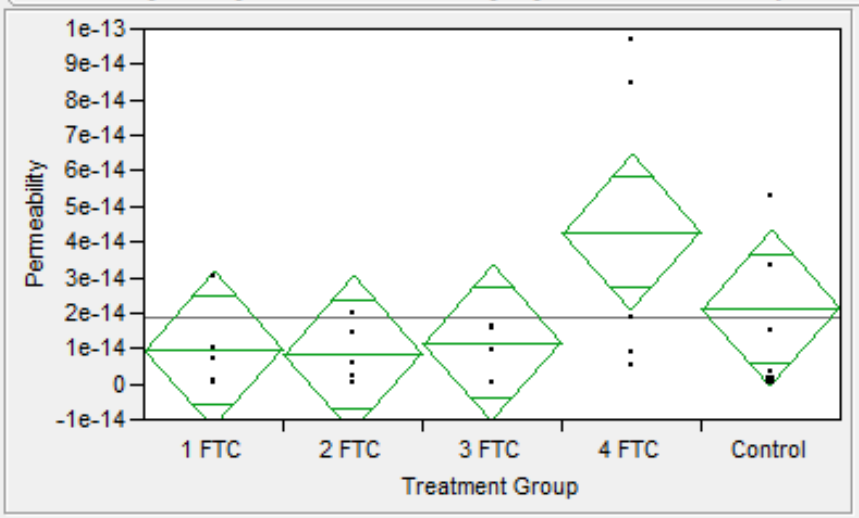

Oneway Anova

Summary of Fit

Rsquare	0.274999
Adj Rsquare	0.129998
Root Mean Square Error	2.33e-14
Mean of Response	1.88e-14
Observations (or Sum Wgts)	25

Analysis of Variance

Source	DF	Sum of Squares	Mean Square	F Ratio	Prob > F
Treatment Group	4	4.105e-27	1.026e-27	1.8965	0.1505
Error	20	1.0822e-26	5.411e-28		
C. Total	24	1.4927e-26			

Means for Oneway Anova

Level	Number	Mean	Std Error	Lower 95%	Upper 95%
1 FTC	5	9.73e-15	1.04e-14	-1.2e-14	3.143e-14
2 FTC	5	8.491e-15	1.04e-14	-1.32e-14	3.019e-14
3 FTC	5	1.168e-14	1.04e-14	-1e-14	3.338e-14
4 FTC	5	4.28e-14	1.04e-14	2.11e-14	6.45e-14
Control	5	2.121e-14	1.04e-14	-4.94e-16	4.291e-14

Std Error uses a pooled estimate of error variance

APPENDIX E

Equipment and Designs

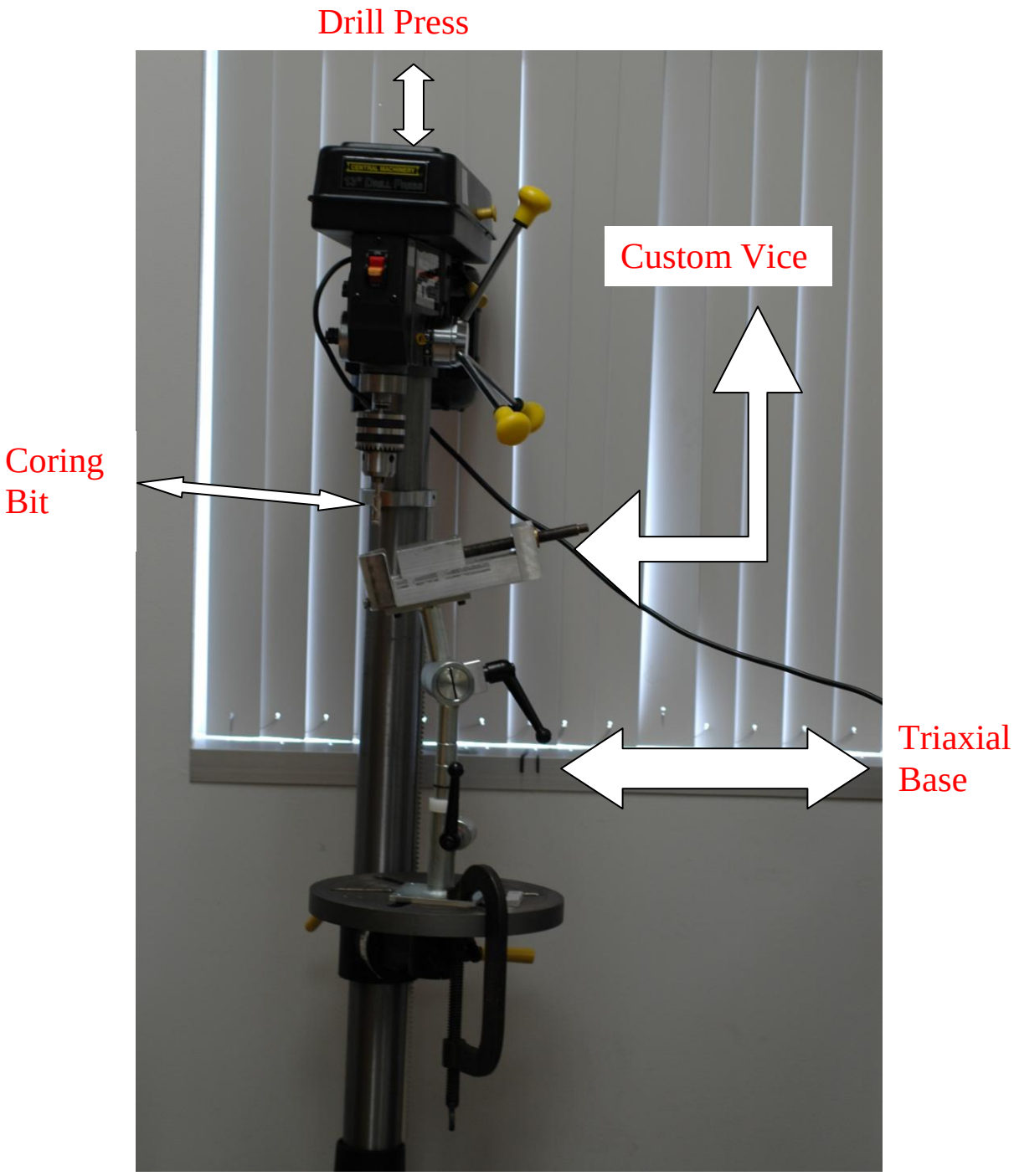

Confined Compression Chamber Design

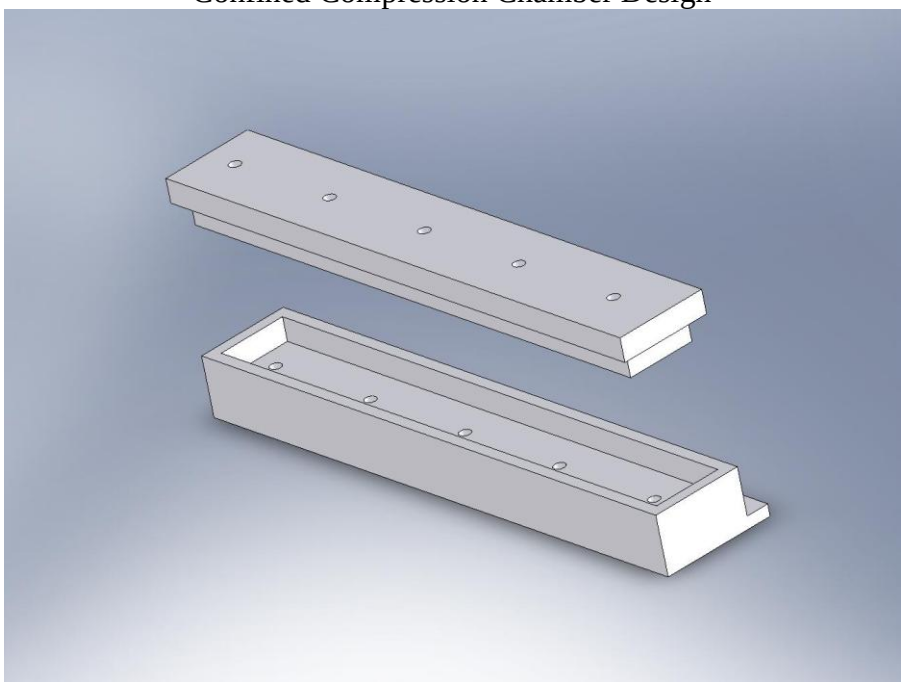

Vice Design

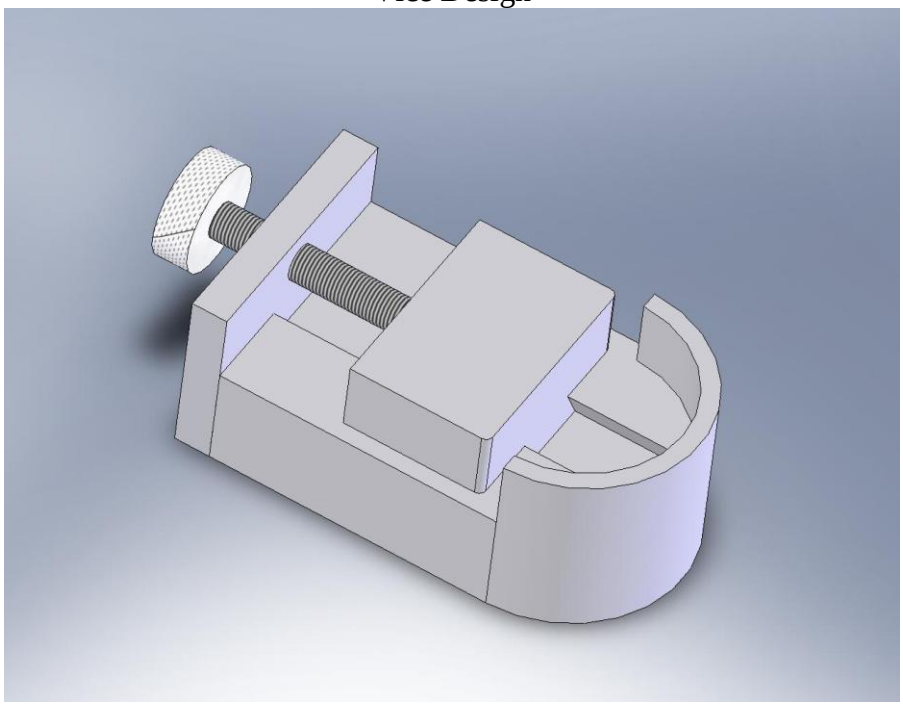

Confined Compression Chamber with Indenters and Weights Design

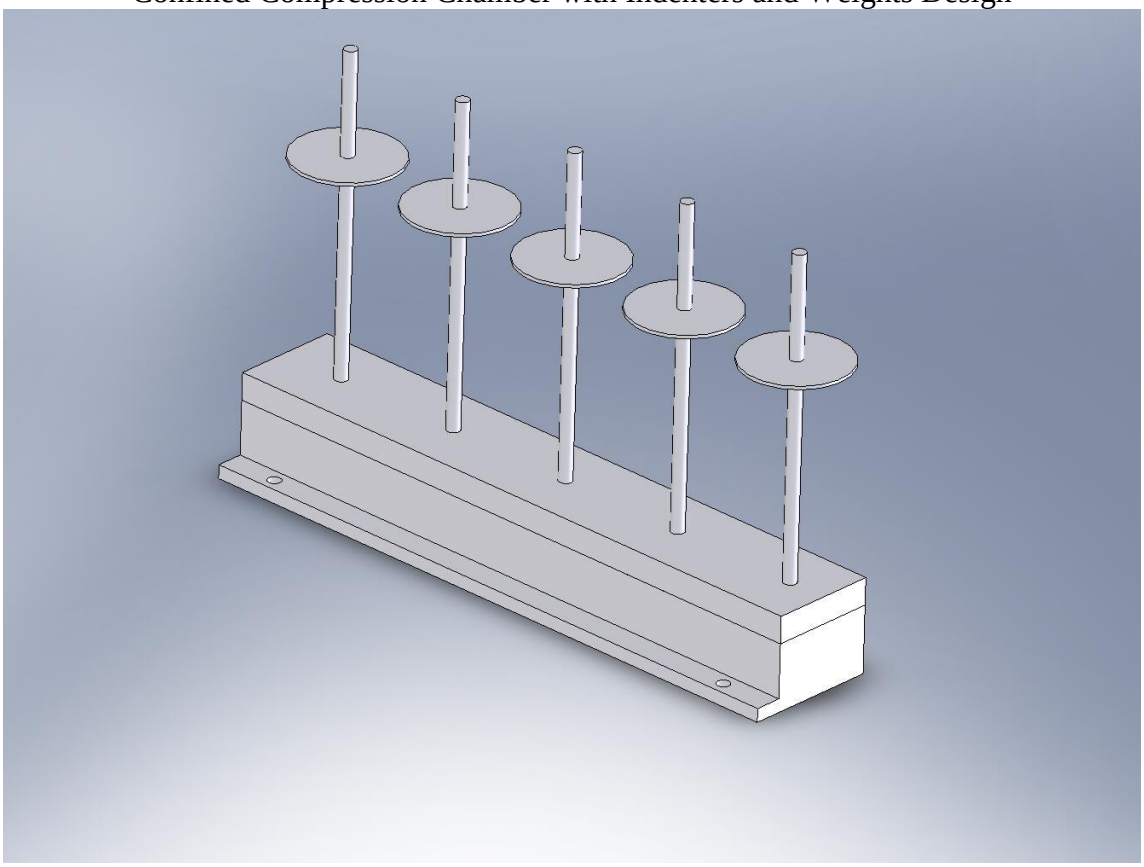

REFERENCES

[1] American Heritage Dictionary [Internet] Boston (MA): Meniscus; c2009. Available from: http://www.bartleby.com/61/imagepages/A4menisc.html

[2] Mow, V.C., Ratcliffe, A., "Chapter 4 Structure and Function of Articular Cartilage and Meniscus" in Basic Orthopaedic Biomechanics 2nd ed., 1997, ed. Mow, V.C., Hayes, W. C., Lippincott-Raven, Philadelphia, pp. 113.

[3] Sweigart, M. A., and Athanasiou, K. A., 2004, "Biomechanical Characteristics of the Normal Medial and Lateral Porcine Knee Menisci." Proc Inst Mech Eng Part H-J Eng Med, 219(1) pp. 53-62.

[4] Swann, A. C., and Seedhom, B. B., 1989, "Improved Techniques for Measuring the Indentation and Thickness of Articular Cartilage." Proc Inst Mech Eng Part H-J Eng Med, 203(3) pp. 143-150.

[5] Hsieh, H., and Walker, P. S., 1976, "Stabilizing Mechanisms of the Loaded and Unloaded Knee Joint." J Bone Joint Surg-Am Vol, 58(1) pp. 87-93.

[6] Ahmed, A. M., and Burke, D. L., 1983, "In-Vitro Measurement of Static Pressure Distribution in Synovial Joints--Part I: Tibial Surface of the Knee." J Biomech Eng, 105(3) pp. 216-225.

[7] Schinagl, R. M., Ting, M. K., Price, J. H., 1996, "Video Microscopy to Quantitate the Inhomogeneous Equilibrium Strain within Articular Cartilage during Confined Compression." Ann Biomed Eng, 24(4) pp. 500-512.

[8] Rijk, P. C., 2004, "Meniscal Allograft Transplantation--Part I: Background, Results, Graft Selection and Preservation, and Surgical Considerations." Arthroscopy, 20(7) pp. 728-743.

[9] Sutton, J. B., 1884, "Nature of Ligaments: Part II." J Anat Phys, 19(Pt 1) pp. 26.1-50.

[10] Fairbanks, T. J., 1948, "Knee Joint Changes After Menisectomy," J Bone Joint Surg Br-Vol 30 pp. 664-670.

[11] Arnoczky, S. P., McDevitt, C. A., Schmidt, M. B., 1988, "The Effect of Cryopreservation on Canine Menisci: A Biochemical, Morphologic, and Biomechanical Evaluation." J Orthop Res, 6(1) pp. 1-12.

[12] American Academy of Orthopedic Surgeons [Internet] Rosemont (IL): Common Knee Injuries; c2009. Available from: http://orthoinfo.aaos.org/fact/thr_report.cfm?thread_id=88&topcategory=knee

[13] Mow, V. C., Athesan, G. A., and Spilker, R. L., 1993, "Biomechanics of Diarthrodial Joints: A Review of Twenty Years of Progress." J Biomech Eng, 115(4B) pp. 460-467.

[14] Lu, X. L., and Mow, V. C., 2007, "Biomechanics of Articular Cartilage and Determination of Material Properties." Med Sci Sports Exerc, 40(2) pp. 193-199.

[15] American Academy of Orthopedic Surgeons [Internet] Rosemont (IL): Meniscal Tear; c2009. Available from: http://orthoinfo.aaos.org/fact/thr_report.cfm?thread_id=277&topcategory=knee

[16] Fithian, D. C., Kelly, M. A., and Mow, V. C., 1990, "Material Properties and Structure-Function Relationships in the Menisci." Clin Orthop Rel Res, (252) pp. 19-31.

[17] Wisnewski, P. J., Powers, D. L., and Kennedy, J. M., 1988, "Glutaraldehyde-Cross-Linked Meniscal Allografts: Mechanical Properties." J Invest Surg, 1(4) pp. 259-266.

[18] Reckers, L. J., Fagundes, D. J., Cohen, M., 2005, "Effects of Different Temperatures and Periods of Preservation in Menisci Cellularity in Rabbits." Acta Cir Bras, 20(6) pp. 428-432.

[19] Hamlet, W., Liu, S. H., and Yang, R., 1997, "Destruction of a Cyropreserved Meniscal Allograft: A Case for Acute Rejection." Arthroscopy, 13(4) pp. 517-521.

[20] Tienen, T. G., Verdonschot, N., Heijkants, R. G., 2004, "Prosthetic Replacement of the Medial Meniscus in Cadaveric Knees: Does the Prosthesis Mimic the Functional Behavior of the Native Meniscus?" Am J Sports Med, 32(5) pp. 1182-1188.

[21] De Groot, J. H., De Vrijer, R., Pennings, A. J., 1996, "Use of Porous Polyurethanes for Meniscal Reconstruction and Meniscal Prostheses," Biomaterials, 17(2) pp. 163-173.

[22] Khalsa, P. S., and Eisenberg, S. R., 1997, "Compressive Behavior of Articular Cartilage is Not Completely Explained by Proteoglycan Osmotic Pressure." J Biomech, 30(6) pp. 589-594.

[23] Lai, W. M., Mow, V. C., and Roth, V., 1980, "Effects of Nonlinear Strain-Dependent Permeability and Rate of Compression on the Stress Behavior of Articular Cartilage." J Biomech Eng, 103(2) pp. 61-66.

[24] Muir, H., Bullough, P., and Maroudas, A., 1970, "The Distribution of Collagen in Human Articular Cartilage with some of its Physiological Implications." J Bone Joint Surg Br-Vol, 52(3) pp. 554-563.

[25] Gu, W. Y., Lai, W. M., and Mow, V. C., 1998, "A Mixture Theory for Charged-Hydrated Soft Tissues Containing Multi-Electrolytes: Passive Transport and Swelling Behaviors." J Biomech Eng, 120(2) pp. 169-180.

[26] Lai, W. M., Hou, J. S., and Mow, V. C., 1991, "A Triphasic Theory for the Swelling and Deformation Behaviors of Articular Cartilage." J Biomech Eng, 113(3) pp. 245-258.

[27] Skurla, C. P., Perera, A., Towe, C. T., 2007, "Development of Photochemical Method for Meniscal Repair: A Preliminary Study." J Biomech, 40(1) pp. 220-224.

[28] Seireg, A., and Arvikar, S., 1975, "The Prediction of Muscular Load Sharing and Joint Forces in the Lower Extremities during Walking." J Biomech, 8(2) pp. 89-102.

[29] Kempson, G. E., Freeman, M. A. R., and Swanson, S. A. V., 1971, "The Determination of a Creep Modulus for Articular Cartilage from Indentation Tests of the Human Femoral Head." J Biomech, 4(4) pp. 239-250.

[30] Armstrong, C. G., and Mow, V. C., 1983, "The Mechanical Properties of Articular Cartilage." Bull Hosp Joint Dis Orthop Inst, 43(2) pp. 109-117.

[31] Kempson, G. E., Muir, H., Swanson, S. A. V., 1970, "Correlations between Stiffness and the Chemical Constituents of Cartilage on the Human Femoral Head." Biochim Biophys Acta-Gen Subj, 215(1) pp. 70-77.

[32] Lechner, K., Hull, M. L., and Howell, S. M., 2000, "Is the Circumferential Tensile Modulus within a Human Medial Meniscus Affected by the Test Sample Location and Cross-Sectional Area?" J Ortho Res, 18(6) pp. 945-951.

[33] Proctor, C. S., Schmidt, M. B., Whipple, R. R., 1989, "Material Properties of the Normal Medial Bovine Meniscus." J Ortho Res, 7(6) pp. 771-782.

[34] Roth, V., and Mow, V. C., 1980, "The Intrinsic Tensile Behavior of the Matrix of Bovine Articular Cartilage and its Variation with Age." J Bone Joint Surg-Am Vol, 62(7) pp. 1102-1117.

[35] Skaggs, D. L., Warden, W. H., and Mow, V. C., 1994, "Radial Tie Fibers Influence the Tensile Properties of the Bovine Medial Meniscus." J Ortho Res, 12(2) pp. 176-185.

[36] Sweigart, M. A., and Athanasiou, K. A., 2005, "Tensile and Compressive Properties of the Medial Rabbit Meniscus." Proc Inst Mech Eng Part H-J Eng Med, 219(5) pp. 337-347.

[37] Wainwright, S.A., Biggs, W.D., Currey, J.D., 1982, Mechanical Design in Organisms, Princeton Univerisity Press, Princeton, pp. 89.

[38] Chen, A. C., Bae, W. C., Schinagl, R. M., 2001, "Depth- and Strain-Dependent Mechanical and Electromechanical Properties of Full-Thickness Bovine Articular Cartilage in Confined Compression." J Biomech, 34(1) pp. 1-12.

[39] Athanasiou, K. A., Agarwal, A., Muffoletto, A., 1995, "Biomechanical Properties of Hip Cartilage in Experimental Animal Models." Clin Orthop Rel Res, (316) pp. 254-266.

[40] Jurvelin, J., Saamanen, A., Arokoski, J., 1988, "Biomechanical Properties of the Canine Knee Articular Cartilage as Related to Matrix Proteoglycans and Collagen." Eng Med, 17(4) pp. 157-162.

[41] Armstrong, C. G., and Mow, V. C., 1982, "Variations in the Intrinsic Mechanical Properties of Human Articular Cartilage with Age, Degeneration, and Water Content." J Bone Joint Surg-Am Vol, 64(1) pp. 88-94.

[42] Roberts, S., Weightman, B., Urban, J., 1986, "Mechanical and Biochemical Properties of Human Articular Cartilage in Osteoarthritic Femoral Heads and in Autopsy Specimens." J Bone Joint Surg-Br Vol, 68(2) pp. 278-288.

[43] Ateshian, G. A., Warden, W. H., Kim, J. J., 1997, "Finite Deformation Biphasic Material Properties of Bovine Articular Cartilage from Confined Compression Experiments." J Biomech, 30(11-12) pp. 1157-1164.

[44] Mow, V. C., Kuei, S. C., Lai, W. M., 1980, "Biphasic Creep and Stress Relaxation of Articular Cartilage in Compression: Theory and Experiments." J Biomech Eng, 102(1) pp. 73-84.

[45] Maroudas, A., 1976, "Balance between Swelling Pressure and Collagen Tension in Normal and Degenerate Cartilage." Nature, 260(5554) pp. 808-809.

[46] Towe, C., 2004, "Effects of Freezing on Intrinsic Circumferential Tensile Properties of Bovine Medial Meniscus," Honors Thesis. Baylor University, Waco, TX

[47] Goertzen, D. J., Budney, D. R., and Cinats, J. G., 1997, "Methodology and Apparatus to Determine Material Properties of the Knee Joint Meniscus." Med Eng Phys, 19(5) pp. 412-419.

[48] Schinagl, R. M., Gurskis, D., Chen, A. C., 1997, "Depth-Dependent Confined Compression Modulus of Full-Thickness Bovine Articular Cartilage." J Ortho Res, 15(4) pp. 499-506.

[49] Morgan, D. S., 2007, "The Effects of Freezing on the Circumferential Tensile Properties of Bovine Medial Meniscus," .Honors Thesis. Baylor University, Waco, TX

[50] Athanasiou, K. A., Agarwal, A., and Dzida, F. J., 1994, "Comparative Study of the Intrinsic Mechanical Properties of the Human Acetabular and Femoral Head Cartilage." J Ortho Res, 12(3) pp. 340-349.

[51] Soltz, M. A., and Ateshian, G. A., 1998, "Experimental Verification and Theoretical Prediction of Cartilage Interstitial Fluid Pressurization at an Impermeable Contact Interface in Confined Compression," J Biomech, 31(10) pp. 927-934.

[52] Bozzola, J.J., and Russell, L.D., 1999, Electron Microscopy: Principles and Techniques for Biologists 2nd Edition, Jones and Bartlett, Sudbury, Massachusetts, pp. 17-77.